UNIVERSITY OF CALIFORNIA

Los Angeles

Uncertainties in the Measurement of Simulated Carbonaceous Aerosols: (I) Characterization of Emissions from a Portable Diesel Generator and Development of the Extended Idealized Aggregate Theory and (II) the Effect of Metal Additives on the Evolved Gas Analysis of Carbon

A dissertation submitted in partial satisfaction of the

requirements for the degree Doctor of Philosophy

in Chemical Engineering

by

Albert Chung

2009

The dissertation of Albert Chung is approved.

Yoram Cohen

Gerassimos Orkoulas

Panagiotis Christofides, Committee Co-Chair

Suzanne E. Paulson, Committee Co-Chair

University of California, Los Angeles

2009

TABLE OF CONTENTS

Chapter 1: Introduction 1

Chapter 2: Particulate Emissions by a Small Non-Road Diesel Engine: Biodiesel and Diesel Characterization and Mass Measurements using the Extended Idealized Aggregates Theory 12
Introduction 12
Effect of EGA Temperature Program 17
Results 18
Characterization of PM Emissions 18
Diesel Particle Morphology and Chemical Composition 26
Derivation of Mass Concentrations from On-Line Measurements
Correction for Aggregates: Theory 28
Validation of Aggregate Correction 30
SMPS Inlet Impactor 32
Health and Atmospheric Impacts 34
References 36

Chapter 3: The Catalytic Effects of Metal Salts and Sulfates on Diesel Aerosols 39
Introduction 39
Experimental 45
Results 50
Catalyst Characterization 56
Catalytic Effect on Carbon Evolution for Diesel Particles During EGA 58
High EC Diesel Particles 58
High OC Diesel Particles 83
Conclusions 95
References 98

Chapter 4: The Catalytic Effects of Metal Salts and Sulfates on Secondary Organic Aerosols and Biodiesel Aerosols 102
Introduction 102
Experimental 107
Results 112
SOA 112
SOA and Diesel Particles 117
Biodiesel Particles, Maximum Load 124
Biodiesel Particles, Idle Load 128
Conclusions 133
References 136

Chapter 5: Conclusions 131
Recommendations 143

LIST OF FIGURES

Chapter 2

Figure 1: SMPS size distributions for particles emitted while running on (a) California #2 low sulfur diesel fuel, and (b) B100 biodiesel 19
Figure 2: 100,000× magnification TEM images of diesel (a) and biodiesel (b) particles emitted during engine idle 21
Figure 3: EC/OC ratio for diesel and biodiesel particles 22
Figure 4: TEM images of diesel particles emitted at 60% load (a) and 100% load (b). 24
Figure 5: Typical biodiesel TEM image at 100,000 × magnification 26
Figure 6: Frequency distribution for all aggregates analyzed. 28
Figure 7: Aggregate size distributions based solely on IA theory and IA theory with the extension to the transition regime 31
Figure 8. Measured diesel aggregate mass with the scanning mobility particle sizer, after correction with the idealized aggregate extension, and filter-based mass derived from gravimetric and total carbon measurements with an EGA 32

Chapter 3

Figure 3-1: Carbon evolution profile for ambient, diesel, and a combination of ambient and diesel PM 53
Figure 3-2: Carbon evolution profile for ambient, diesel, and a combination of ambient and diesel PM 55
Figure 3-3: The effect of diesel PM mass loading on catalytic activity of ambient aerosol 56
Figure 3-4: TEM image of $CaCl_2$ catalysts sampled directly from the small Teflon chamber.... 57
Figure 3-5: Particle sizes of the aerosolized metal catalysts 58
Figure 3-6: Thermograms of carbon evolution of high EC/OC diesel particles with and without a $CaCl_2$ catalyst using the NIOSH (1999) and Conny et al. (2003) temperature programs 59
Figure 3-7: The effect of metal salts on the oxidation temperature of the low volatility carbon associated with diesel soot 61
Figure 3-8: Carbon evolution profiles of high EC diesel particles mixed with $FeCl_3$ using the NIOSH (1999) temperature protocol 66
Figure 3-9: The change in soot oxidation temperature due to the addition of a metal catalyst plotted against the reduction in EC/OC split time during EGA 72
Figure 3-10: Relationship between the percent change in the EC/OC ratio to the resulting change in split time when using a metal catalyst 73
Figure 3-11: Correlation between a metal compound's ability to affect the diesel EC/OC ratio and the oxidation temperature of soot 74
Figure 3-12: Relationship between mobility diameters of metal chlorides/sulfates measured by the SMPS to the change in oxidation temperature of diesel soot 75
Figure 3-13: The melting points of metal chlorides and sulfates plotted against the corresponding reduction in oxidation temperature. 76
Figure 3-14: Carbon evolution profile for diesel PM mixed with a combination of NaCl and $FeCl_2$ 81
Figure 3-15: Carbon evolution profile for diesel PM mixed with a combination of NaCl and $CuCl_2$ 82
Figure 3-16: EGA thermogram of the $CuCl_2$ and idle diesel particles 92

LIST OF FIGURES CONTD.

Figure 3-17: Correlations between the two measures of char to the M/C ratio deposited on the quartz filter 93
Figure 3-18: Correlation of the two measurements of char from EGA using the NIOSH (1999) and Conny et al. (2003) protocol for diesel particles emitted at idle load conditions sampled with a denuder 94
Figure 3-19: Correlation between the percentage of change in the EC/OC ratio and the M/C ratio of the sample 95

Chapter 4
Figure 4-1: SMPS distribution showing a bi-modal distribution for the mixture of diesel particles and SOA (top). TEM image of SOA and diesel particles (bottom) 110
Figure 4-2: EGA thermogram of SOA and a mixture of SOA and $CuCl_2$ 115
Figure 4-3: Correlation between the two measures of char for SOA 116
Figure 4-4: EGA thermogram of SOA and diesel particles (D) formed at maximum load with and without $CuCl_2$ analyzed by the NIOSH (1999) method 117
Figure 4-5: Correlation between the change in oxidation temperature of biodiesel and diesel particles in the presence of catalytic metals 127
Figure 4-6: EGA thermogram of biodiesel particles with and without NaCl 128
Figure 4-7: EGA thermograms of idle biodiesel particles (BD) alone and in the presence of $CuCl_2$ 132

LIST OF TABLES

Chapter 2

Table 1: Morphological description of aggregates emitted from the diesel generator operating on diesel or biodiesel fuel at various loads 26

Chapter 3

Table 3-1: Temperatures and durations of each step for the NIOSH (1999) and Conny et al. (2003) method 47

Table 3-2: Measured chemical composition of TSP in the ambient atmosphere. 51

Table 3-3a: Experiments conducted to determine the catalytic effect of metal salts and sulfates on the oxidation of high EC soot particles – NIOSH (1999) method 62

Table 3-3b: Experiments conducted to determine the catalytic effect of metal salts and sulfates on the oxidation of high EC soot particles – Conny et al. (2003) method 63

Table 3-4a: Resulting EC/OC measurements of high EC diesel particles with and without the presence of metal catalysts. Adjusted EC/OC split time – NIOSH (1999) method..... 68

Table 3-4b: Resulting EC/OC measurements of high EC diesel particles with and without the presence of metal catalysts. Adjusted EC/OC split time – Conny et al. (2003) method 69

Table 3-5a: Experiments conducted to determine the catalytic effect of a combination of metal salts on the oxidation of high EC soot particles. 78

Table 3-5b: Experiments conducted to determine the catalytic effect of a combination of metal salts on the oxidation of high EC soot particles. 79

Table 3-6: Experiments conducted to determine the catalytic effect of a combination of metal salts on the oxidation of high EC soot particles with adjusted split times..... 80

Table 3-7a: High OC diesel particles without sampling with a denuder. 85

Table 3-7b: High OC diesel particles without sampling with a denuder. $CaCl_2$. Manual adjustment of EC/OC split point. 86

Table 3-8a: Experiments conducted to determine the catalytic effect of metal salts and sulfates on the oxidation of high OC soot particles with use of a denuder – NIOSH (1999) method..... 88

Table 3-8b: Experiments conducted to determine the catalytic effect of metal salts and sulfates on the oxidation of high OC soot particles with use of a denuder – Conny et al. (2003) method 89

Table 3-9a: Experiments conducted to determine the catalytic effect of metal salts and sulfates on the oxidation of high OC soot particles with use of a denuder – NIOSH (1999) method. Adjusted EC/OC split point..... 90

Table 3-9b: Experiments conducted to determine the catalytic effect of metal salts and sulfates on the oxidation of high OC soot particles with use of a denuder – Conny et al. (2003) method. Adjusted EC/OC split point 91

Chapter 4

Table 4-1: Temperatures and durations of each step for the NIOSH (1999) and Conny et al. (2003) method used for TOT-EGA 111

Table 4-2: EC/OC ratios and measures of char for SOA 113

Table 4-3a: EC/OC ratios and measures of char for mixtures of SOA and high EC diesel particles with and without the presence of metals. NIOSH (1999) method. 120

Table 4-3b: EC/OC ratios and measures of char for mixtures of SOA and high EC diesel particles with and without the presence of metals. Conny et al. (2003) method. 121

Table 4-4a: EC/OC ratios and measures of char for mixtures of SOA and high EC diesel particles with and without the presence of metals. NIOSH (1999) method. Adjusted EC/OC split point 122

LIST OF TABLES CONTD.

Table 4-4b: EC/OC ratios and measures of char for mixtures of SOA and high EC diesel particles with and without the presence of metals. Conny et al. (2003) method. Adjusted EC/OC split point 123
Table 4-5: Effect of metal compounds on the EC/OC measurement of biodiesel particles emitted by a diesel generator operating at maximum load 125
Table 4-6: Effect of metal compounds on the EC/OC measurement of biodiesel particles emitted by a diesel generator operating at maximum load. Adjusted EC/OC split point 126
Table 4-7: Effect of metal compounds on the EC/OC measurement of biodiesel particles emitted by a diesel generator operating at maximum load 129
Table 4-8: Effect of metal compounds on the EC/OC measurement of biodiesel particles emitted by a diesel generator operating at idle load. Adjusted EC/OC split point 130

VITA

August 26, 1975	Born, Stamford, Connecticut
1997	B.S. Civil Engineering The University of Texas Austin, Texas
2002	M.S. Environmental Engineering The University of California Davis, California
2005	M.S. Chemical Engineering The University of California Los Angeles, California

PUBLICATIONS AND PRESENTATIONS

Chung, A., Paulson, S.E., Lall, A.A. (2008) Particulate Emissions by a Small Non-Road Diesel Engine: Characterization and Mass Measurements using the Extended Idealized Aggregates Theory, Atmospheric Environment 42(9): 2129-2140.

Barkey, B., Paulson, S.E., Chung, A. (2007) Genetic Algorithm Inversion of Dual Polarization Polar Nephelometer Data to Determine Aerosol Refractive Index. Aerosol Science and Technology, 41 (8), 751 – 760.

Chung, A. (February 2007). Measurements of diesel and secondary organic aerosol particles. Presented at the Symposium on Photochemical and Kinetic Processing. Los Angeles, CA.

Chung, A. (October 2006). The characterization of internal and external mixtures of carbonaceous aerosols in an outdoor teflon photochemical chamber. Presented at the Department of Energy (DOE) Science Team Meeting, Denver, CO.

Chung A. (February 2006). The calibration of a polar nephelometer to measure the refractive index of submicron particles. Presented at the American Chemical Society 40th Western Regional Meeting, Anaheim, CA.

Chung, A., Herner, J.D., Kleeman, M.J. (2001) Detection of Alkaline Ultrafine Atmospheric Particles at Bakersfield, CA. Environmental Science and Technology, 35 (11), 2184 – 2190.

Chung, A., Chang, D.P.Y., Kleeman, M.J., Perry, K.D., Cahill, T.A., Dutcher, D., McDougall, E.M., Stroud, K. (2001) Comparison of Real-Time Instruments Used to Monitor Airborne Particulate Matter. Journal of Air and Waste Management, 51, 109 – 120.

ABSTRACT OF THE DISSERTATION

Uncertainties in the Measurement of Simulated Carbonaceous Aerosols: (I) Characterization of Emissions from a Portable Diesel Generator and Development of the Extended Idealized Aggregate Theory and (II) the Effect of Metal Additives on the Evolved Gas Analysis of Carbon

by

Albert Chung

Doctor of Philosophy in Chemical Engineering

University of California, Los Angeles, 2009

Professor Suzanne E. Paulson, Co-Chair

Professor Panagiotis Christofides, Co-Chair

Several studies have characterized emissions from on-road diesel engines; however, non-road diesel engines, have received less attention. Although non-road diesel engines contribute a small fraction of the total number of diesel engines in operation, because they have minimal emissions control, they account for a disproportionate fraction of the PM emissions - in the US their contribution is estimated at 44% of the total diesel PM emissions. Emissions from a small 4.8 kW diesel generator running on ultra-low sulfur diesel and biodiesel fuels are characterized. Aerosol characteristics such as

particle size distribution, carbon content, and morphology were similar to that published for larger on-road diesel sources. The use of biofuel (B100) is important due to its increasing role as an alternative energy source. Results showed that the biodiesel particles were compact, irregular, and lack the clearly defined primary particles of diesel aggregates. At high loads they had similar elemental (EC) and organic (OC) ratios as diesel particles; however at lower loads this ratio was much smaller.

Mass measurements of aerosols are often conducted using gravimetric methods which offer poor time resolution. The idealized aggregate (IA) theory developed by Lall and Friedlander, 2006 was extended to the transition regime for diesel aggregates to determine aerosol mass from real-time measurements. Results showed that the calculated mass concentrations from the extended IA theory were in good agreement with the mass concentrations from gravimetric and total carbon measurements.

There has been limited amount of work understanding the effect of metals on the thermal stability of carbon during its measurement in evolved gas analysis (EGA) thus biasing the measurement of the EC/OC ratio. Metal chlorides and sulfates were externally mixed with a variety of primary and secondary carbonaceous aerosols. Measurements showed that metals in the presence of a carbonaceous aerosol decreased its oxidation temperature and enhanced OC charring. Not only do different metals have different effects on the thermal stability of carbon, but different types of carbonaceous aerosols reacted differently with the same metal during EGA. An attempt was made to correlate these findings to changes to the EC/OC ratio measurement and a discussion on recommendations is given.

Chapter 1: Introduction

Carbonaceous particulate matter (PM) continues to be the subject of intense study due to its role in global climate change, both on a local and global scale (e.g., Ramanathan and Carmichael 2008). A unique characteristic of atmospheric carbonaceous PM is its ability to both warm and cool the earth's atmosphere, although uncertainties remain (Kanakidou et al. 2005; Bond 2007; Keil 2007). The organic carbon (OC) fraction, such as secondary organic aerosols (SOA), scatters incoming sunlight and is considered to result in negative radiative forcing (Penner et al., 1998; Myhre et al., 2008). "Elemental" carbon (EC), or "black" carbon (BC) strongly absorbs both visible and infrared radiation thus increasing the deposition of energy to the atmosphere while obscuring visibility and reducing the amount of light that reaches the Earth's surface. Climate forcing of EC is thought to exceed that of methane gas and is second only to CO_2 (Jacobson 2001; Ramanathan and Carmichael 2008). In the ambient atmosphere; however, cooling and heating aerosols are always mixed and in consequence, complicates the estimation of an overall aerosol radiative forcing (Fuller et al, 1999; Jacobson 2001). In addition to direct effects of aerosols on climate, indirect effects such as increased cloudiness due to elevated cloud condensation nuclei numbers (Choularton et al., 2008) and the increased probability and severity of rainfall (Bell et al., 2008) expand the impacts of carbonaceous aerosols.

Climate impacts of direct emissions of aerosols are not a local phenomenon. Koch et al. (2007) determined that 65 to 90% of direct emissions are transported beyond the area of production. Bond (2007) showed that the radiative forcing of direct emissions

can affect an area 40 times greater than the initial 'hot spot'. Simulations by Levy et al. (2008) showed that warming potential of black carbon particles can be responsible for up to 40% of the total increase of surface temperature by the year 2100. This conclusion was also found by Kirkevag (2008) which stated that within the next 100 years the sign of the aerosol radiative forcing will go from negative to positive due to the contribution of black carbon (BC). The aerosol radiative forcing has been shown to be sensitive to the OC and EC emission factors used. Wang et al. (2007) showed that the radiative forcing for biomass aerosols ranges from -3.1 to 1.6 W m^{-2} depending on the ratio of OC to EC used for model inputs.

In addition to climate effects, epidemiological studies have shown a strong relationship between PM and health outcomes, including increased mortality (Schlesinger et al., 2006). Ultrafine particles, of which diesel aggregates make up a large share in urban air, appear to be toxic due to their ability to penetrate into the cardiovascular system and other organs (Xia et al. 2007). Although possibly producing less PM, biodiesel emissions have been shown to have elevated levels of NO_x (Swanson et al., 2007) and cause increased cytotoxic effects in biological assays by a factor of four compared to conventional diesel fuel (Bunger et al., 2000).

Primary emissions of carbonaceous aerosols originate from the incomplete combustion of fossil fuels in transportation, energy generation, and various industrial applications. Diesel engine emissions generate fractal-like agglomerates of solid carbon nano-particles, typically coated with organics (Surakai et al. 2003). The aggregates have mobility diameters in the ultrafine range (< 0.15 μm) however can span several hundred

nanometers in length (Chung et al., 2008). From an optical standpoint, emissions from diesel engines can either be light scattering due to the presence of organic droplets or light absorbing from the high EC aggregates. Once in the atmosphere, combustion particles can also be mixed with the pre-existing ambient aerosols such as SOA and various inorganic ions and metals.

A large fraction of particulate OC is attributed to SOA which is formed in the atmosphere from the oxidation of volatile organic compounds (VOCs). It has been estimated that 10 to 40% of the global organic aerosol mass is attributed to SOA with about 90% of that being biogenic in nature (Volkamer et al, 2006); however large uncertainties remain in the estimate of the yearly SOA production (Bonn and Lawrence, 2005). SOA can have significant impacts on visibility and climate however their impact relative to other aerosols is highly uncertain (Kanakidou et al., 2005). Model simulations have suggested that the global SOA burden will increase by 36% by 2100 with biogenic aerosols resulting in 26% of that increase (Heald et al., 2008). Estimates were achieved by updating the Community Atmosphere Model (CAM3) with recent laboratory results for SOA yield from various organic pre-cursors. Biogenic emissions were simulated using the Model of Emissions of Gases and Aerosols (MEGAN2) within the Community Land Model (CLM3).

Biodiesel, an (at least partly) "carbon neutral" drop-in replacement for regular diesel fuel is currently gaining attention and market share as a source for alternative energy. Both the American Jobs Creation Act of 2004, which provided distributors of biodiesel fuel federal tax credits, and the Energy Policy Act of 2005, in effect will

significantly increase the demand for biodiesel fuel. The American Jobs Creation Act alone contributed to a 300% increase in the U.S. biodiesel production from just 2004 to 2005 (Swanson et al., 2007). The Law and Economics Consulting Group (LECG) LLC (Emeryville, CA), an international expert services company, has predicted that the demand for biodiesel fuel will increase from 75 million gallons in 2005 to over 600 million gallons by the year 2015. Due to its potential growth, the emissions of biodiesel combustion are important to quantify both from a chemical composition and climate standpoint. Extensive literature is available examining innovative ways to produce biodiesel (Ranganathan et al. 2008; Du et al. 2008; Jin et al., 2008); however the research into biodiesel particulate emissions is limited. Unlike diesel fuel which has its chemical composition regulated, biodiesel fuels can be made by a number of methods and sources. This inconsistency in biodiesel production introduces the possibility of data on biodiesel particulate matter being specific to the source fuel. The biodiesel fuel that is commercially available in Los Angeles is formulated from used vegetable oil (www.conservfuel.com) and is used in this study. The few studies that have been published on biodiesel fuel emissions have shown that combustion of biodiesel produces lower particle mass emissions and smaller particles than conventional diesel fuel (Lapuerta et al., 2008; Chung et al., 2008).

Carbonaceous PM ranks as some of the most difficult aerosols to measure, such that basic atmospheric measurements of these materials carry variability of at least 30-50% (Heubert and Charlson, 2000). Taken together, EC and OC are often referred to as total carbon (TC). Categorically speaking, some materials fall between OC and EC; for

example, bound polyaromatic hydrocarbons (PAHs) on the surface of soot particles are not extractable by the same methods that other organics are, and have a higher C/H ratio than most organics. The most common method of quantifying elemental and organic material in the atmosphere is the offline, or more recently semi-continuous, technique of using evolved gas analyzers (EGA), which provides EC and OC mass based on their respective thermal stabilities. The EGA works by evolving material through heating a quartz filter punch and oxidizing it to CO_2 and then reducing it to methane and quantifying it with a flame ionization detector (FID). The step-wise heating process initially takes place in an inert (He) environment. During this phase, the evolved material is typically classified as OC. The oven then cools and then resumes the step-wise heating in an oxidizing (He/O_2) atmosphere. Ideally, the material evolved in the oxidizing phase can be classified as EC.

Several studies have characterized PM emissions from on-road diesel engines; however, non-road diesel engines, have received much less attention. Although non-road diesel engines contribute a small fraction of the total number of diesel engines in operation, because they typically have minimal emissions control, they account for a disproportionate fraction of the PM and NO_x emissions. In the US, the contribution is estimated at 44% of the diesel PM and 12% of the NO_x mobile source emissions. The smallest class of diesel generator (< 19 kW) made up 18% of the U.S. non-road market in 2000 (EPA, 2004).

The emissions of a small 4-stroke, air cooled direct injection 4.8 kW diesel generator (L70V6, Yanmar Corporation) within its first 100 hours of operation will be

characterized. Both conventional low-sulfur diesel fuel and vegetable oil derived biodiesel fuel will be used, and the applied load will be varied. Offline measurements such as EGA and online measurements such as the scanning mobility particle sizer (SMPS), which provides high resolution continuous measurements of size distributions, based on particle electrical mobility diameter were used to characterize diesel and biodiesel emissions. In the measurements of EC and OC, two approaches have been applied to avoid OC sampling artifacts, one of the major sources of uncertainty in EC/OC measurements.

A method to determine online mass concentrations from SMPS measurements will also be presented. The software accompanying the SMPS allows the calculation of mass concentrations from measured particle distributions assuming particles of constant density and spherical structure. For aggregates however, mass concentrations based on spherical particle calibrations can be overestimated up to a factor of ten. To address this issue, Lall and Friedlander (2006) developed a new method for interpreting SMPS data for aggregates. The method applies to idealized aggregates (IA) composed of uniform primary particles in the free molecule size range, and assumes that each primary particle is equally exposed to the surrounding gas. This is a reasonable approximation for aggregates with low fractal dimension ($D_f < 2$). The IA method relates the number and the radius of primary particles that compose the aggregates to the mobility diameter. The relation is obtained by equating aggregate migration velocity to that of spheres with the same mobility diameter. In this way the ultrafine aggregate number, surface area and volume distributions can be calculated from SMPS measurements corrected for aggregate

drag and charging efficiency. The aggregate mass distribution can be then calculated, if the primary particle density is known.

The IA theory makes use of free molecular drag on aggregates to calculate the migration velocities in the electric field. When the primary particles are comparable to the mean free path (transition regime), the drag on aggregates is calculated using the adjusted sphere method by interpolating between continuum and free molecular regime (Dahneke, 1982). Good agreement was found for this extended IA (EIA) method and TEM-derived aggregate volumes from Park et al. (2004) for diesel aggregates composed of primary particles with a diameter of 31.9 nm (Lall and Friedlander, 2006).

The transition regime extension is here verified for the first time against mass measurements by comparing SMPS size distributions corrected using the EIA theory with filter-based gravimetric and EGA of total carbon (TC). For both diesel and biodiesel particles, TEM analyses were performed to extensively characterize engine emissions, including (for diesel PM) the primary particle size, which is a necessary input for the SMPS correction for aggregates, as well as fractal dimension and several other morphological characteristics, as a function of engine load. The loss of aggregates in the inlet impactor shipped with the SMPS by the manufacturer is also characterized, in addition to elemental and organic carbon content of the particles for both diesel and biodiesel particles as a function of engine load.

The second portion of this work examines the effect of non-carbonaceous components, such as metals, on the measurement of carbon aerosols using EGA. Metals comprise a significant fraction of the ambient aerosol mass. Coarse (2.5 um < d_p < 10

um) and accumulation mode (0.1 um < d_p < 2.5 um) particles comprise the majority of the aerosol mass concentration (over 85%) in the Los Angeles area (Sardar et al., 2005). Coarse mode particles typically have high concentrations of metals (over 50% by mass) including aluminum, silicon, calcium, and iron and relatively low carbon mass concentrations. The accumulation mode frequently contains lower concentrations of metals and a higher fraction of carbon. For ultrafine particles, carbon often dominates the aerosol mass (Hughes et al., 1998; Sardar et al., 2005); however, Chung et al. (2001) found that metals exceed 50% of the ultrafine particle mass for aerosols collected in Bakersfield, CA with calcium being the predominant metal. Whether externally or internally mixed with carbonaceous aerosols, it is possible that metals affect the thermal stability of carbon during EGA.

The Lawrence Berkeley Laboratory method (Novakov and Corrigan 1995, Kirchstetter et al. 2001), which utilizes a steady temperature ramp in an oxidizing environment, shows that source-dominated samples from a vehicle tunnel contained "black" carbon that evolved from a filter at much higher temperatures than that for ambient samples. Further, by externally mixing aerosols on filters, Turner and Hering (1994) showed that the evolution temperature for the black carbon from the tunnel is lowered if ambient aerosol sample is added to the tunnel sample, and attributed the different oxidation profiles of the soot to the non-carbonaceous constituents of the ambient aerosol. In addition to the non-carbonaceous component of ambient aerosols, the metals associated with diesel PM itself may affect its oxidation in the EGA. Studies have

shown that diesel PM can include high levels of Fe, Ca, Mn and Zn, while coal PM has associated Fe, Ti, Al, Mn, V, and Ni (Finlayson-Pitts and Pitts 2000, Wang et al. 2003).

Neeft et al. (1996) determined that the degree of contact between soot particles and catalyst is a key parameter in soot oxidation using a model soot (Printex-U, Degussa Inc.). They showed that catalysts with "tight" contact with soot particles are more effective in oxidation than when there is "loose" contact. "Tight" contact was produced by mechanically milling the catalyst and Printex-U into a mixture, whereas "loose" contact consisted of hand mixing the aerosols with a spatula. Mul et al. (1998) found that $PbCl_2$, $CuCl_2$, and CuCl are very active in the oxidation of Printex-U whereas $HgCl_2$, $BaCl_2$, and $CaCl_2$ had little effect. They suggested that the activity of these metal chlorides is induced by in-situ formation of contact with the soot by gas phase transport during oxidation. Silva et al. (1997) showed that nickel, cobalt, and molybdenum as well as their mixtures have the ability to catalyze charcoal. Although not a metal, Yu et al. (2002) showed that ammonium bisulfate altered the thermal evolution of several OC standards such as levoglucosan, starch, and cellulose, when using a EGA-TOT running off the UST-2 thermal method.

The catalytic effect of metals on the thermal stability of carbon during EGA can possibly contribute to a source of uncertainty in using EGA, which is determining the exact location of the OC/EC split. During the inert phase, OC may pyrolize and produce char, resulting in the darkening of the filter spot. Charred OC requires the addition of O_2 to remove it from the filter – similar to EC. The instrument accounts for charred OC that would otherwise be classified as EC by the laser transmittance or reflectance through the

sample, otherwise known as thermo-optical transmittance (TOT) or thermo-optical reflectance (TOR). The EC/OC split is located at the point where the transmittance or reflectance level returns to its initial level after a reduction of laser response due to charring. By affecting the thermal stability of carbon during EGA, it is possible that the metals will cause the oxidation of carbon at lower temperatures, or enhance the production of char, and in effect bias the resulting EC/OC ratio. For EGA, the standard temperature protocol for a TOT instrument is specified by the National Institute of Occupational Safely and Health (NIOSH) (NIOSH, 1999). The method developed by Conny et al. (2003) which performed an extensive factorial study to optimize the temperature program of EGA-TOTs, will also be used. Their method attempts to minimize the charring of OC and to eliminate the possibility of native EC evolving during the helium phase and being miscounted as OC.

Understanding how metals can affect the thermal stability of carbon during EGA is necessary in determining any effect these inorganic species may have on the measurement of OC and EC. For this study, diesel particulates with varying compositions of EC and OC will be studied. Lab generated SOA will also be analyzed, along with mixtures of SOA with high EC diesel particles, and biodiesel particles. Catalytic metals chosen for study were determined by their measured presence in the local ambient aerosol as well as reports from the literature (Sardar et al., 2005; Zhao and Gao, 2008; Yin and Harrison, 2008). Solutions of individual catalytic alkali, alkaline, and transition metal chlorides and sulfates were aerosolized and used to pre-treat baked quartz fiber filters before exposing the filters to the diesel engine exhaust. The effect of

metal chlorides and sulfates on the behavior of both EC and OC during EGA is determined and then related to any changes in the EC/OC ratios due to the catalytic additives. The synergistic catalytic affect of metal mixtures on diesel particles high in EC is also discussed.

In summary the objectives of this work are the following

1. Characterize the emissions of a small non-road diesel generator operating on diesel fuel and compare to published data for larger on-road diesel engines.
2. Add to the limited amount of data regarding the particle characteristics resulting from the combustion of biodiesel fuel.
3. Extend the idealized aggregate (IA) theory developed by Lall and Friedlander (2006) to determine the mass concentrations of diesel particles from real-time measurements, possibly presenting an advantage over gravimetric measurement methods which offer poor time resolution.
4. Study the effect of metals, which are typically in the ambient atmosphere, on the thermal stability of carbonaceous particles during their measurement for carbon content and to correlate the effects to any resulting biases to the measured EC/OC ratio.
5. Determine if the type of carbon within a particle plays an important role in its interactions with metals during EGA.

Chapter 2: Particulate Emissions by a Small Non-Road Diesel Engine: Biodiesel and Diesel Characterization and Mass Measurements using the Extended Idealized Aggregates Theory

Introduction

Diesel particles were produced from a 4-stroke, air cooled direct injection 4.8 kW diesel generator (L70V6, Yanmar Corporation) within its first 100 hours of operation. The generator supplied power to four electrical appliances which each pulled 1.42 kW, equivalent to about a 30% load per appliance. For 100% load, one of the four appliances was operated at partial capacity. The generator was operated either on commercially available California #2 ultra low sulfur fuel (less than 15 ppmw sulfur) or 100% biodiesel fuel (B100), and was warmed up for 10 minutes at idle and then another 10 minutes at the load investigated. For most of the measurements presented here, samples were collected 80 cm away from the generator's exhaust outlet. In several cases however the particles were diluted into a chamber (below). In the first case, particles are unperturbed by a dilution tunnel or other extensive sampling device, so they are representative of fresh real world emissions. In the latter case, particles passed through a 1.8 m × 3.3 cm ID stainless steel tube, in which there is some agglomeration.

The outdoor chamber had a volume of approximately 34 m^3 and had dimensions of 4.5 × 7.5 × 1 m in a pillow geometry. The chamber was constructed by sealing 2 mil FEP Teflon sheets using an impulse heat sealer (PI-G35, Packaging Aids) and reinforcing the seals with greenback tape (3M). A padded steel frame (0.75 m high) with an open

mesh ((0.1 m)^2 × 0.5 mm strand thickness) nylon netting (U.S. Netting) was used as the support for the chamber and to secure it during high winds. Air was supplied to the chamber by two 33 gallon air compressors after passing through a series of packed bed scrubbers filled with Purafil Triple Blend (Purafil Inc.), activated charcoal, and a HEPA capsule filter (Gelman). The scrubbed air had < 50 particles cm^{-3} and NO_x and O_3 levels in the ppt range. The chamber was emptied and flushed with clean air in full sun for 10 hours in preparation for additional experiments. Access to the inside of the chamber was provided by custom Teflon sampling ports. Sampling lines for filter measurements were conductive ¼" OD × 30 cm copper tubing that was extended 15 cm into the chamber; the SMPS sampling line was 1.5 m. Although the chamber was always allowed time to equilibrate, sampling lines were inserted into the same port to avoid complications from possible sample inhomogeneity.

Particles were characterized as follows. Continuous, on-line measurements of particle distributions (7 – 1000 nm) were made with an SMPS (differential mobility analyzer (DMA) 3081, condensation particle counter (CPC) 3010, TSI). EC/OC analyses were performed on aerosols collected on pre-baked (24 hours @ 550° C) 25 mm quartz fiber filters (Pall Life Sciences). A backup filter was sandwiched behind the front filter, and samples were collected for 20 min. at 25 LPM.

Gravimetric measurements were made by collecting aerosols on 47 mm Teflon membrane filters (Pallflex) in stainless steel housings at 40 LPM for 10-20 minutes. Teflon filters were pre-weighed in a temperature and humidity controlled room using a microbalance (± 1 μg, Sartorius). Charges were removed from the filters by passing them

over a polonium strip. Prior to reweighing, the filters were allowed to re-equilibrate for 24 hrs in the weighing room.

Particles deposited onto a 400 mesh copper grid with formvar carbon support film (Electron Microscopy Sciences) were analyzed for morphology. The TEM grids were attached with adhesive tape to the center of 25mm filter screen and placed inside a filter holder. Particles were sampled at a flow rate of 20 LPM for 10 to 30 min. The TEM grids were studied using a JEOL 100CX TEM at magnification of 20 to 100,000 ×, and the film was developed and scanned into tagged image format using a Microtek Scanmaker E6 (Redondo Beach, CA).

Fractal dimension (D_f) and the number of primary particles (N_p) were analyzed by a method developed by Xiong and Friedlander (2001). Using Corel Draw (Eastman Kodak Company, version 10.0), each primary particle in an aggregate was manually outlined. A Corel script was used to determine the number, size, and position of each circle. D_f is then calculated from:

$$N_p = A\left(\frac{R_g}{a}\right)^{Df} \qquad (1)$$

where N_p is the number of primary particles, A is the pre-factor, R_g is the radius of gyration, which equals $\left[\ \frac{1}{M}\left(\sum m_i r_i^2\right)\ \right]^{1/2}$, m_i is the mass of the i^{th} particle, $M = \sum m_i$, r_i is the distance of the i^{th} particle from the aggregate center of mass, and a = average primary particle radius.

The overlapping of primary particles will introduce error to the 2-D analysis of 3-D particles, although for chain-like, low fractal aggregates, the results were reasonable.

The side-by-side overlapping (necking) was taken care of by carefully fitting each circle to the maximum dimensions of the adjacent primary particles. The dark and light regions of the aggregates were used to identify the more significant problem of overlapping on top of each other.

Organic Carbon Sampling Artifacts

To address the issue of OC sampling artifacts, samples were collected in several configurations of denuders and filters, as follows. For the results shown in Fig. 3, a parallel carbon filter plate denuder (Sunset Laboratory) was used upstream of the filter holder to remove any vapor phase organics which may condense on the front filter and to a lesser degree on the backup filter. SMPS measurements showed that particle losses in the denuder were about 14% by number, however almost all of the particles lost were smaller than 20 nm. Particle losses for the 20-1000 nm were less than 2%, so that the denuder has a minimal effect on mass concentrations measurements. The denuder reduced the OC mass observed on the filters by an average of 46% removing the least for idle conditions and the most for maximum load. With the denuder in place, any OC measured on the backup filter was assumed to be OC originally present on the particles trapped on the front filter that volatilized and re-condensed onto the backup filter (Mader et al., 2003). This OC was added to the front filter measurement, resulting in a corrected OC concentration. Backup filter OC averaged 27% (range: 9 - 57%) of the front filter OC for all loads and fuels tested. There was no observed relationship between load and amount of OC on the backup filter for either diesel and biodiesel particles.

An additional estimate of the OC positive and negative artifacts for diesel particles was derived as follows. Three parallel filter holders sampled the exhaust of the diesel generator operating with diesel fuel at 100% load without denuders. One sampling line had 2 quartz filters ('quartz behind quartz' or QBQ). In this configuration, vapor phase organics likely deposited on the front filter, and the back filter traps some additional vapor phase OC together with some OC volatilized from particles trapped on the front filter (e.g., Mader *et al.*, 2003). The second had a Teflon followed by a quartz filter (QBT). The OC collected on this backup quartz filter (QBT) was likely to be gas phase organics that would otherwise be collected on a front quartz filter. A third sampling unit had a diesel particle-laden Teflon filter upstream of a quartz filter (QBDT). Diesel particles were deposited onto the Teflon filter prior to the experiment. The OC on this backup quartz filter should be a combination of gas phase organics passing through the Teflon filter plus any organics from the particles deposited on the front filter that may have volatilized and re-condensed on the backup filter. Comparison of OC measurements between the QBT and the front Q filter showed that gas phase organics contribute to about half of the total OC. This was in close agreement with the denuder result above. Comparing the OC concentrations on the QBT and QBDT filter, indicated that about 30% of the OC present on backup filters results from the volatilization of particle phase OC on the front filter and its re-condensation on the backup filter. This estimate of volatilzed OC was also in very good agreement with the amount of OC on the backup filter when a denuder is used (~27%).

Effect of EGA Temperature Program

A thermal optical transmission evolved gas analyzer (Sunset Laboratories) was used to measure OC and EC from the quartz filters. In this measurement, OC was evolved first by heating the filter punch in the absence of O_2, to avoid oxidation of EC in the sample. The filter punch was then allowed to cool and oxygen was added to the gas stream, followed by a second heating program. During the O_2-free heating step however, some of the organic material inevitably charred (e.g., Conny et al., 2003), darkening the filter spot. Charring was monitored by the decrease of transmittance of laser light through the filter punch. As char was removed from the filter in the second heating stage, the laser transmittance gradually increases. The point at which the transmittance equals its initial value determined the EC/OC split point. Precise EGA temperature programs can have a substantial effect on the OC charring of OC and as a result the partition between EC and OC. To provide some insight into the magnitude of the error introduced by the temperature programs, all samples were analyzed on the widely used NIOSH 5040 protocol (NIOSH, 1999), and the recent protocol developed by Conny et al. (2003) to minimize charring. For the emissions as a function of load, the resulting EC/OC ratios differed from one another by 7 to 32%, although the average of the two methods were in good agreement with one another (within 3%). Total carbon values derived with the two methods were more closely correlated, however the Conny et al. (2003) method averaged about 8% lower than the NIOSH method.

RESULTS

1. Characterization of PM Emissions

Number distributions, TEM images and EC/OC for diesel and biodiesel particles at various loads are shown in Figs. 1-5.

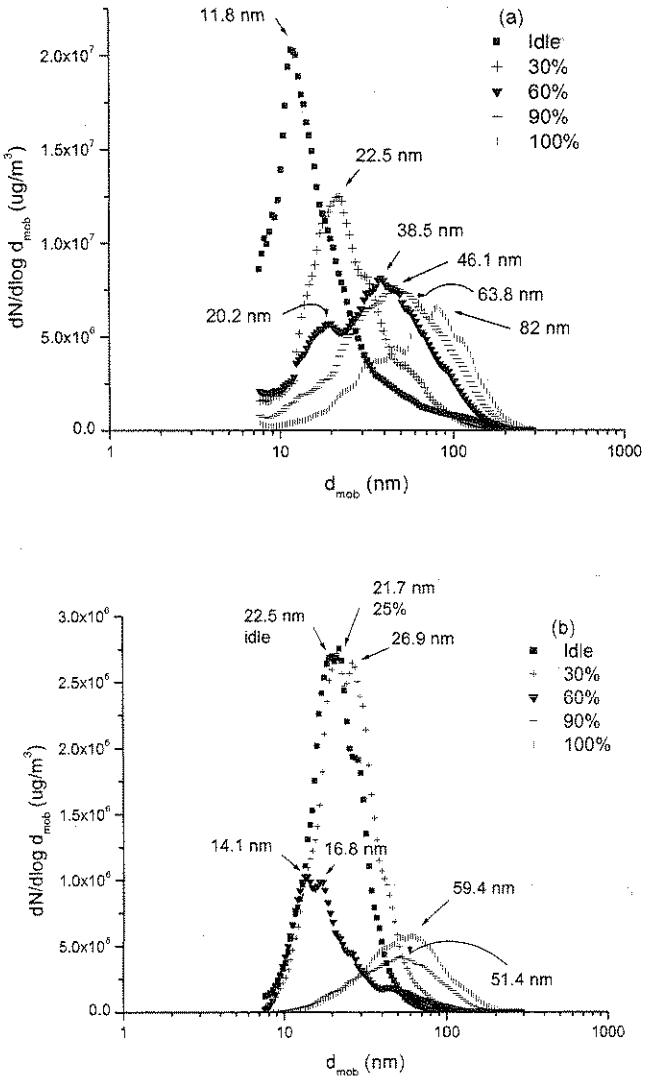

Figure 1. SMPS size distributions for particles emitted while running on (a) California #2 low sulfur diesel fuel, and (b) B100 biodiesel.

During idle operation, diesel particles (Fig. 1a) had a large single peak with a maximum at 12 nm and a tail extending past 100 nm. TEM images of this aerosol show halos from many small liquid drops together with a small number of aggregates (Fig. 2a), which were generally larger than the halos and likely correspond to the much higher mobility diameters. Over the entire grid, about 97% of the particles were spherical, with the remaining 3% being black carbon aggregates, however this ratio may be skewed somewhat by the sampling configuration. The low EC/OC ratio, 0.5 (Fig. 3), for particles emitted during idle operation was broadly consistent with the notion that the spherical particles were primarily organic in composition; the comparatively large EC/OC ratio relative to the number ratio of droplets to EC-dominated aggregates may result from the much larger volume of the latter. Liquid droplets were common in diesel emissions at idle and low load. Earlier studies have shown that these particles are OC and sulfate (e.g., Liu et al., 2005). Our particles likely contained much less sulfate as our fuel is 15 ppmw sulfur, in contrast to 0.05 – 0.3 % in earlier fuels.

Biodiesel particles emitted during idle operation also had a single large peak in the nuclei mode (Fig. 1b), but it was nearly double that for diesel particles, at 22 nm. This result was similar to those made by Bunger et al. (2000), who found that larger non-road diesel engines (52 kW) operating on biodiesel emitted smaller numbers of larger particles when compared to diesel fuel. Biodiesel particles were primarily irregular compact solid particles (Fig. 2b) in sharp contrast to the liquid droplets observed from diesel. The EC/OC ratio of the biodiesel particles, 0.09, was much smaller than that of regular diesel particles at idle (Fig. 3).

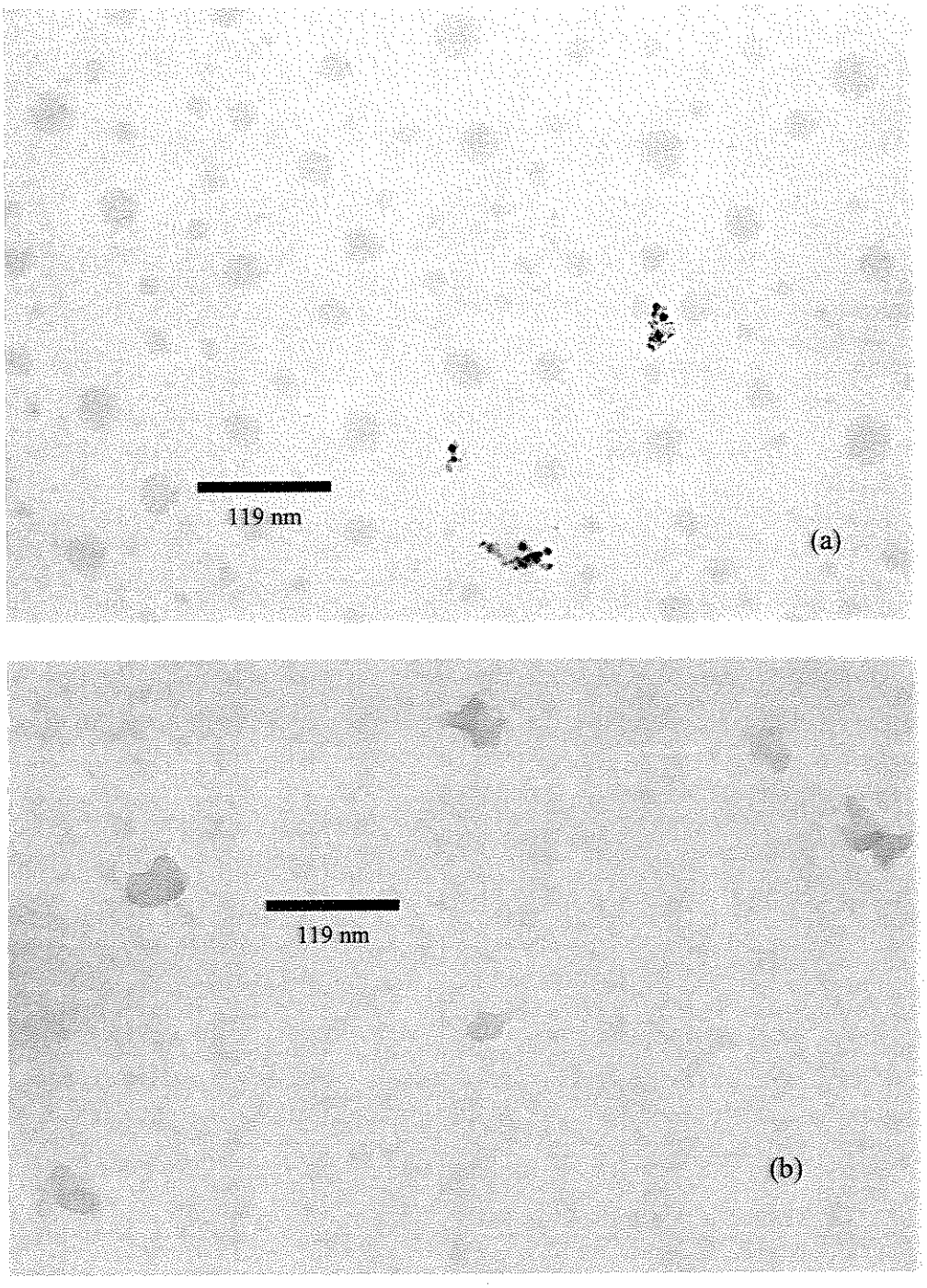

Figure 2: 100,000× magnification TEM images of diesel (a) and biodiesel (b) particles emitted during engine idle.

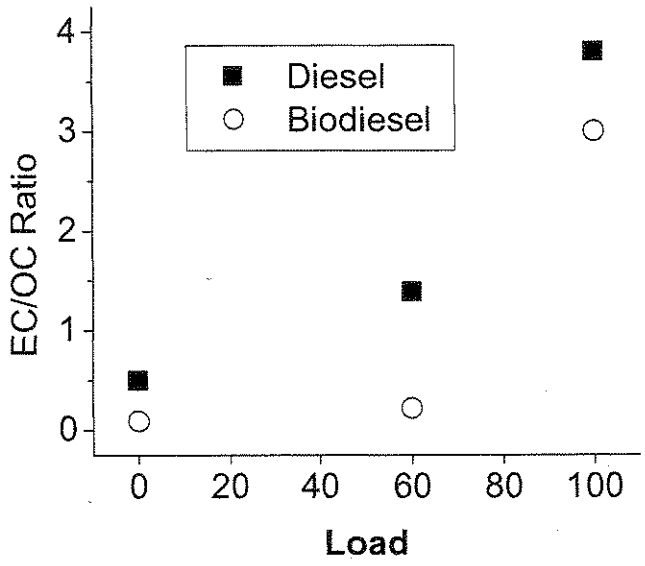

Figure 3: EC/OC ratio for diesel and biodiesel particles. Results from the Conny et al. (2003) and NIOSH 5040 protocols were averaged.

The mobility diameter of diesel particles increased with applied load. For particles emitted at low loads, there was a large peak in the nuclei mode (dp < 30 nm) with a shoulder forming in the aggregate accumulation mode (dp > 30 nm). As load was increased, the peak in the nuclei mode was much less prominent, and the shoulder becomes more dominant. At maximum load, the nuclei mode peak disappeared and a dominant peak at 82 nm with a shoulder at 47 nm was observed. TEM images and the bimodal SMPS size distributions showed that once a load was applied to the generator, the spherical droplets disappear, and a combination of aggregates and small compact solid particles were emitted (Figs. 1a and 4a). This transfer of number to the accumulation mode as load was increased has been observed in previous studies

involving on-road diesel engines (Sakurai et al., 2003). As the load was increased, image analysis showed that a higher fraction of the emitted particles were chain aggregates (Figure 4b) and the EC/OC ratio increases at the same time (Fig. 3), to 1.4 at 60% load and then to 3.8 at max load.

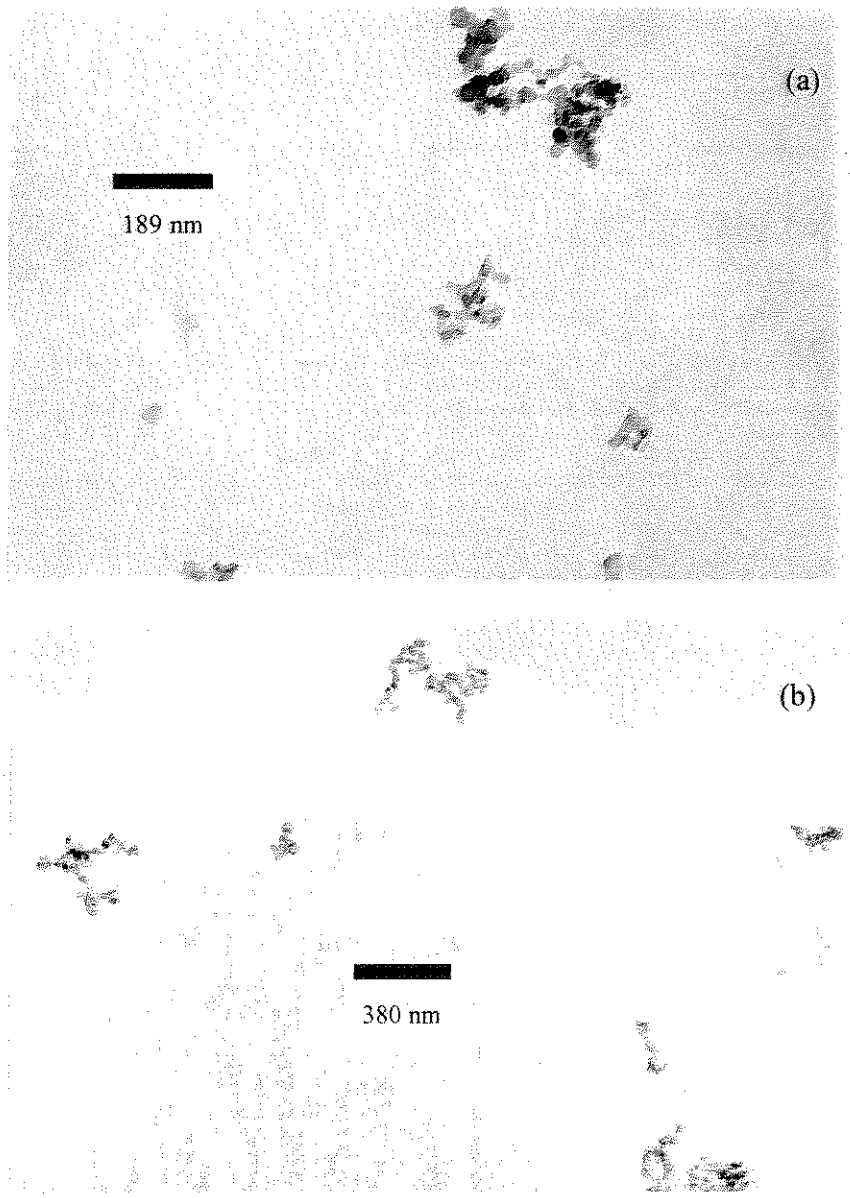

Figure 4: TEM images of diesel particles emitted at 60% load (a) and 100% load (b). At lower loads, the aerosol was a combination of aggregates and compact irregular shaped particles. At maximum load, the aerosol consisted of only aggregates.

This was in contrast to the results of Shah et al. (2004) who tested three 300-350 kW back-up generators and observed that EC/OC maxima were at 50% load, and smaller EC/OC ranges than observed here, 0.5-1.0, 1.5-2.5, and 2.5-4.5 depending on generator and load respectively. In contrast, Liu et al. (2005) monitored an 80 kW diesel generator and found a similarly increasing EC/OC – load trends as ours, although the maximum EC/OC ratios were above 5 at higher loads.

The mobility diameter of the biodiesel particles was nearly unchanged as the load was increased from idle to 30%, and curiously, it decreases at 60% load (Fig. 1b). Variability in emissions from diesel engines operating on alternative fuels as a function of applied load had been observed in other studies; smoke opacity for biodiesel blended fuels did not show a distinct relationship with engine load, (Labeckas and Slavinskas 2005). We speculate that the instability in the combustion of biodiesel blended fuels by the diesel generator resulted in the inconsistent particle size emissions as a function of load. As the load was increased further, the distribution shifts toward a single mode at higher mobility diameters, peaking at 51 and 60 nm for loads of 90 and 100%, respectively, smaller than diesel particles. This was in good agreement with the results of Jung et al. (2006) who observed a peak mobility diameter of 62 nm for a 93 kW, 4 cylinder direct injection non-road diesel engine operating at 75% load. The EC/OC ratio of biodiesel particles also increased with applied load, reaching 3.0 at max load, similar to diesel particles. TEM images showed that the particles were still much more compact than diesel particles (Fig. 5), and although the primary particles became darker and more defined, primary particles were still difficult to discern individually.

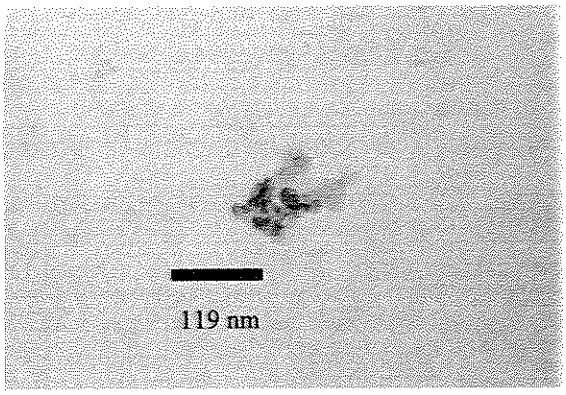

Figure 5: Typical biodiesel TEM image at 100,000 × magnification.

Diesel Particle Morphology and Chemical Composition

Table 1 summarizes the means, ranges, and standard deviations for particle D_f, N_p, and d_p, for diesel particles emitted by the generator at several loads.

			Fractal Dimension, Df			Primary Particle Size (nm), dp			Primary Particle #, Np		
Description	Load	N[a]	Avg.	Range	Sx	Avg.	N[b]	St. Dev	Avg.	Range	Sx
Diesel	100%	10	1.67	1.44-1.9	0.13	29.2	1097	3	110	43-149	29
Diesel	90%	7	1.75	1.42-1.96	0.14	30.5	413	4.9	59	24-84	17
Diesel	60%	8	1.56	1.44-1.77	0.06	31.7	242	4.4	30	21-38	5
Diesel	30%	5	1.5	1.27-1.71	0.16	35	137	4.9	27	14-35	6

[a]The number of particles characterized
[b]The number of primary particles characterized

Table 1: Morphological description of aggregates emitted from the diesel generator operating on diesel or biodiesel fuel at various loads. For diesel particles emitted during idle, and all biodiesel particles, D_f, d_p, and N_p are unavailable due to the lack of distinct primary particles.

A total of 1,899 primary particles (46 aggregates) were analyzed, and had mean and median diameters of 31 ± 9 and 29 nm, respectively. The range of primary particle sizes observed was quite broad, at 9 to 62 nm, with a log-normal distribution (Figure 6). The few aggregates observed at idle did not have sufficiently distinct primary particles for image analysis. The fractal dimension (D_f) averaged 1.63 (range of 1.5 to 1.75 for the different loads), and for individual particles 1.27 to 1.96; the largest D_f was at 90% load, however the differences were not statistically significant. The aggregates' fractal dimensions and primary particle diameters fall well within the ranges of values observed for all other types of diesel engines. Literature reports of mean d_p fell in a fairly narrow range, from 19 to 35 nm, with the most common values between 25-32 nm (Sakurai et al., 2003; Wentzel et al., 2003; Park et al., 2004; Zhu et al., 2005; Mathis et al., 2005, Neer and Koylu, 2006); however for individual engines the standard deviation of d_p was typically somewhat smaller (< 25%, Park et al., 2004) than that observed here. D_p had been observed to increase somewhat with engine load, although the results were scattered (Neer and Koylu, 2006); in our investigation this parameter actually decreased from 35 to 29. In good agreement with our results, measured literature values of the average D_f also fell in a tight range, from 1.5 to 1.9, with 1.7 as by far the most common value (Wentzel et al., 2003; Park et al., 2004; Zhu et al., 2005; Neer and Koylu, 2006). In their extensive study of 14 on and non-road diesel engines, Shah et al. (2004) found that the EC/OC ratio was less than unity (0.05-0.6) at idle, and from about 1 to 4.8 for cruise/high load conditions. The EC content from the small generator investigated here fell well within both ranges (Fig. 3).

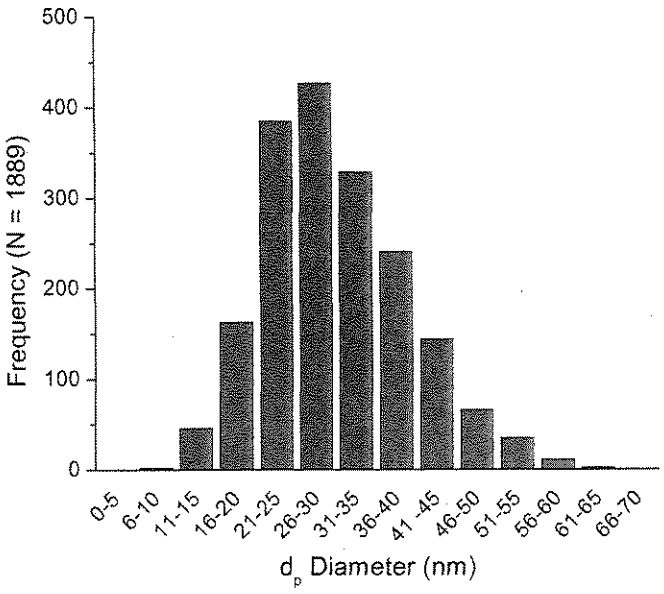

Figure 6: Frequency distribution for all aggregates analyzed. Median primary particle size is 29 nm.

Derivation of Mass Concentrations from On-line Measurements

Correction for Aggregates: Theory

The IA theory (Lall and Friedlander, 2006) was used in an expanded form that included the unequal ion mobility ratio characteristic of the ^{85}Kr source. The IA method applies to idealized aggregates with low fractal dimension and uniform primary particles in the free molecule size range, and uses two calculation modules. Module 1 related N_p and the radius (a) of primary particles that compose the aggregates to their mobility diameter (d_m). The relation was obtained by equating the migration velocity of the aggregates to that of spheres with equivalent mobility diameter:

$$\frac{d_m}{C(d_m)} = \frac{c^* N_p a^2}{3\pi\lambda} \qquad (2)$$

where $C(d_m)$ is the electrical mobility-based Cunningham slip correction factor, and λ is the mean free path of the gas. For aggregates oriented parallel to their relative motion (which is assumed here), the dimensionless drag force, c^* is equal to 6.62 (Dahneke 1982). If the primary particle size is known, aggregate volume and surface area can be obtained by summing the surface areas and volumes of the primary particles in the aggregate. Module 2 combines Eq. 2 with the aggregate charging efficiency (different from that of spheres) to obtain the aggregate number distributions:

$$n_{agg} = n_{sph} \frac{\eta_{sph}}{\eta_{agg}} \tag{3}$$

where, n_{sph} and n_{agg} are the number distribution functions for spheres and aggregates, respectively. η_{sph} and η_{agg} are the fraction of singly charged spheres and aggregates, respectively. (Small) multiple charging is ignored. The fraction of aggregates with charge q is given by Wen *et al.* (1984),

$$\eta_{agg} = \frac{e}{(\pi D_{qe} kT)^{1/2}} \exp\left[\frac{-(q-\bar{q})^2 e^2}{D_{qe} kT}\right] \tag{4}$$

where D_{qe} is the charging equivalent diameter of the aggregate ($N = 10$)

$$D_{qe} = \frac{2aN}{\ln(2N)} \tag{5}$$

and

$$\bar{q} = \frac{D_{qe} kT}{e^2} \ln\left(\frac{N_+ Z_+}{N_- Z_-}\right) \tag{6}$$

where the ion mobility ratio Z_+/Z_- is assumed equal to 1.4/1.9.

This treatment can be extended to apply to primary particles in the transition regime as follows. The adjusted aggregate drag c_a^* was determined from the ratio of the continuum drag, $c(0)$, and the slip correction factor based on the Knudsen number (Kn_a) of the adjusted sphere:

$$c_a^* = \frac{c(0)}{C(Kn_a)} \tag{6}$$

where

$$Kn_a = \frac{Kn}{A + B\left[\frac{c(0)}{c^*}\right]} \tag{7}$$

where, $Kn_a = \lambda/a$ is the Knudsen number based on the primary particle radius. A and B are 1.234 and 0.414, the constants of the Cunningham slip correction factor (Dahneke 1982). The dimensionless continuum drag force, $c(0)$, is a function of the number of primary particles that compose an aggregate.

Validation of the Aggregate Correction

The diesel aggregates investigated (generated at maximum load) had a median primary particle diameter of 29 nm, therefore requiring the EIA theory. Figure 7 shows a comparison between SMPS aggregate mass distributions based on IA theory compared to IA theory extended to the transition regime, for two primary particle diameters, 25 nm (Fig. 7a) and 30 nm (Fig. 7b). The total mass concentration based on EIA theory was about 25-30% more than when only IA theory was applied.

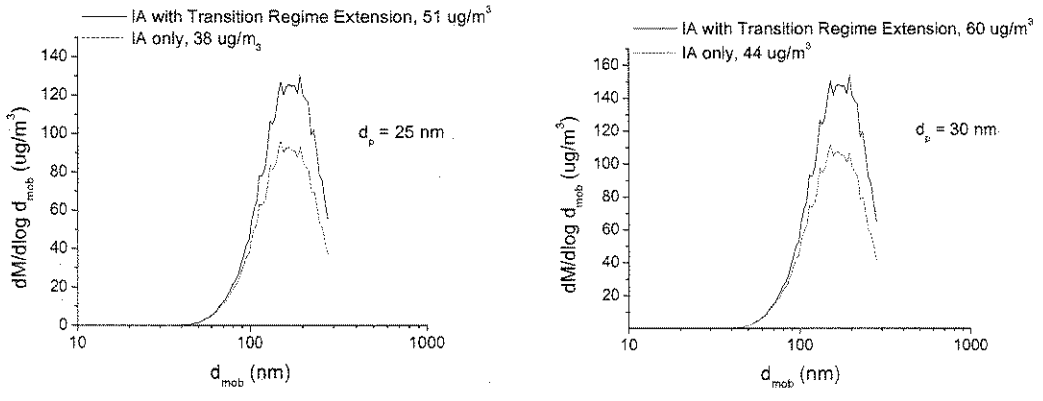

(a) (b)

Figure 7: Aggregate size distributions based solely on IA theory (dashed black) and IA theory with the extension to the transition regime (solid black), for primary particles with diameter 25 nm (a) and 30 nm (b).

Five experiments were performed to compare the SMPS measurements of diesel aggregates with gravimetric and total carbon measured by EGA (NIOSH 5040 method, Fig. 8) using particles in the chamber. During each experiment, aerosols were sampled simultaneously with the SMPS (at 2-minute resolution) and the filter-based measurements (20 minutes per sample). SMPS mass concentrations were averaged over the filter sampling periods. Fig. 8 shows correlations between the SMPS measurements, corrected with EIA, and the filter-based measurements, together with the uncertainties of each measurement. The correlations were excellent in both cases ($R^2 = 0.99$), and the slopes were close to unity; 1.04 for the gravimetric-corrected SMPS comparison and 0.89 for the TC-corrected SMPS comparison. The lower slope for the SMPS-TC comparison may be partially explained by some sulfur and trace metals in the particles, which cannot be detected by the EGA.

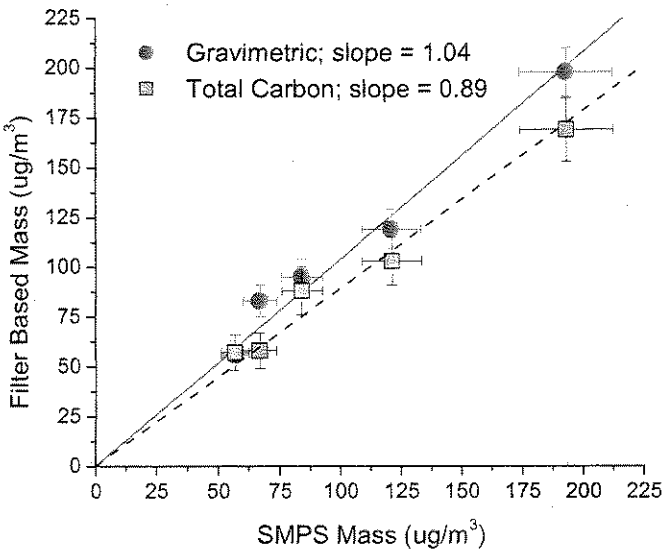

Figure 8. Measured diesel aggregate mass with the scanning mobility particle sizer, after correction with the idealized aggregate extension, and filter-based mass derived from gravimetric and total carbon measurements with an EGA.

SMPS Inlet Impactor

Currently TSI SMPS instruments come equipped with inlet impactors. The impactor serves two purposes: the inlet flow rate is calculated from the measured pressure drop across this impactor, and the size of the largest particles entering the SMPS system, assumed to equal the cut-off diameter of this impactor, is used to make a multiple charging correction. Aggregate inertial deposition, however, differs from that of spheres and is controlled primarily by the size of the spherules rather than the mobility diameter. This suggests that aggregates with mobility diameters well below the cut-off of the impactor might be lost in the impactor, and furthermore that the cut-off cannot be used to determine the largest aggregates that enter the SMPS (Barone et al., 2006).

To determine aggregate loss in the SMPS inlet impactor, the total number concentrations of diesel aggregates in the chamber (around 40,000 particles/cm^3) measured by two TSI SMPS systems were compared. Both systems used the same model electrostatic classifier (#3080), but the CPCs were slightly different: SMPS #1 used model #3775, and SMPS #2 used model #3010. With both SMPS systems operating without inlet impactors, number concentrations (after EIA correction) measured by the SMPS #1 were lower by 14%, a level of disagreement that was expected (Mamakos et al., 2004). Installation of the standard impactor (orifice diameter 0.071 cm) on SMPS #1 resulted in a difference of 37%, indicating a net aggregate loss of 23% due to the impactor.

In a separate set of chamber measurements, the loss of aggregates in the impactor as a function of mobility diameter was monitored. For these measurements, the TSI impactor was connected downstream of the DMA column. The current, which is proportional to the particle concentration, was measured using an aerosol electrometer (#3068A, TSI). We used the electrometer in lieu of a CPC for this configuration because the pressure drop in the impactor may interfere with CPC measurements. Electrometer readings with and without the impactor for mobility classified aggregates of 80, 90, 100, 110,120, and 150 nm revealed a reduction in current due to the impactor of 25 ± 5 %. It is worth noting that the impactor loss was a strong function of the *primary* particle diameter (Barone et al., 2006) thus care should be taken when applying the 25% loss to other aggregate systems. In light of these findings, when monitoring aggregates, the SMPS system was run without the impactor and the flow rate was manually measured.

Health and Atmospheric Impacts

Because the PM emissions from the small diesel generator investigated here are quite similar to those from larger and on- and non-road diesel engines, this type of generator is a convenient and relevant diesel particle source for climate and health studies. Non-road diesel engines, which include backup generators, contribute substantially to PM emissions in the US, which in turn contribute to anthropogenic alterations of the Earth's climate. Additionally, in contrast to on-road diesel engines where human exposure is typically distant from the exhaust, non-road diesel emissions tend to be in close proximity to human populations, and their emissions can have elevated importance from a health perspective.

As biodiesel becomes a larger part of the fuel pool, its PM emissions will become more important. Particles produced from biodiesel fuel are morphologically very different than those produced using diesel fuel; biodiesel particles are compact aggregates mostly lacking in clearly distinguishable primary particles. While at maximum load biodiesel particles have indistinguishable EC/OC ratios from diesel particles, at idle biodiesel particles have almost no EC, but they still exhibit irregular structures indicative of some solid material. EC sometimes serves as a proxy for chain aggregates in urban air (e.g., Schlesinger et al., 2006). Biodiesel particles have the potential however to contribute a substantial EC content while not maintaining fractal-like aggregated structures. Since optical absorption, scattering, and atmospheric lifetimes are a strong function of the shape of the particles, biodiesel particles need further study to determine their atmospheric implications.

Acknowledgements: This research was supported primarily by the U.S. Department of Energy's Atmospheric Science Program (Office of Science, BER, Grant No. DE-FG02-05ER64011). The authors thank Yoji Reichert for assistance with the experiments and image analysis, and the late Prof. Sheldon K. Friedlander for his relentless enthusiasm for all particle matters.

REFERENCES

Barone, T. L., Lall, A. A., Zhu, Y. F., Yu, R. C. and Friedlander, S. K., 2006. Inertial deposition of nanoparticle chain aggregates: Theory and comparison with impactor data for ultrafine atmospheric aerosols. Journal of Nanoparticle Research 8, 669-680.

Bunger, J., Krahl, J., Baum, K., Schroder, O., Muller, M., Westphal, G., Ruhnau, P., Schulz, T. G. and Hallier, E., 2000. Cytotoxic and mutagenic effects, particle size and concentration analysis of diesel engine emissions using biodiesel and petrol diesel as fuel. Archives of Toxicology 74, 490-498.

Conny, J. M., Klinedinst, D. B., Wight, S. A. and Paulsen, J. L., 2003. Optimizing thermal-optical methods for measuring atmospheric elemental (black) carbon: A response surface study. Aerosol Science and Technology 37, 703-723.

Dahneke, B., 1982. Viscous resistance of straight chain aggregates of uniform spheres. Aerosol Science and Technology 1, 179-185.

Heubert B.J. and Charlson, R. J., 2000. Uncertainties in data on organic aerosols. Tellus 52B, 1249-1255.

Jung, H. J., Kittelson, D. B. and Zachariah, M. R., 2006. Characteristics of SME biodiesel-fueled diesel particle emissions and the kinetics of oxidation. Environmental Science & Technology 40, 4949-4955.

Labeckas G. and Slavinskas S., 2005. Performance and exhaust emission characteristics of direct-injection Diesel engine when operating on shale oil. Energy Conversion and Management 46, 139 – 150.

Lall, A. A. and Friedlander, S. K., 2006. On-line measurement of ultrafine aggregate surface area and volume distributions by electrical mobility analysis: 1. Theoretical analysis. Journal of Aerosol Science 37, 260-271.

Liu, Z. F., Lu, M. M., Birch, M. E., Keener, T. C., Khang, S. J. and Liang, F. Y., 2005. Variations of the particulate carbon distribution from a nonroad diesel generator. Environmental Science & Technology 39, 7840-7844.

Mader, B., Schauer, J., Seinfeld, J., Flagan, R., Yu, J., Yang, H., Lim, H., Turpin, B., Deminter, J., Heidemann, G., Bae, M., Quinn, P., Bates, T., Eatough, D., Huebert, B., Bertram, T. and Howell, S., 2003. Sampling methods used for the collection of particle-phase organic and elemental carbon during ACE-Asia. Atmospheric Environment 37, 1435-1449.

Mamakos, A., L. Ntziachristos and Z. Samaras, 2004. Comparability of particle emission measurements between vehicle testing laboratories: a long way to go. Meas. Sci. & Tech. 15: 1855-1866

Mathis, U., Mohr, M., Kaegi, R., Bertola, A. and Boulouchos, K., 2005. Influence of diesel engine combustion parameters on primary soot particle diameter. Environmental Science & Technology 39, 1887-1892.

Myhre, G., Bellouin, N., Berglen, T. F., Berntsen, T. K., Boucher, O., Grini, A., Isaksen, I. S. A., Johnsrud, M., Mishchenko, M. I., Stordal, F. and Tanre, D., 2007. Comparison of the radiative properties and direct radiative effect of aerosols from a global aerosol model and remote sensing data over ocean. Tellus Series B-Chemical and Physical Meteorology 59, 115-129.

Neer, A. and Koylu, U. O., 2006. Effect of operating conditions on the size, morphology, and concentration of submicrometer particulates emitted from a diesel engine. Combustion and Flame 146, 142-154.

NIOSH, 1999. Elemental Carbon (Diesel Particulate). NIOSH Manual of Analytical Methods (NMAM). NIOSH: Method 5040 Issue 3.

Park, K., Kittelson, D. B. and McMurry, P. H., 2004. Structural properties of diesel exhaust particles measured by transmission electron microscopy (TEM): Relationships to particle mass and mobility. Aerosol Science and Technology 38, 881-889.

Saathoff, H., Naumann, K.-H., Schnaiter, M., Schock, W., Mohler, O., Schurath, U., Weingartner, E., Gysel, M. and Baltensperger, U., 2003. Coating of soot and (NH4)2SO4 particles by ozonolysis products of a-pinene. Journal of Aerosol Science 34, 1297-1321.

Sakurai, H., Tobias, H. J., Park, K., Zarling, D., Docherty, S., Kittelson, D. B., McMurry, P. H. and Ziemann, P. J., 2003. On-line measurements of diesel nanoparticle composition and volatility. Atmospheric Environment 37, 1199-1210.

Schlesinger, R. B., Kunzli, N., Hidy, G. M., Gotschi, T. and Jerrett, M., 2006. The health relevance of ambient particulate matter characteristics: Coherence of toxicological and epidemiological inferences. Inhalation Toxicology 18, 95-125.

Shah, S. D., Cocker, D. R., Miller, J. W. and Norbeck, J. M., 2004. Emission rates of particulate matter and elemental and organic carbon from in-use diesel engines. Environmental Science & Technology 38, 2544-2550.

Sharp, C. A., 1998. Characterization of Biodiesel Exhaust Emissions for EPA 211 (b) - Final Report for the National Biodiesel Board, Jefferson City, MO. San Antonio, TX, Southwest Research Institute.

Swanson, K. J., Madden, M. C. and Ghio, A. J., 2007. Biodiesel exhaust: The need for health effects research. Environmental Health Perspectives 115, 496-499.

U.S. EPA, May 2004. Final Regulatory Analysis: Control of Emissions from Nonroad Diesel Engines, Office of Transportation and Air Quality, Assessment and Standards Division.

Wentzel, M., Gorzawski, H., Naumann, K. H., Saathoff, H. and Weinbruch, S., 2003. Transmission electron microscopical and aerosol dynamical characterization of soot aerosols. Journal of Aerosol Science 34, 1347-1370.

Xia, T., Kovochich, M. and Nel, A. E., 2007. Impairment of mitochondrial function by particulate matter (PM) and their toxic components: implications for PM-induced cardiovascular and lung disease. Frontiers in Bioscience 12, 1238-1246.

Xiong, C. and Friedlander, S. K., 2001. Morphological properties of atmospheric aerosol aggregates. Proceedings of the National Academy of Sciences of the United States of America 98, 11851-11856.

Zhu, J. Y., Lee, K. O., Yozgatligil, A. and Choi, M. Y., 2005. Effects of engine operating conditions on morphology, microstructure, and fractal geometry of light-duty diesel engine particulates. Proceedings of the Combustion Institute 30, 2781-2789.

Chapter 3: The Catalytic Effects of Metal Salts and Sulfates on Diesel Aerosols

3.1 Introduction

Carbonaceous particulate matter (PM) continues to be the subject of intense study due to its role in global climate change, both on a local and global scale (Ramanathan and Carmichael 2008). Atmospheric carbonaceous PM has been shown to both warm and cool the earth's atmosphere, but uncertainties are large (Kanakidou et al. 2005; Bond 2007; Keil 2008). The organic carbon (OC) fraction scatters incoming sunlight (e.g., Penner et al., 1998). "Elemental" carbon (EC), or "black" carbon (BC) strongly absorbs both visible and infrared radiation. Climate forcing of EC is thought to exceed that of methane and is second only to CO_2 (Jacobson 2001; Ramanathan and Carmichael 2008). In addition to direct effects, indirect effects such as increased cloudiness due to elevated cloud condensation nuclei numbers (Choularton et al. 2008) and the increased probability and severity of rainfall (Bell et al. 2008) expands the impact of carbonaceous aerosols. It is often believed that the climate impacts of direct emissions of aerosols are a local phenomenon; however, Koch et al. (2007) determined that 65 to 90% of direct emissions are transported beyond the area of production. Bond (2007) showed that the radiative forcing of direct emissions can affect an area 40 times greater than the initial 'hot spot'. Simulations by Levy et al. (2008) showed that warming potential of black carbon particles can be responsible for up to 40% of the total increase of surface temperature by the year 2100. This conclusion was also found by Kirkevag et al. (2008) which argued

that within the next 100 years the sign of the aerosol radiative forcing will go from negative to positive due to the contribution of black carbon (BC). The aerosol radiative forcing has been shown to be sensitive to the OC and EC emission factors used. Wang et al. (2007) showed that the radiative forcing for biomass aerosols ranges from -3.1 to 1.6 W m^{-2} depending on the ratio of OC to EC used for model inputs.

Carbonaceous PM ranks as some of the most difficult aerosol to measure, such that basic atmospheric measurements of these materials carry uncertainties of at least 30-50% (Huebert and Charlson 2000). Taken together, EC and OC are often referred to as total carbon (TC). Categorically speaking, some materials fall between OC and EC; for example, bound polyaromatic hydrocarbons (PAHs) on the surface of soot particles are not extractable by the same methods that other organics are, and have a higher C/H ratio than most organics, part way to soot. A large fraction of particulate OC results from the photo-oxidation of gas phase organics to form secondary organic aerosols (SOA). Primary emissions of carbonaceous aerosols originate from the incomplete combustion of fossil fuels in transportation, energy generation, and various industrial applications. Depending on the source and method of operation, primary emissions vary widely in OC and EC composition (Shah et al. 2004; Chung et al. 2008).

The most common method of quantifying elemental and organic material in the atmosphere is the offline, or more recently semi-continuous, technique of using evolved gas analyzers (EGA), which provides EC and OC mass based on their respective thermal stabilities. The EGA works by evolving material through heating a quartz filter punch and oxidizing it to CO_2 and then reducing it to methane and quantifying it with a flame

ionization detector (FID). The step-wise heating process initially takes place in an inert (He) environment. During this phase, the evolved material is typically classified as OC. The oven then cools and then resumes the step-wise heating in an oxidizing (He/O_2) atmosphere. Ideally, the material evolved in the oxidizing phase can be classified as EC.

One of the largest sources of uncertainties in using EGA is determining the exact location of the OC/EC split. During the inert phase, OC may pyrolize and produce char, resulting in the darkening of the filter spot. Charred OC requires the addition of O_2 to remove it from the filter – similar to EC. The instrument accounts for charred OC that would otherwise be classified as EC by the laser transmittance or reflectance through the sample, otherwise known as thermo-optical transmittance (TOT) or thermo-optical reflectance (TOR). The EC/OC split is located at the point where the transmittance or reflectance level returns to its initial level after a reduction of laser response due to charring after a small correction for the temperature dependence of the laser response. The National Institute of Occupational Safely and Health (NIOSH) specifies a standard temperature protocol for a TOT instrument (NIOSH 1999). In addition to the NIOSH (1999) method, Conny et al. (2003) performed an extensive factorial study to optimize the temperature program of EGA-TOTs, to minimize the charring of OC and to eliminate the possibility of native EC evolving during the helium phase and being miscounted as OC.

Another complication in the analysis of OC and EC is the possibility that the non-carbonaceous components in aerosols may affect the thermal stability of carbon during EGA analysis. The chemical composition of aerosols typically shifts according to

particle size. Coarse (2.5 um < d_p < 10 um) and accumulation mode (0.1 um < d_p < 2.5 um) particles comprise the majority of the aerosol mass concentration (over 85%) in the Los Angeles area (Sardar et al. 2005). Coarse mode particles typically have high concentrations of metals (over 50% by mass) including aluminum, silicon, calcium, and iron and relatively low carbon mass concentrations. The accumulation mode frequently contains lower concentrations of metals and a higher fraction of carbon. For ultrafine particles, carbon often dominates the aerosol mass (Hughes et al. 1998; Sardar et al. 2005); however, Chung et al. (2001) found that metals exceed 50% of the ultrafine particle mass for aerosols collected in Bakersfield, CA, with calcium being the predominant metal.

The Lawrence Berkeley Laboratory method (Novakov and Corrigan 1995; Kirchstetter et al. 2001), which utilized a steady temperature ramp in an oxidizing environment, showed that source-dominated samples from a vehicle tunnel contained "black" carbon that evolved from a filter at much higher temperatures than that for ambient samples. Further, by externally mixing aerosols on filters, Turner and Hering (1994) showed that the evolution temperature for the black carbon from the tunnel is lowered if ambient aerosol sample is added to the tunnel sample, and attributed the different oxidation profiles of the soot to the non-carbonaceous constituents of the ambient aerosol. Grosjean et al. (1994) observed even larger reductions in oxidation temperatures when mixing ambient tunnel samples with lab generated NaCl particles. In addition to the non-carbonaceous component of ambient aerosols, the metals associated with diesel PM itself may affect its oxidation in the EGA. Studies have shown that diesel

PM can include high levels of Fe, Ca, Mn and Zn, while coal PM has associated Fe, Ti, Al, Mn, V, and Ni (Finlayson-Pitts and Pitts 2000; Wang et al. 2003). Prior analysis of high load diesel particles in our lab showed significant levels of Na, Zn, Ca, Fe, and Cu.

Several laboratory studies have investigated the oxidation of soot and graphitic carbon for various applications. Murphy et al. (1981) discovered that copper chloride dissolved in methanol reduces the temperature at which diesel soot is oxidized. Lin and Friedlander (1988) studied the enhancement of soot oxidation in the presence of sodium and suggested that at elevated temperatures used in EGA, sodium, as often present in aerosols, will catalyze the oxidation of soot. For their experiments the sodium was naturally present in the glass fiber filters. Even though diesel particles only on the initial deposit layer are in contact with the catalyst surface, they showed that reactions still take place despite limited contact. In contrast, Neeft et al. (1996) determined that the degree of contact between soot particles and catalyst is a key parameter in soot oxidation using a model soot (Printex-U, Degussa Inc.). They showed that catalysts with "tight" contact with soot particles are more effective in oxidation than when there is "loose" contact. "Tight" contact was produced by mechanically milling the catalyst and Printex-U into a mixture, whereas "loose" contact consisted of hand mixing the aerosols with a spatula. Mul et al. (1998) found that $PbCl_2$, $CuCl_2$, and CuCl are very active in the oxidation of Printex-U whereas $HgCl_2$, $BaCl_2$, and $CaCl_2$ had little effect. They suggested that the activity of these metal chlorides was induced by in-situ formation of contact with the soot by gas phase transport during oxidation. Silva et al. (1997) showed that nickel, cobalt, and molybdenum as well as their mixtures had the ability to catalyze charcoal. Although

not a metal, Yu et al. (2002) showed that ammonium bisulfate altered the thermal evolution of several OC standards such as levoglucosan, starch, and cellulose, when using a EGA-TOT running off the UST-2 thermal method.

There is extensive literature investigating the use of metals to catalyze the gasification of biomass fuels. In contrast to the problem of quantifying EC/OC, the production of char in biomass combustion is desirable, since char can be used as a substrate for subsequent gasification and production of combustible gases for energy. Several studies have investigated wood charring (Richards and Zheng 1991; Edye et al. 1993). Richards and Zheng (1991) found that wood treated with acetate salts of alkali metals (i.e., copper and iron) and calcium, increased yields of char during vacuum pyrolysis. Acetates were used to ensure a high pH to ionize the acid groups on the wood surface so that the metal ions would bind to the surface. Shimada et al. (2008) found that alkaline earth metal chlorides enhance the pyrolysis of cellulose, which in turn increased the yield of produced char. Edye *et al.* (1991) compared the charring of wood using copper and iron acetate with and without any indigenous cations (such as K and Ca) associated with the wood samples. Experiments with copper showed that the natural cations acted as retardant for char formation, in contrast to iron, which showed enhanced wood charring when the natural cations were present. Similarly for coal samples Yu et al. (2006) found that adding aqueous ferric chloride solution enhanced char as compared to untreated coal. These studies indicated that many metals enhance the oxidation of soot, and also enhance charring or organic carbon material of various types. The catalytic community has not thus far been successful at developing a predictive model for which

metals will or will not have high catalytic activities, and thus rely on empirical observations (Dr. Selim Senkan - personal communication).

Understanding how inorganic species, such as metals, can affect the thermal stability of carbon during EGA is necessary in determining accurate OC and EC concentrations for carbonaceous particles. For this study diesel particulates emitted from a non-road diesel generator was used as the carbon aerosol (Chung et al. 2008), since metals interact with EC and OC differently, two chemically distinct types of diesel particles were generated – particles high in EC by operating the generator at maximum load and high in OC with operation of the generator at lower loads. Catalytic metals were chosen for study were based on their measured presence in the local ambient aerosol as well as reports from the literature (Sardar et al. 2005; Wojas and Almquist 2007; Yin and Harrison 2008). Solutions of individual catalytic alkali, alkaline, and transition metal chlorides and sulfates were aerosolized and used to pre-treat baked quartz fiber filters before exposing the filters to the diesel engine exhaust. The effect of metal chlorides and sulfates on the behavior of both EC and OC during EGA was determined and then related to any changes in the EC/OC ratios due to the catalytic additives. Also, the synergistic catalytic affect of metal mixtures on diesel particles high in EC will be discussed.

3.2 Experimental

To determine which metals in ambient aerosols may affect the carbon analysis of diesel particles, ambient total suspended particles (TSP) were collected on the roof of the UCLA math sciences building at a flow rate of 32 L min^{-1} onto a 47 mm Teflon filter

(Pall Life Sciences) during December 5-7, 2007. Sampling times varied from 2 to 6 hours depending on the atmospheric mass concentration as determined by the scanning mobility particle sizer (SMPS) (differential mobility analyzer (DMA) 3081, condensation particle counter (CPC) 3010, TSI). Teflon filters were pre-weighed in a temperature and humidity controlled room using a microbalance ($\pm$ 1 μg, Sartorius) after removing charges from the filters by passing them over a polonium strip. Prior to weighing, the filters were allowed to re-equilibrate for 24 hrs in the weighing room. After gravimetric analysis, the aerosols deposited on the Teflon filter were extracted in preparation for analysis by inductively coupled plasma atomic electron spectroscopy (ICP-AES) for elemental composition. Individual Teflon filters were placed in sterile polycarbonate Petri dishes and material was extracted with 10 mL of 5% HNO_3 solution for 48 hours. Calibration solutions were provided by Dr Amir Liba (Director, UCLA Molecular and Instrumentation Center) and calibration curves were performed at concentrations of 0, 50, 100, 400, 700, and 1000 ppm for the desired metals with correlation coefficients for these calibrations being above 0.999.

In parallel with the Teflon filter, ambient aerosols were deposited on two 47 mm quartz filters (Pall Life Sciences) at a flow rate of 20 L min^{-1}. All quartz filters used in this study were pre-baked in a furnace at 550° C for over 24 hours to remove any carbon impurities. One quartz filter was used for EC/OC analysis of the native ambient aerosol. The second quartz filter was then used to sample diesel PM on top of the layer of ambient particles. Sampling occurred at 20 L min^{-1} less than 1 m away from the exhaust of a 4-stroke, air cooled direct injection 4.8 kW diesel generator (L70V6, Yanmar Corporation).

Loads were applied to the generator by connecting electrical appliances, each pulling 1.42 kW, equivalent to about a 25% load per appliance. The generator was operated on commercially available California #2 ultra low sulfur fuel (less than 15 ppmw sulfur) or B99 biodiesel fuel. The biodiesel fuel was locally purchased and was manufactured from a combination of used restaurant grease and various agricultural oils (http://www.conservfuel.com/). Before use, the diesel generator was warmed up for 5 minutes at idle and then another 5 minutes at the load investigated.

A thermal optical transmittance (TOT) EGA (Sunset Laboratories) was used to measure OC and EC from the quartz filters. To provide some insight into the magnitude of the error introduced by the temperature programs, all samples were analyzed on the widely used NIOSH 5040 protocol (NIOSH 1999) and the recent protocol developed by Conny et al. (2003) to minimize charring. The durations and temperatures of each step for the NIOSH (1999) and Conny et al. (2003) protocol are shown in Table 3-1.

		NIOSH (1999)		Conny et al. (2003)	
	Step	Temp (°C)	Time (s)	Temp (°C)	Time (s)
He Phase	1	250	90	190	90
	2	500	60	365	60
	3	650	60	610	60
	4	850	90	835	72
O_2-He Phase	1	650	30	550	180
	2	750	30	700	60
	3	850	60	850	60
	4	940	120	900	90-120

Table 3-1: Temperatures and durations of each step for the NIOSH (1999) and Conny et al. (2003) method used for TOT-EGA. After step 4 there is a about a 50 second period of cooling before the O_2-He phase begins.

The concentrations of chlorides and sulfates in the ambient atmosphere are highly variable, so it is necessary to understand if the chloride or sulfate component of the aerosol plays any role in the oxidation of soot. Metal solutions were prepared by weighing out the appropriate mass of metal chloride/sulfate powder on a microbalance (± 0.001 g, Shimadzu) and were subsequently dissolved in purified de-ioninized water (18 M Ω). Solutions of metal chlorides and sulfates were nebulized into a small indoor Teflon chamber for 2 min at a flow rate of 3.3 L min^{-1}. The chamber had a volume of approximately 0.13 m^3 in a pillow geometry and was constructed by sealing 2 mil FEP Teflon sheets with a impulse heat sealer (PI-G35, Packaging Aids). The seals were then reinforced with greenback tape (3M). The chamber air was less than 25% relative humidity, so the aerosol leaving the nebulizer was directly injected into the chamber without the use of a drier. This resulted in a total relative humidity between 30 and 40%. Chamber air was supplied by an oil-free air compressor and was purified prior to filling the chamber by a series of packed bed scrubbers filled with Purafil Triple Blend (Purafil Inc.), activated charcoal, and a HEPA capsule filter (Gelman). The background particle concentration in a clean filled chamber was < 20 particles cm^{-1}. Conductive rubber tubing was used to sample from the chamber through Teflon sampling ports. 47 mm filter holders equipped with a Teflon and quartz filter sampled the nebulized aerosols from the chamber simultaneously at a flow rate of 20 L min^{-1} for 30 seconds. The SMPS was also used to characterize the aerosol size distribution.

Once the metal aerosols were deposited onto the quartz filter, diesel PM was deposited on top of the metal catalyst layer. In parallel, a diesel sample (considered the

control) was collected on a clean quartz filter at 20 L min^{-1} 1 m away from the generator exhaust. Since mass emission rates are proportional to engine load (Symonds et al. 2007) sampling times varied from 30 seconds to 15 minutes depending on the applied load. Also taken into account when determining an appropriate sampling time was the quantity of metals deposited onto the filter prior to sampling the diesel PM. Attempts were made to make the mass ratio of metals to carbon deposited on the filter similar to that typically found in the atmospheric aerosol. Literature shows that typical PM 2.5 metal to carbon ratios in the Los Angeles area ranged from 0.2 to 0.5 depending on location with higher ratios found in the downtown area smaller ratios in the rural areas (Sardar et al. 2005).

Blank quartz filters were analyzed and showing carbon being evolved from the filters at concentrations less than the recommended range of the EGA. Since concentrations were less than the recommended operating range of the instrument, the samples were not blank corrected for carbon concentrations. Laser transmission through the blanks fluctuated by a few percent during the duration of the analysis. Baked quartz filters deposited with only metals also showed carbon concentrations less than the recommended operating range of the EGA. For all metals, with the exception of iron, the laser transmission fluctuated slightly during analysis, similar to the clean baked filter. Due to darkening of the iron during heating, the transmission through the filter significantly decreased during analysis. The complication of the iron species affecting the laser transmission through the quartz filter will be discussed in later sections.

The morphology of the aerosolized metal catalysts was determined by transmission electron microscopy (TEM). Aerosols were deposited onto a 400 mesh

copper grid with formvar carbon support film (Electron Microscopy Sciences) for analysis. The TEM grids were attached with adhesive tape to the center of 25mm filter screen and placed inside a filter holder. Particles were sampled at a flow rate of 20 LPM for 30 seconds to a minute. The TEM grids were studied using a JEOL 100CX TEM at magnification of 20 to 100,000×. The pressure inside the TEM was maintained at 0.0007 Pa. Pictures of individual particles were taken and subsequently scanned into electronic image format using a Microtek Scanmaker E6 (Redondo Beach, CA).

3.3 Results

Table 3-2 shows the chemical composition of TSP for the December 5-7, 2007 experiments.

Metal [a]	12/5/2007 $\mu g/m^3$	12/6/2007 $\mu g/m^3$	12/7/2007 $\mu g/m^3$
Na	6.44	7.48	7.42
Al	0.42	0.27	0.06
Ba	0.15	0.06	0.02
Ca	2.84	1.93	0.49
Co	0.00	0.00	0.00
Cr	0.05	0.02	0.01
Cu	0.37	0.07	0.02
Fe	1.77	0.78	0.19
K	0.47	0.24	0.20
Mg	1.06	0.97	0.85
Ni	0.01	0.01	0.00
Si	0.75	0.41	0.26
Ti	0.04	0.02	0.00
V	0.11	0.03	0.09
Zn	0.43	1.25	0.05
Sum:	15	14	10
TC (EGA)	15	9	2
EC/OC Ratio	0.14	0.16	0.11
Unknown	49	34	10
Total	79	57	22
Metal/diesel PM/ ratio [b]	0.16	1.77	3, 1.3
Shift in Oxidation Temperature [c]	158° C	158° C	160° C

[a] Cobalt was below the detection limit in all samples.
[b] Ratio of diesel PM added to filters with ambient aerosol, to the sum of measured metals in the ambient aerosol.
[c] Shift in oxidation temperature is determined by the difference in temperature at which the peak of the carbon evolution occurs between diesel and a mixture of diesel and ambient aerosols.

Table 3-2: Measured chemical composition of TSP in the ambient atmosphere. Metals are analyzed by ICP-AES and TC was measured from EGA using the NIOSH (1999) temperature protocol.

Gravimetric analysis was conducted to determine the total aerosol mass deposited onto the Teflon filters. For all three samples, a large fraction of the mass was unaccounted for and was most likely a mixture of water soluble ions (such as nitrates, sulfates, and phosphates), various metals not analyzed for in ICP-AES, and water. Data

from the literature have shown that the difference between the metal and carbon mass from the total PM10 was similar in percentage to what is allocated as being "unknown" for our TSP samples (Sardar et al. 2005; Yin and Harrison 2008; Zhao and Gao 2008). For our samples, the bulk of the known mass was carbon for the first two experiments. Sodium becomes the predominant metal for the third experiment. The most abundant metal in the three ambient samples was sodium, with significant contributions from calcium, magnesium, and iron.

For the 12/5/07 experiment TSP was collected for 2 hours on two quartz filters before exposing one of them to diesel exhaust for 3 minutes. One quartz filter was measured with EGA to obtain the TC of the ambient aerosol. The total ambient carbon mass deposited onto the filter was 28 μg. The amount of diesel carbon deposited on top of the ambient layer was 171 μg. Visually comparing the darkness of the ambient to the ambient/diesel samples verified this overwhelmingly large amount of diesel particulate deposited onto the filter. These carbon masses were determined by EGA using the NIOSH (1999) method. Even with the large diesel to ambient carbon ratio, figure 3-1 shows that there was still a significant reduction in the oxidation temperature for soot by close to 200° C. The carbon from ambient/diesel PM sample began to oxidize at the same temperature that ambient carbon begins to oxidize. The addition of ambient aerosol to the diesel PM did not affect the volatilization profiles for carbon during the inert phase (< 320 sec). The resulting carbon evolution of the ambient and diesel PM aerosol during the inert heating phase was a weighted average of the ambient and diesel carbon evolution. There was no change in evolution profile during this phase. The EC/OC ratio

was 4.31 and 1.49 for diesel particles alone and when mixed with ambient aerosols. The EC/OC ratio change was not a weighted average of the two types of aerosols. Knowing the mass of diesel particles (17.5 mg) and ambient aerosols (3.5 mg) on the quartz filter and their respective EC/OC ratios, the weighted EC/OC ratio of the resulting aerosol mixture would be 3.54.

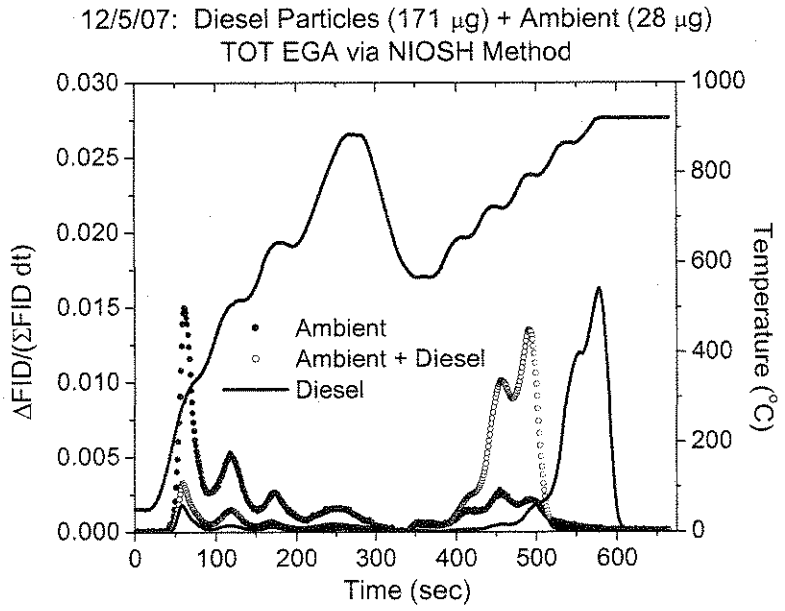

Figure 3-1: Carbon evolution profile for ambient, diesel, and a combination of ambient and diesel PM. The FID response is normalized to the total FID response for a given sample. The area under the curve is proportional to the total carbon evolved.

The second and third experiment attempted to make the carbon mass loading of diesel and ambient PM more equal. For the 12/6/07 experiment, 66 μg of diesel carbon was deposited on top of 33 μg of ambient carbon and for the 12/7/07 experiment, 18 μg of diesel carbon was deposited on top of 11 μg of ambient carbon. For both experiments

the oxidation temperature of diesel PM was still lowered significantly (~175^{o} C) with the addition of ambient aerosols (Figure 3-2). Regardless of the relative amount of diesel and ambient carbon deposited on the filter, the oxidation temperature was reduced due to the catalytic components of the ambient PM. To further validate that the oxidation temperature was reduced regardless of the diesel to ambient carbon mass ratio deposited on the filter, the 12/7/08 sample was loaded with an additional 25 μg of diesel carbon. From figure 3-3 it can be seen that the oxidation temperature was unchanged even though more diesel was added. The diesel to ambient carbon ratio for each curve is shown in the legend. The reduction of the oxidation temperature of the low volatility carbon, regardless of the carbon mass on top of a layer of ambient aerosols was consistent with the results of Turner and Hering (1994).

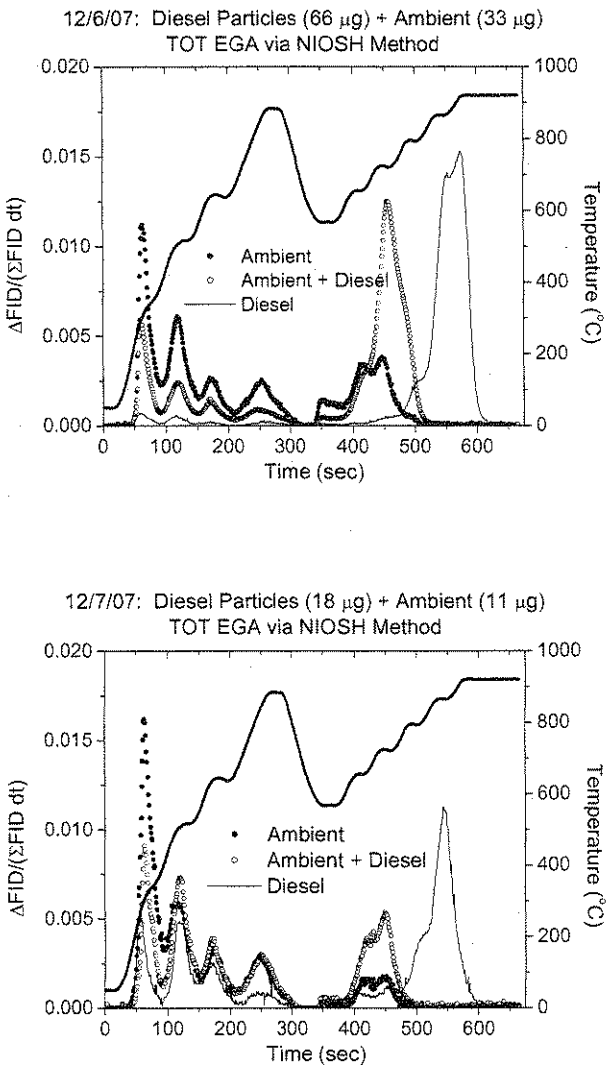

Figure 3-2: Carbon evolution profile for ambient, diesel, and a combination of ambient and diesel PM.

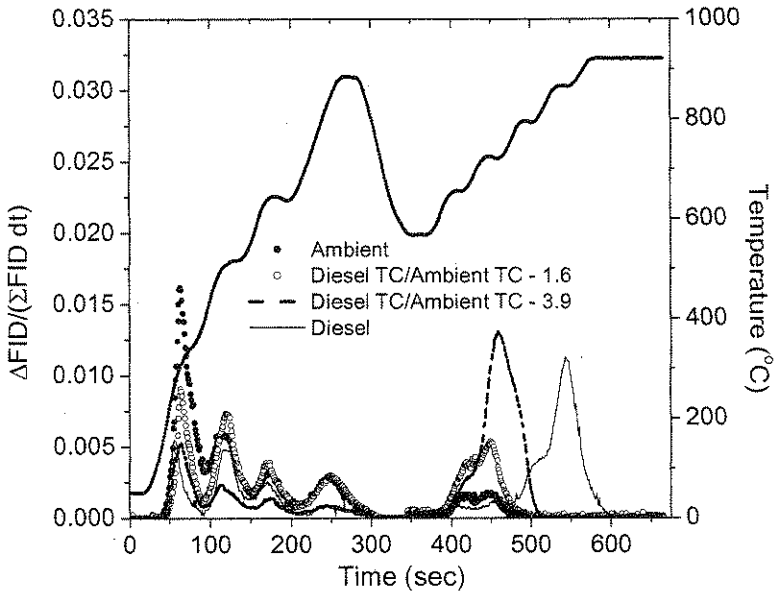

Figure 3-3: The effect of diesel PM mass loading on catalytic activity of ambient aerosol

Catalyst Characterization

It was evident that there are elements in atmospheric aerosol that cause reductions in the oxidation temperature of the low volatile soot that could potentially bias the measured EC and OC concentrations. Literature has shown that in the Los Angeles area, the coarse and accumulation mode aerosols have significant amounts of iron, calcium, potassium, silicon, and aluminum (Sardar et al., 2005). Wojas and Almquist (2007) found large amounts of copper in addition to crustal elements, such as magnesium, manganese, calcium, and potassium, in TSP samples in Oxford, OH. Manganese is also of relevance due to the work of (Fung et al. 2002) which uses oxides of manganese to assist in the speciation of OC and EC during EGA. Taking into account the literature and the elemental analysis of the three ambient TSP samples, metal chlorides chosen for

study were calcium, magnesium, manganese, copper (I and II), iron (II and III), sodium and potassium. Sodium and magnesium sulfate were also investigated to determine possible effects of different anions.

For each metal chloride or sulfate, a 0.1 M solution was nebulized into the chamber. From TEM images the catalyst particles were irregularly shaped (Figure 3-4) and were most likely metal hydrates and not crystalline metal particles. Also, these particles were not deliquesced because of the low RH (< 40%) maintained in the chamber after aerosol injection. Deliquescence points for the metal chlorides and sulfates were not readily available; however, the RH inside the chamber was most likely well below this value. Using the number concentration and particle size data from the SMPS, it was calculated that there were multiple layers of deposition of metal aerosols onto the quartz filter.

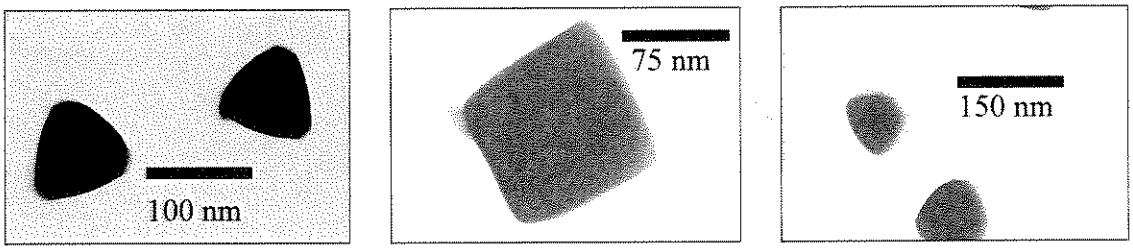

Figure 3-4: TEM image of $CaCl_2$ catalysts sampled directly from the small Teflon chamber.

The SMPS measured the particle size of the metal catalysts directly from the chamber. Several distributions were measured and the median diameters (shown in Figure 3-5) ranged from 42 to 122 nm.

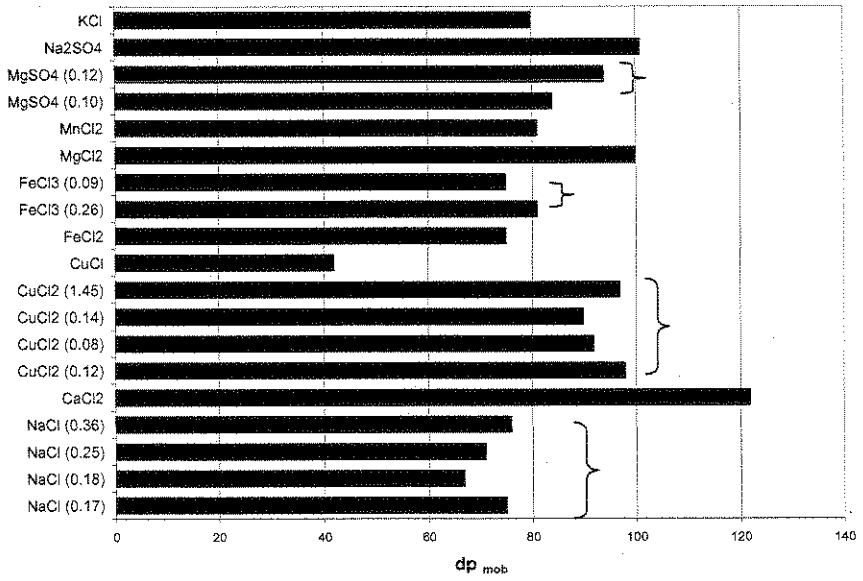

Figure 3-5: Particle sizes of the aerosolized metal catalysts. For metals where multiples experiments were conducted, the resulting metal to carbon mass ratio deposited on the filter is shown in parenthesis.

Catalytic Effect on Carbon Evolution for Diesel Particles During EGA

I. High EC Diesel Particles

An example EGA thermogram of high load diesel particles (i.e., high EC) with and without a $CaCl_2$ catalyst analyzed using the NIOSH (1999) and Conny et al. (2003) protocol is shown in Figure 3-6. The $CaCl_2$ catalyst enhanced the evolution of carbon during the last temperature stage (200 to 300 s) of the inert phase for both protocols; however, because the fraction of carbon evolved during this period as small and these values were close to the minimum detection limits of the EGA, it is difficult to make any remarks about this observation. For $CaCl_2$, along with most other metal catalysts used in this study, a large catalytic effect on carbon evolution was observed during the oxidation phase of EGA which is the period beyond 320 sec. As the NIOSH (1999) protocol

resumes heating and the Conny et al. (2003) method initiates the constant temperature step, oxygen was introduced in the carrier gas and the carbon begins to evolve earlier, and at much lower temperatures when a metal catalyst was present. Accompanied with the earlier evolution of the low volatile soot comes earlier removal of all remaining carbon from the quartz filter during EGA. A difference observed from the evolution of carbon during the oxygen phase was the emergence of a bi-modal carbon evolution distribution using the Conny et al. (2003) method. A bi-modal oxidation profile occurred in several instances but not a majority of the time. A small fraction of the carbon evolved at 750°C and a majority of the material evolved at higher temperatures (850 to 900° C).

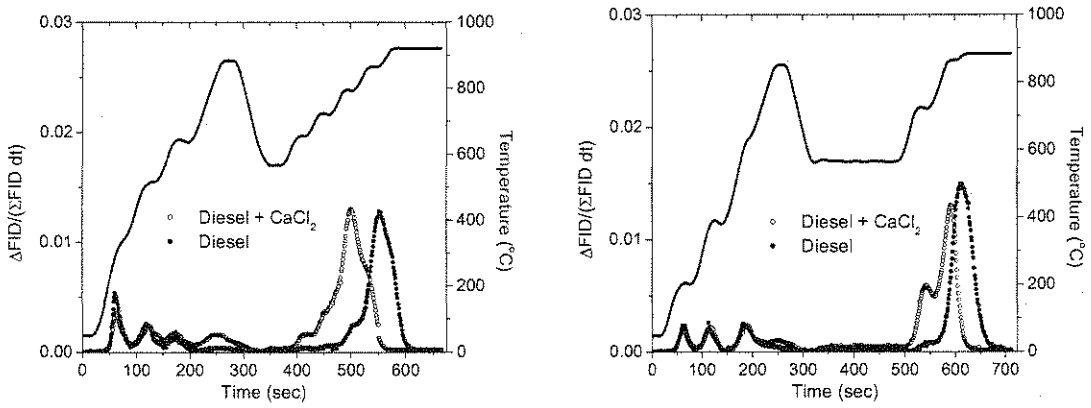

Figure 3-6: Thermograms of carbon evolution of high EC/OC diesel particles with and without a $CaCl_2$ catalyst using the NIOSH (1999) (left) and Conny et al. (2003) (right) temperature programs.

Table 3-3a and 3b shows the effect of metal additives to carbon stability during EGA and the resulting effect on the measurement of EC/OC ratios using the NIOSH (1999) and Conny et al. (2003) method. The change in oxidation temperature was measured by comparing the temperature at which the peak of the carbon oxidation occurs

with and without a catalyst. Several metals were selected to determine if the ratio of metal to diesel carbon mass (M/C ratio) deposited onto the filter affects the oxidation temperature of carbon.

It was evident that the oxidation temperature of diesel particles was lowered substantially in the presence of metal catalysts. Figure 3-7 compares the change in carbon oxidation temperature of carbon when in the presence of metals. All of the catalysts, with the exception of the magnesium species, reduced the oxidation temperature of EC. $CuCl_2$ had the largest affect on the oxidation temperature of carbon and was the only metal that resulted in oxidation temperatures reductions similar to that of ambient aerosols. All the other metals tested affected the oxidation temperature of carbon to a lesser degree than ambient aerosols.

Iron (II) reduced the soot oxidation temperature by 26° to 30° C. Iron (III) showed that its affect on oxidation temperature depended on the temperature program used. There was a reduction of 73° to 86° C and 22° to 29° C when using the NIOSH (1999) and Conny et al. (2003) method. Cu (I) had a much smaller affect then Cu (II), at 15° or 20° C for Cu (I) and 143° to 166° for Cu (II) for the NIOSH and Conny et al. (2003) method, respectively. Murphy et al. (1981) dissolved copper (II) chloride in methanol and added it to diesel soot and showed a reduction in the temperature at which carbon becomes oxidized of about 170° C. NaCl reduced the oxidation temperature by 27° to 90° C depending on the temperature protocol. Considering five of the six NaCl experiments resulted in oxidation reductions of 60° C or higher, the 27° C change may be an outlier. These results were in agreement with Grosjean et al. (1994) which observed a

reduction in oxidation temperature when lab generated NaCl was deposited on top of ambient tunnel samples. $CaCl_2$ resulted in an oxidation temperature reduction of 75° to 85° C, in contrast to Mul et al. (1998) which showed that $CaCl_2$ mixed with a model diesel soot (Printex-U) had little effect on the oxidation temperature.

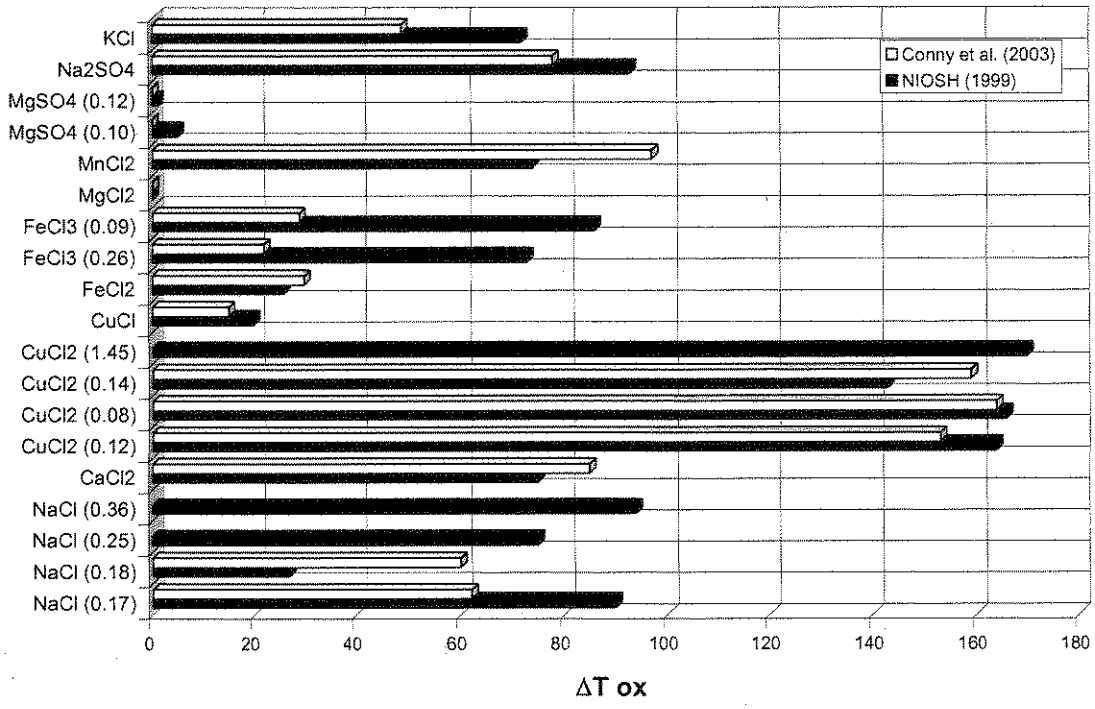

Figure 3-7: The effect of metal salts on the oxidation temperature of the low volatility carbon associated with diesel soot. For metals where multiples experiments were conducted, the resulting M/C ratio deposited on the filter is shown in parenthesis.

Metal	TC (μg/filter) w/cat	TC (μg/filter) w/o cat	M/C Ratio	EC/OC w/cat	EC/OC w/o cat	EC/OC % diff	Split Time w/cat	Split Time w/o cat	Split Time Δ	Temp (°C) w/cat	Temp (°C) w/o cat	Temp (°C) Δ
$CaCl_2$	62.1	70.8	1.07	1.69	1.80	-6	347	529	-182	792	867	-75
$MnCl_2$	108.4	124.0	0.28	1.54	2.25	-32	416	518	-102	791	865	-74
CuCl	53.7	57.9	0.09	1.81	1.46	24	461	501	-40	865	885	-20
$CuCl_2$	61.7	45.3	0.12	2.99	2.65	11	406	503	-97	721	885	-164
	106.5	107.5	0.08	1.64	1.44	14	431	546	-115	724	890	-166
	71.3	69.1	0.14	3.84	1.87	105	239	521	-282	722	865	-143
	43.6	46.1	1.45	1.15	0.94	18	417	544	-127	698	868	-170
$FeCl_2$	46.7	58.3	0.17	1.77	2.01	-12	449	532	-83	790	816	-26
$FeCl_3$	59.6	58.3	0.26	4.41	2.01	119	144	532	-388	794	867	-73
	103.8	100.8	0.09	4.27	2.34	83	307	534	-227	794	880	-86
KCl	64.1	55.8	0.27	1.55	2.44	-36	472	329	143	793	865	-72
NaCl	109.4	100.2	0.17	1.52	2.45	-38	447	537	-90	755	845	-90
	83.4	76.3	0.18	1.30	1.39	-7	491	541	-50	858	885	-27
	30.0	30.4	0.25	1.67	2.20	-32	445	520	-75	790	865	-75
	43.2	39.8	0.36	1.19	2.83	-138	425	541	-116	771	865	-94
Na_2SO_4	92.5	86.0	0.11	1.55	1.27	22	434	537	-103	775	868	-93
$MgCl_2$	37.7	57.4	0.30	2.13	2.57	-17	322	300	22	865	865	0
$MgSO_4$	75.0	75.3	0.10	2.02	2.19	-8	319	542	-223	914	919	-5
	65.0	66.7	0.12	1.81	3.59	-50	521	458	63	869	870	-1
				Avg:	2.09			503			870	
				σ_d:	0.63			70			20	

Table 3-3a: Experiments conducted to determine the catalytic effect of metal salts and sulfates on the oxidation of high EC soot particles. The M/C ratio deposited on the filter is shown. Data shown is analysis of samples by the NIOSH (1999) method.

Metal	TC (µg/filter)		M/C	EC/OC			Split Time			Temp (°C)		
	w/cat	w/o cat	Ratio	w/cat	w/o cat	% diff	w/cat	w/o cal	Δ	w/cat	w/o cat	Δ
$CaCl_2$	48.8	71.2	1.07	1.65	1.96	-16	302	601	-299	792	877	-85
$MnCl_2$	119.7	103.6	0.28	1.83	2.21	-17	360	598	-238	772	869	-97
CuCl	66.9	62.9	0.09	1.80	1.44	25	529	603	-74	866	881	-15
$CuCl_2$	63.1	55.4	0.12	1.73	1.91	9	496	593	-103	728	881	-153
	105.4	114.3	0.08	5.79	3.07	89	337	593	-256	720	884	-164
	81.8	72.3	0.14	1.38	1.95	-29	460	584	-124	722	881	-159
	-	-	-	-	-	-	-	-	-	-	-	-
$FeCl_2$	55.4	55.8	0.17	2.67	2.45	9	283	586	-303	751	781	-30
$FeCl_3$	60.0	55.8	0.26	2.49	2.45	2	274	586	-312	860	882	-22
	100.2	97.1	0.09	4.52	5.86	-23	282	558	-276	856	885	-29
KCl	65.6	57.2	0.27	2.01	2.59	-22	441	555	-114	825	874	-49
NaCl	100.9	101.9	0.17	3.36	4.23	-21	546	596	-50	821	883	-62
	84.5	80.7	0.18	1.12	1.72	-35	580	600	-20	815	875	-60
	-	-	-	-	-	-	-	-	-	-	-	-
	-	-	-	-	-	-	-	-	-	-	-	-
Na_2SO_4	87.6	83.2	0.11	3.13	2.69	16	535	589	-54	803	881	-78
$MgCl_2$	35.6	59.5	0.30	2.10	2.11	0	453	537	-84	821	821	0
$MgSO_4$	73.8	84.9	0.10	2.01	2.67	-25	444	589	-145	884	884	0
	64.0	63.7	0.12	3.93	4.29	-8	316	316	0	884	884	0
				Avg:	2.73			568			870	
				σ_d:	1.15			70			28	

Table 3-3b: Experiments conducted to determine the catalytic effect of metal salts and sulfates on the oxidation of high EC soot particles. The M/C ratio deposited on the filter is shown. Data shown is analysis of samples by the Conny et al. (2003) method.

For the few experiments investigating the effect of the M/C ratio deposited on the filter (i.e., $CuCl_2$, $FeCl_2$, NaCl), there was no consistency in the relationship between this ratio to the resulting change in the oxidation temperature. The variability in soot oxidation temperature for the control data (i.e., diesel particles only) may explain some of the variability in the reduction in soot oxidation temperature from metal to metal. The NaCl and Na_2SO_4 effects on soot oxidation temperature were both reasonably similar within variability; likewise, $MgCl_2$ and $MgSO_4$ behaved very similarly with both having almost no effect on the oxidation temperature.

Due to the large range in reported values for EC/OC ratios for the control data set, it was difficult to determine the effect of the metals on this measurement. For the NIOSH (1999) method, EC/OC ratios were in the range of 0.94 to 3.59 with an average value of 2.09 (σ_d = 0.63). The Conny et al. (2003) method had even larger variability with measured ratios in the range of 1.44 to 5.86 resulting in an average value of 2.73 (σ_d = 1.15. To detail the influence in the variability of data for the control, the $CaCl_2$ catalyst seemed to affect the EC/OC ratio with a resulting reduction of 6 to 16%; however, this reduction may be coupled with the sample to sample variability in this measurement, in addition to being related to the affect of the metal additive.

The cause for the large range in EC/OC ratios for the control was inconsistent determination of the EC/OC split point. Inspection of the laser transmission profiles showed inconsistent determination of the EC/OC split points. Correct designation of an EC/OC split point was especially important for high EC diesel particles because a majority of the mass evolves off the filter in the time range where the EC/OC split

normally occurs. Slight variations of the split point, even by seconds, can have a huge effect on the resulting EC/OC ratio. After charring of the particulate OC, the laser transmission will gradually increase and eventually surpass the transmission level initially observed before starting the analysis. This is the point where the EC/OC split point should occur. For most of the samples, the split point was found to be at a laser transmission level that was higher than that measured initially leading to underestimations of the amount of EC. Although further research is necessary to determine a method to correctly adjust the EC/OC split point, for purposes of this paper, of the EC/OC split point will be adjusted to the point where the laser transmission during analysis increases to that initially observed.

Two unique characteristics of high EC diesel particles that caused complications during EGA was the fact that very little charring occurs during inert heating of the sample during analysis and that a large fraction of the carbon evolved in the period where split times typically occur. With the near constant laser transmission through the filter during analysis, the software had difficulty distinguishing when the laser transmission returns back to the original level. The sensitivity of the EC/OC ratio to split point was illustrated in the thermogram for diesel particles with (bold) and without (non-bold) the presence of a $FeCl_3$ catalyst (Figure 3-8). From the thermograms, a bulk of the carbon mass evolved from the filter during a time where the EC/OC split occurred for the control. Since there was very little OC in these particles, the slightest deviation in the EC/OC split will have large impact on the resulting EC/OC ratio. Both carbon evolution and laser tramission through the filter are shown. For both samples it was determined

that the EC/OC split time was inappropriately set. The split time for the control was initially determined to be at 534 s; however the time at which the laser transmission reaches the initial level was 525s. By changing the split time by 9 s for the control sample in the above figure, the EC/OC ratio changed from 2.34 to 2.85, almost a 22% increase

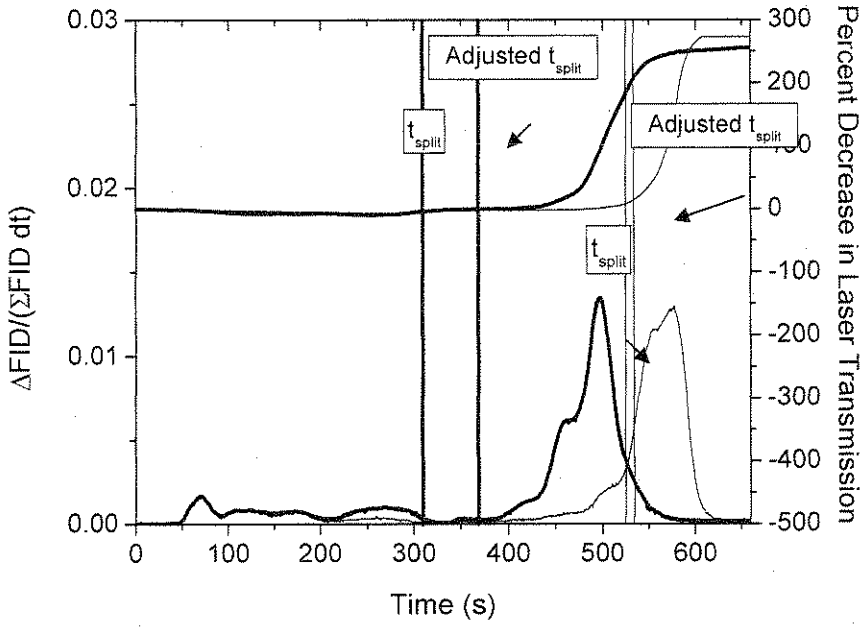

Figure 3-8: Carbon evolution profiles of high EC diesel particles mixed with $FeCl_3$ using the NIOSH (1999) temperature protocol. The control is shown in non-bold and the effect of adding $FeCl_3$ is shown in bold.

Manually setting the EC/OC split point resulted in a narrower range of measurements for the pure diesel particles and values of EC/OC ratios more similar to those published in the literature (Chung et al., 2008). In comparison, the NIOSH (1999) (Table 3-4a) method results in smaller EC/OC ratios with less spread in the data than the

Conny et al. (2003) method (Table 3-4b). There was also less variation in the EC/OC split times of the control after making the adjustment. Considering the better reproducibility in the data for the control using data with manually adjusted EC/OC split point, all forthcoming analysis will be using EC/OC split adjusted data.

Metal	TC (µg/filter)		M/C	EC/OC			Split Time			Temp (°C)		
	w/cat	w/o cat	Ratio	w/cat	w/o cat	% diff	w/cat	w/o cat	Δ	w/cat	w/o cat	Δ
$CaCl_2$	62.1	70.8	1.07	1.69	2.76*	-39	347	500*	153	792	867	-75
$MnCl_2$	108.4	124.0	0.28	1.93*	2.77*	-30	402*	503*	101	791	865	-74
CuCl	53.7	57.9	0.09	1.81	1.91*	-5	461	465*	4	865	885	-20
$CuCl_2$	61.7	45.3	0.12	2.99	2.65	13	406	503	97	721	885	-164
	106.5	107.5	0.08	3.93*	2.73*	44	400*	526*	126	724	890	-166
	71.3	69.1	0.14	3.38*	2.61*	30	260*	495*	235	722	865	-143
	43.6	46.1	1.45	2.36*	2.30*	16	320*	500*	180	698	868	-170
$FeCl_2$	46.7	58.3	0.17	1.77	2.91*	-39	449	509*	60	790	816	-26
$FeCl_3$	59.6	58.3	0.26	4.41	2.91*	52	144	509*	365	794	867	-73
	103.8	100.8	0.09	4.08*	2.85*	43	360*	525*	165	794	880	-86
KCl	64.1	55.8	0.27	1.99*	2.44	-18	456*	329	-127	793	865	-72
NaCl	109.4	100.2	0.17	1.52	2.45	-38	447	537	90	755	845	-90
	83.4	76.3	0.18	2.01*	2.38*	-16	457*	509*	52	858	885	-27
	30.0	30.4	0.25	3.00*	2.72*	10	421*	475*	54	790	865	-75
	43.2	39.8	0.36	2.83*	2.85*	1	425*	500*	75	771	865	-94
Na_2SO_4	92.5	86.0	0.11	2.61*	2.7*	-3	414*	493*	79	775	868	-93
$MgCl_2$	37.7	57.4	0.30	2.13	2.57	-17	322	300	-22	865	865	0
$MgSO_4$	75.0	75.3	0.10	2.02	2.84*	-29	319	525*	206	914	919	-5
	65.0	66.7	0.12	2.31*	2.46*	-6	502*	512*	10	869	870	-1
				Avg:	2.53			417			870	
				σ_d:	0.10			120			20	

Table 3-4a: Resulting EC/OC measurements of high EC diesel particles with and without the presence of metal catalysts. The cells noted with (*) indicate data which required manual adjustment of the EC/OC split point. Data shown is analysis of samples by the NIOSH (1999) method.

Metal	TC (µg/filter)		M/C	EC/OC			Split Time			Temp (°C)		
	w/cat	w/o cat	Ratio	w/cat	w/o cat	Δ	w/cat	w/o cal	Δ	w/cat	w/o cat	Δ
$CaCl_2$	48.8	71.2	1.07	1.65	2.94*	-44	302	580*	278	720, 863	877	-86
$MnCl_2$	119.7	103.6	0.28	1.42*	2.21	-36	396*	598	202	772	869	-97
CuCl	66.9	62.9	0.09	1.80	2.19*	-18	529	582*	53	866	881	-15
$CuCl_2$	63.1	55.4	0.12	2.71*	2.77*	-2	400*	425*	25	728	881	-153
	105.4	114.3	0.08	5.79	3.07	89	337	593	256	720	884	-164
	81.8	72.3	0.14	1.75*	2.82*	-38	410*	440*	30	722	881	-159
	-	-	-	-	-	-	-	-	-	-	-	-
$FeCl_2$	55.4	55.8	0.17	2.58*	3.36*	-23	330*	467*	137	751	781	-30
$FeCl_3$	60.0	55.8	0.26	2.49	3.36*	-26	274	467*	193	860	882	-22
	100.2	97.1	0.09	4.52	5.86	-23	282	558	276	856	885	-29
KCl	65.6	57.2	0.27	2.01	2.59	-22	441	555	114	825	874	-49
NaCl	100.9	101.9	0.17	3.36	4.23	-21	546	596	50	821	883	-62
	84.5	80.7	0.18	1.58*	2.64*	-40	566*	570*	4	815	875	-60
	-	-	-	-	-	-	-	-	-	-	-	-
	-	-	-	-	-	-	-	-	-	-	-	-
Na_2SO_4	87.6	83.2	0.11	4.13*	4.39*	-6	400*	500*	100	803	881	-78
$MgCl_2$	35.6	59.5	0.30	2.15*	2.71*	-21	440*	509*	69	821	821	0
$MgSO_4$	73.8	84.9	0.10	2.01	3.23*	-38	444	560*	116	884	884	0
	64.0	63.7	0.12	3.93	3.01*	31	316	585*	269	884	884	0
				Avg:	3.21			537			870	
				σ_d:	0.93			59			28	

Table 3-4b: Resulting EC/OC measurements of high EC diesel particles with and without the presence of metal catalysts. The cells noted with (*) indicate data which required manual adjustment of the EC/OC split point. Data shown is analysis of samples by the Conny et al. (2003) method.

For both temperature programs, significant effects were observed with the exception of Na_2SO_4. Although both NaCl and Na_2SO_4 had similar affects on the oxidation temperature of soot, the catalytic nature of NaCl seems to have a larger impact on the EC/OC ratio than Na_2SO_4. Metals which did not affect the oxidation temperature of soot such as $MgSO_4$ and MgCl, resulted in large effects on the EC/OC ratio. Changes to the EC/OC ratio caused by the addition of metals varied from -39% to +52% and -44% to +89% for the NIOSH (1999) and Conny et al. (2003) method. The catalytic effects of $CuCl_2$ and $FeCl_3$ were dependent on the temperature program used. The $CuCl_2$ additive resulted in a 13 to 44% increase in the measurement of the EC/OC ratio for diesel particles when analyzed by the NIOSH (1999) method. The same sample analyzed by the Conny et al. (2003) method showed much greater variability in the results with anywhere from a decrease of 38% to an increase of 89%. $FeCl_3$ resulted in a large reduction in the EC/OC ratio (43 to 52%) for the NIOSH (1999) method over a large range of metal to carbon mass ratios deposited on the filter. Analysis by the Conny et al. (2003) method showed decreases of the EC/OC ratio for high EC diesel particles up to 26% caused by the $FeCl_3$ catalyst.

It should be noted that the iron chloride compounds discolored during heating. EGA of metal aerosols deposited on a quartz filter showed that the laser transmission decreased by about 23% during EGA when 18 μg of $FeCl_3$ was deposited on a quartz filter. In comparison to other metals, NaCl and $CuCl_2$ darkened slightly by 6 and 8% when 15 and 42 μg were deposited, respectively; however this decrease was negligible

because a clean quartz filter being heated in EGA resulted in similar decreases in laser transmission.

The darkening of iron was highly problematic because EGAs rely on laser transmittance through the filter during analysis to determine the location of the EC/OC split and to correct for charring. Due to any darkening of atmospheric inorganic species on the quartz filter during heating, the laser transmittance in the EGA will be overly reduced thus creating the incorrect appearance that char is being formed. The increased laser absorption due to the metal oxides was not recovered as the filter continues to be heated. Even if this was recovered, it most likely happened later in the temperature program so that the EC/OC split was applied later than it should. From Table 3-4a and 4b, the darkening effect of iron compounds had an opposite effect on the location of the EC/OC split as anticipated and produced the largest reductions in EC/OC split times. For Fe (II) there was either a reduction of 23 to 39% in the EC/OC ratio when analyzing by the NIOSH (1999) or Conny et al. (2003) profile. Another striking difference in results was observed when using the $FeCl_3$ catalyst. The NIOSH (1999) method showed very large increases in the EC/OC ratio (43 to 52%) whereas the Conny et al. (2003) method showed a reduction of 23 to 36%.

Figure 3-9 plots each metal's effect on the reduction of soot oxidation temperature to the resulting change in split time. High EC particles char very slightly, so the location of the EC/OC split was more a function of the removal of dark carbon from the filter (i.e, EC or BC). Since metal catalysts reduce the oxidation temperature of this carbon, it was expected to also reduce EC/OC split times. Even at small changes in oxidation

temperature there were large changes in the EC/OC split time. The data seems to show a large reduction in oxidation temperature with a drop in split time; however, the scatter was significant and it is difficult to make any conclusions.

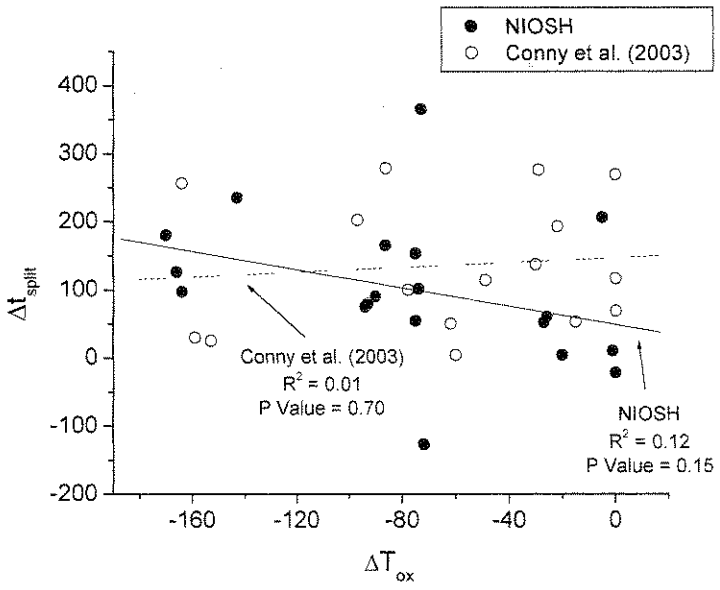

Figure 3-9: The change in soot oxidation temperature due to the addition of a metal catalyst plotted against the reduction in EC/OC split time during EGA.

Generally it was expected that earlier split times will partition more carbon to EC than OC and thus be correlated with higher EC/OC ratios, and the plot of change in split time compared to measured EC/OC ratio for our samples in figure 3-10 shows a trend in this direction; however, the intercept was not zero and reductions in split time up to 300 s were associated with lower EC/OC ratios. Presumably this was because while metals tend to increase char, they also catalyzed its oxidation and this latter effect dominates. In principle the laser transmittance through the filter should compensate for the extra charring and early evolution of the char, but according to the measurements,

transmittance alone was insufficient in correcting for the effect of catalytic metal additives.

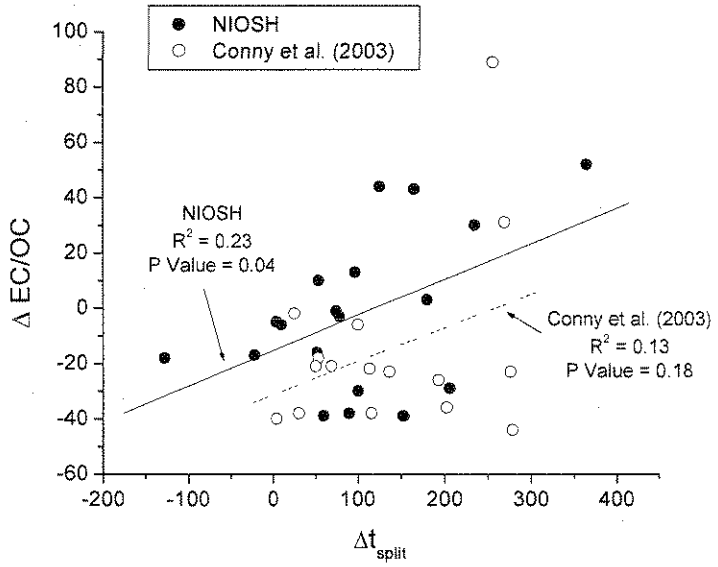

Figure 3-10: Relationship between the percent change in the EC/OC ratio to the resulting change in split time when using a metal catalyst

Figure 3-11 plots the change of soot oxidation temperature to the change in EC/OC ratio. Most all of the metals tested resulted in lower EC/OC ratios compared to the control diesel soot. The dashed line indicates no change in EC/OC ratio. If the EGA was able to correct for the early oxidation of soot, all the data points should line up along this line. For a reference point, the vertical line shows the reduction in oxidation temperature of diesel soot when ambient TSP was used as the catalyst. Even though the metals tested do not affect the oxidation temperature to the degree that TSP did, there was still a large effect on the EC/OC ratios, even with small reductions in the oxidation

temperatures. From the data available, there was no correlation between a metal's ability to reduce the oxidation of carbon to the resulting measurement of the EC/OC ratio.

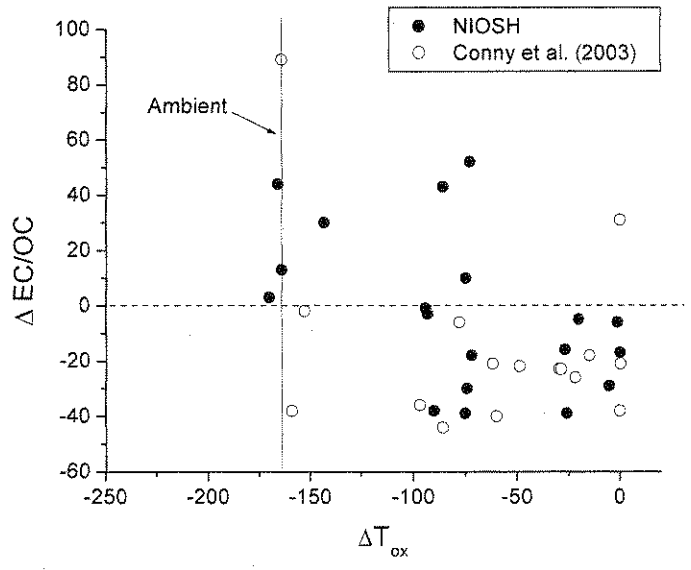

Figure 3-11: Correlation between a metal compound's ability to affect the diesel EC/OC ratio and the oxidation temperature of soot.

Catalytic Mechanisms

Both the NIOSH (1999) and Conny et al. (2003) methods showed very similar, yet poor, R^2 and P values when correlating the change in oxidation temperature and catalyst mobility particle size. (Figure 3-12). Data for MgCl and $MgSO_4$ were not included in this graph since they did not exhibit any catalytic effect on the oxidation temperature of soot. Although having small R^2 values, a general trend, relative to the other correlations, was observed showing that metal aerosols with higher mobility diameters may cause larger reductions in the oxidation temperature.

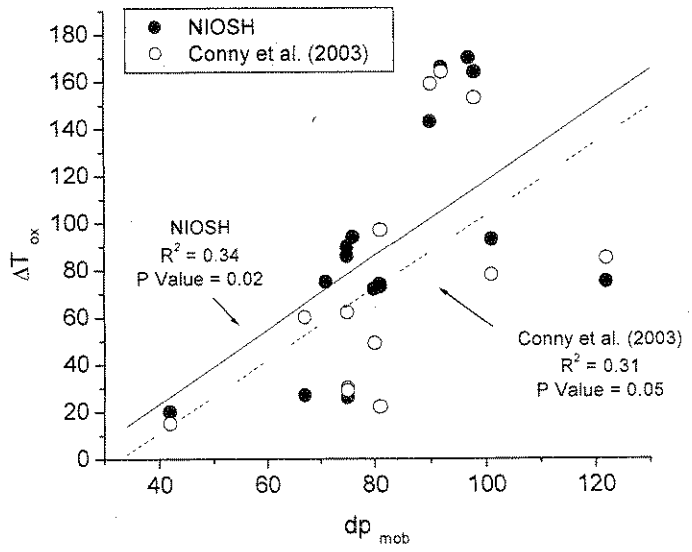

Figure 3-12: Relationship between mobility diameters of metal chlorides/sulfates measured by the SMPS to the change in oxidation temperature of diesel soot.

Several reports in the literature have shown a relationship between the reduction in soot oxidation temperature and the melting point of the metal chloride catalyst (Neeft et al. 1996; Mul et al. 1998; Stanmore et al. 2001). It should be noted that in these references, dry metal chloride powder was physically mixed with Printex-U before thermal analysis. There was no initial phase of heating in an inert atmosphere; they heated their sample solely in an oxidizing atmosphere in contrast to the EGA method. These workers suggested that metal chlorides with low melting points and high vapor pressures were more effective as catalysts due to their increased mobility through the soot during heating. In Figure 3-13, there was a weak relationship between the melting points of the metal chloride and its catalytic effect; however, metals with lower melting points seemed to result in larger reductions in the oxidation temperature. Both the Conny et al.

(2003) and NIOSH (1999) temperature protocol reached temperatures close to 900 °C, above the melting points of all of the compounds tested.

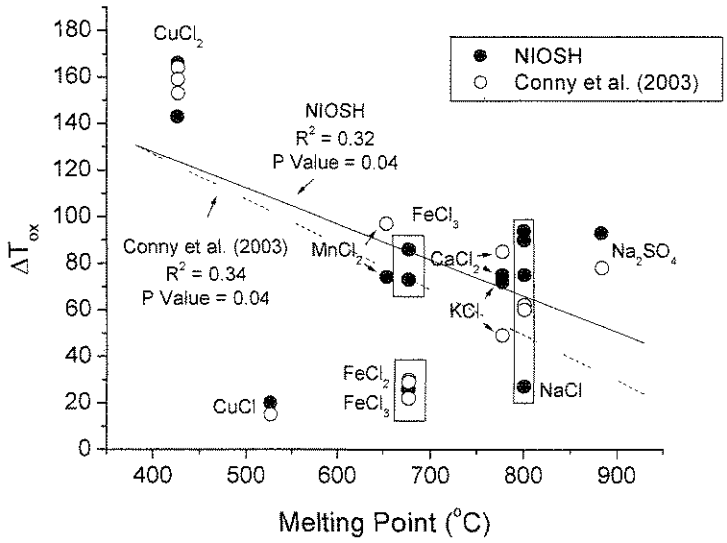

Figure 3-13: The melting points of metal chlorides and sulfates plotted against the corresponding reduction in oxidation temperature.

Catalytic Effects of Metal Chloride Combinations on High EC Particles

Since the ambient aerosol is a complex mixture of various metals, it is important to understand how combinations of various metals affect thermal stability and measurement of EC/OC ratios for diesel particles. Experiments using NaCl with a combination of $CaCl_2$, $FeCl_2$, or $CuCl_2$ were used as the metal catalysts and were combined with high EC diesel particles on a quartz filter. A sensitivity analysis was also conducted to determine how the proportion of metals in a catalyst mixture affects the carbon measurement of diesel particles. Table 3-5a and 5b shows the amount of metal and carbon mass deposited on the quartz filter along with the resulting change in

oxidation temperature, EC/OC ratio, and split time caused by the addition of a mixture of metal catalysts. Table 3-6 shows EC/OC ratios after the adjustment of split times.

The addition of NaCl to $CaCl_2$ showed no effect on the oxidation temperature of EC for either temperature protocols. Even though there was a reduction in oxidation temperature, this change was very similar to that when using $CaCl_2$ alone as a catalyst (~792° C). The thermograms in figure 3-14 shows the catalytic effect on soot oxidation temperature when NaCl is mixed with $FeCl_2$. When a small amount of Na was added to Fe (II) (Na:Fe – 0.36) it was observed that the oxidation temperature is similar to that of when $FeCl_2$ alone was used as a catalyst. As more Na (Na:Fe – 2.14) was added to the catalyst, the soot oxidation temperature dropped more by about 150° C. This dependence of oxidation temperature on the catalyst's Na/Fe (II) mass ratio was seen using both the NIOSH (1999) and the Conny et al. (2003) method.

Figure 3-15 shows a thermogram of diesel particles mixed with a Na/Cu catalyst. A Na/Cu (II) mass ratio of 1.6 resulted in a drop in oxidation temperature of 160° C which was very similar to that when using only $CuCl_2$ (143° to 166° C). When using a smaller Na/Cu (II) mass ratio the oxidation temperature of soot was reduced by only 80° C. Using the Conny et al. (2003) method, there was also a very large drop in oxidation temperature (180° C) with the Na:Cu catalyst mass ratio of 1.6. When $CuCl_2$ was solely used as a catalyst there was a drop in oxidation temperature of (153° to 164° C) using the same temperature program. The catalyst with a Na:Cu ratio of 0.8 resulted in a smaller change in oxidation temperature of only 25°C. As opposed to iron, sodium did not seem to enhance the reduction of oxidation temperature of $CuCl_2$.

Metal	Catalyst (μg/filter)	NIOSH (1999)		Conny et al. (2003)		NIOSH (1999) T_{ox}				Conny et al. (2003) T_{ox}			
		w/cat	w/o cat	w/cat	w/o cat	w/cat	w/o cat	Δ	Control	w/cat	w/o cat	Δ	Control
NaCl - $CaCl_2$	34 (Ca) / 20 (Na)	39.0	44.5	40.1	51.5	780	870	90	792	850	900	50	791
NaCl - $FeCl_2$	7 (Fe) / 15 (Na)	35.7	22.6	36.7	32.3	710	860	150	790	710	880	170	751
NaCl - $FeCl_2$	14 (Fe) / 5 (Na)	28.3	22.6	22.9	32.3	795	860	65	790	850	880	30	751
NaCl - $FeCl_2$	16 (Fe) / 11 (Na)	28.7	22.6	31.9	32.3	770	860	90	790	710	880	170	751
NaCl - $CuCl_2$	5 (Cu) / 8 (Na)	43.6	38.4	44.2	36.3	710	870	160	716	710	890	180	723
NaCl - $CuCl_2$	6 (Cu) / 5 (Na)	33.7	38.4	31.9	36.3	790	870	80	716	865	890	25	723
						Avg:	865			**Avg:**	887		
						σ_d:	5			σ_d:	8		

Control column is the oxidation temperature of high EC diesel particles when mixed with only $CaCl_2$, $FeCl_2$, or $CuCl_2$ (Table 4a and 4b)
For $CuCl_2$ the control oxidation temperature is an average of the multiple experiments

Table 3-5a: Experiments conducted to determine the catalytic effect of a combination of metal salts on the oxidation of high EC soot particles.

Catalyst	NIOSH (1999)						Conny et al. (2003)					
	EC/OC Ratio			Split Time			EC/OC Ratio			Split Time		
	w/cat	w/o cat	% diff	w/cat	w/o cat	Δ	w/cat	w/o cat	% diff	w/cat	w/o cat	Δ
NaCl - $CaCl_2$	2.34	2.99	-22	431	459	28	2.75	3.29	-16	480	590	110
NaCl - $FeCl_2$	0.68	2.93	-77	319	454	135	1.52	3.22	-53	442	562	120
NaCl - $FeCl_2$	0.83	2.93	-72	324	454	130	0.41	3.22	-87	564	562	-2
NaCl - $FeCl_2$	0.95	2.93	-68	299	454	155	0.94	3.22	-71	321	562	241
NaCl - $CuCl_2$	0.63	2.59	-76	462	504	42	0.86	3.15	-73	526	503	-23
NaCl - $CuCl_2$	0.45	2.59	-83	438	504	66	0.45	3.15	-86	529	503	-26
	Avg:	2.83		**Avg:**	471		**Avg:**	3.21		**Avg:**	547	
	σ_d:	0.18		σ_d:	25		σ_d:	0.05		σ_d:	35	

Table 3-5b: Experiments conducted to determine the catalytic effect of a combination of metal salts on the oxidation of high EC soot particles.

Catalyst	NIOSH (1999)						Conny et al. (2003)					
	EC/OC Ratio			Split Time			EC/OC Ratio			Split Time		
	w/cat	w/o cat	% diff	w/cat	w/o cat	Δ	w/cat	w/o cat	% diff	w/cat	w/o cat	Δ
NaCl - $CaCl_2$	2.34	2.99	-22	431	459	28	2.75	3.29	-16	480	590	110
NaCl - $FeCl_2$	0.68**	2.93	-77	347*	454	107	1.68*	3.22	-48	414*	562	148
NaCl - $FeCl_2$	0.65*	2.93	-78	450*	454	4	0.55*	3.22	-83	556*	562	6
NaCl - $FeCl_2$	0.70*	2.93	-76	450*	454	4	0.86*	3.22	-73	446*	562	116
NaCl - $CuCl_2$	0.70*	2.59	-73	455*	504	49	0.94*	3.15	-73	493*	503	10
NaCl - $CuCl_2$	0.62*	2.59	-76	419*	504	85	0.69*	3.15	-80	461*	503	42
	Avg:	2.83			471			3.21			547	
	σ_d:	0.18			25			0.05			35	

Table 3-6: Experiments conducted to determine the catalytic effect of a combination of metal salts on the oxidation of high EC soot particles with adjusted split times. Data marked with a (*) indicate those which changed due to adjustment of split time. Cell marked with (**) indicates that split time adjustment was necessary but no resulting change in the EC/OC ratio.

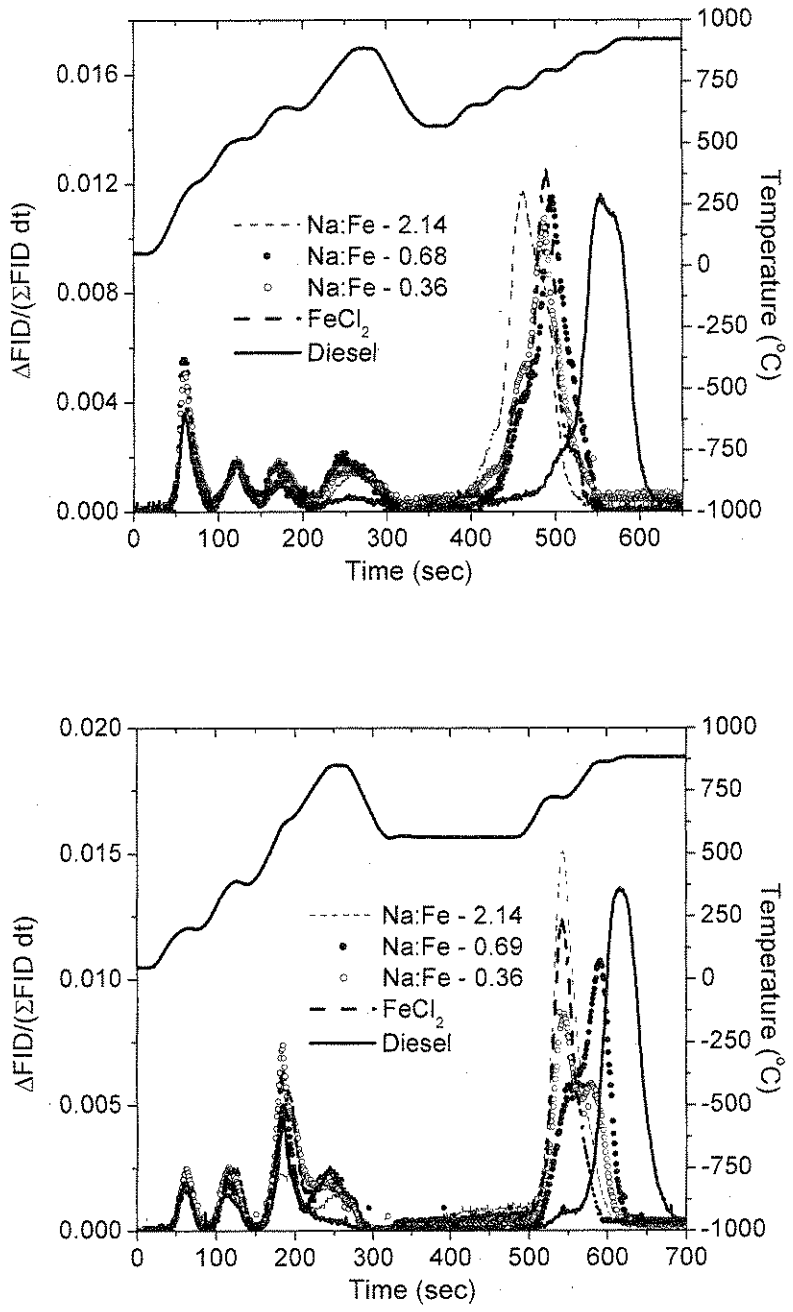

Figure 3-14: Carbon evolution profile for diesel PM mixed with a combination of NaCl and $FeCl_2$ analyzed by the NIOSH (1999) (top) and Conny et al. (2003) (bottom) method.

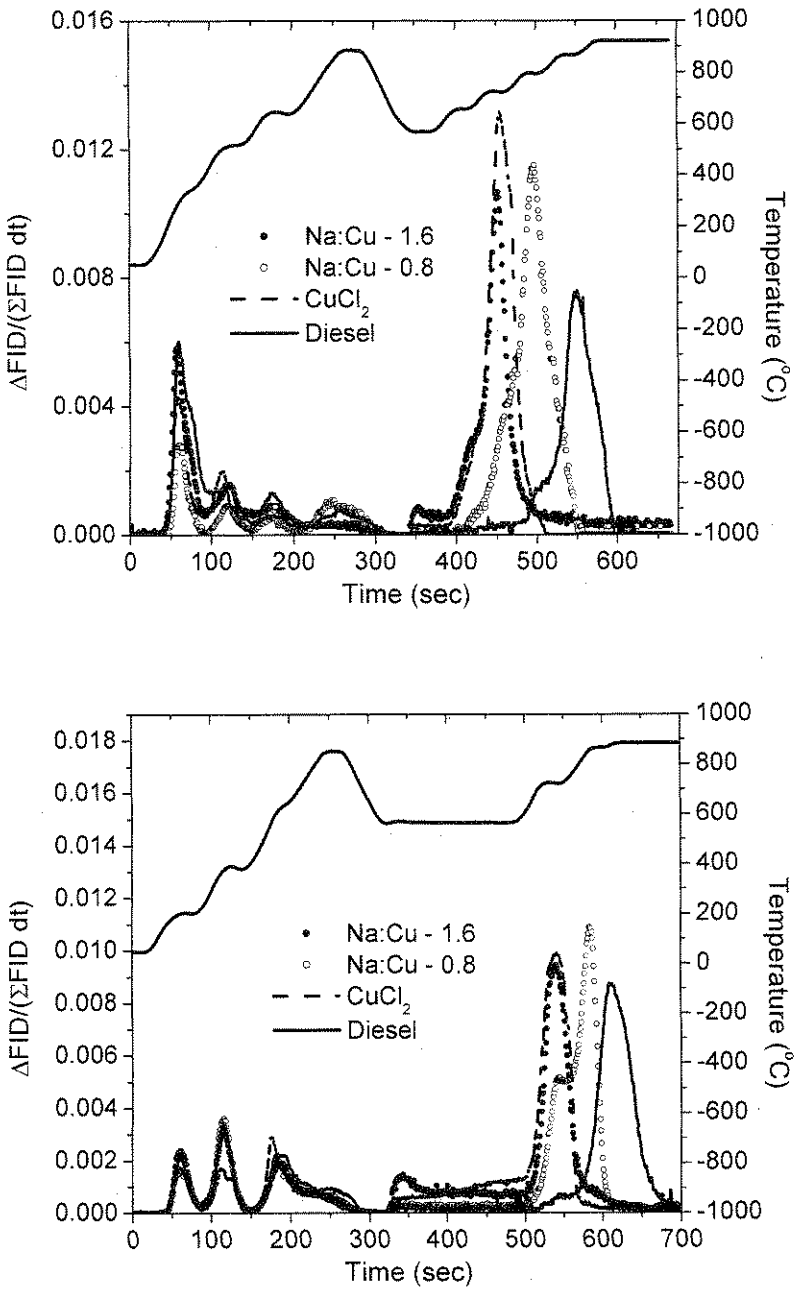

Figure 3-15: Carbon evolution profile for diesel PM mixed with a combination of NaCl and $CuCl_2$ analyzed by the NIOSH (1999) (top) and Conny et al. (2003) (bottom) method.

The largest effect observed was for the measurement of the EC/OC ratios with the exception of the $NaCl/CaCl_2$ catalyst. It was previously shown that, regardless of temperature program, $CaCl_2$ reduced the EC/OC ratio of diesel particles by about 39% to 44%. By adding NaCl to the catalyst mixture, a reduction of 22% and 16% for the EC/OC ratios using the NIOSH (1999) and Conny et al. (2003) profile was observed. Taking the average reduction in EC/OC ratios for the $NaCl/FeCl_2$ experiments there was a reduction of 77% and 68% when the NIOSH (1999) and Conny et al. (2003) profile were used. This was a much greater reduction as opposed to using $FeCl_2$ alone (23 to 39% reduction). The most drastic catalytic effect on the EC/OC ratio was the combination of NaCl and $CuCl_2$. When averaging the reduction in EC/OC ratio when high EC diesel particles are in the presence of the $NaCl/CuCl_2$ catalyst, there was a drop in EC/OC ratio in excess of 75% regardless of temperature program. When looking at the ratios for when diesel particles were mixed with $CuCl_2$ alone, the EC/OC ratio changed anywhere from a decrease of 38% to an increase of 89%.

II. High OC Diesel Particles

Metal catalysts not only affected the oxidation temperature of the low volatile soot, but they also increased the production of char during the initial inert heating phase of the EGA. The diesel generator was operated at low loads to produce particles high in OC content. Char was quantified using two different measures. The first was the amount of carbon removed from the filter between the introduction of oxygen into the carrier gas to the point where laser transmission increased to its initial value. The amount of carbon

evolved during this period was expressed as a percentage of the total carbon evolved during the entire analysis, and is referred to here as char by evolution. The second measure of char was the percent reduction of laser transmission through the filter during the inert heating phase of EGA and is called char by transmission.

The first set of experiments was conducted on diesel particles emitted at low loads without the use of a denuder upstream of the filter holder. Table 3-7a and 7b summarizes the data obtained with and without adjustments to the EC/OC split point. $CaCl_2$ and NaCl were mixed with diesel particles emitted at 25% load, hence the higher baseline EC/OC ratios, whereas the other metals were mixed with diesel particles at lower loads. Both NaCl and $CaCl_2$ reduced the EC/OC ratio and enhanced the char production during inert heating. $CaCl_2$ resulted in more carbon being evolved as charred OC as compared to NaCl; however the NaCl catalyst resulted in more darkening of the filter spot. Since it was shown earlier that $CaCl_2$ reduces the oxidation oxidation temperature of EC to a greater extent than NaCl, it was possible that some native EC evolved during the period where char was classified, thus overestimating the amount. This hypothesis was tested by noting that during the time of the EC/OC split when using $CaCl_2$ on particles emitted at 25% load analyzed by the NIOSH (1999) method, the temperature was 795° C. According to the data for native EC particles emitted at high load (Tables 3-4a and 4b), the native EC evolution peaked at about 792° C which was 3° C less than the temperature at the EC/OC split for the diesel particles emitted at 25% load. From this example it was evident that due to the reduction in oxidation temperature of carbon, some of the native EC was evolved as char.

NIOSH (1999)																
	TC (µg/filter)		M/C	EC/OC			Split Time			Char (Evolution)			Char (Transmission)			
Metal	w/cat	w/o cat	Ratio	w/cat	w/o cat	% diff	w/cat	w/o cat	Δ	w/cat	w/o cat	% diff	w/cat	w/o cat	%dif	
$CaCl_2$	117.8	125.6	0.19	0.07	0.14	-50	500	506	-6	23	17	35	33	27	22	
NaCl	122.9	125.6	0.22	0.09	0.14	-36	464	506	-42	20	17	18	37	27	37	
$MnCl_2$	153.9	163.3	0.15	0.014	0.024	-42	543	532	11	23	15	53	53	47	13	
CuCl	260.6	283.9	0.07	0.040	0.060	-33	473	520	-47	21	22	-5	57	55	4	
$CuCl_2$	214.5	283.9	0.11	0.027	0.060	-55	513	520	-7	25	22	14	60	55	9	
							Avg:	516								
							σ_d:	11								

Conny et al. (2003)																
	TC (µg/filter)		M/C	EC/OC			Split Time			Char (Evolution)			Char (Transmission)			
Metal	w/cat	w/o cat	Ratio	w/cat	w/o cat	% diff	w/cat	w/o cal	Δ	w/cat	w/o cat	% diff	w/cat	w/o cat	%dif	
$CaCl_2$	128.7	146.7	0.19	0.07	0.35	-80	579	590	-11	28	25	12	33	27	22	
NaCl	120.3	146.7	0.22	0.12	0.35	-66	534	590	-56	22	25	-12	37	27	37	
$MnCl_2$	158.3	166.0	0.15	0.016	0.08	-80	595	601	-6	28	25	12	53	47	13	
CuCl	258.3	277.3	0.07	0.039	0.048	-19	545	601	-56	22	32	-31	57	55	4	
$CuCl_2$	207.6	277.3	0.11	0.021	0.048	-56	602	601	1	31	32	-3	60	55	9	
							Avg:	597								
							σ_d:	6								

Table 3-7a: High OC diesel particles without sampling with a denuder. $CaCl_2$ and NaCl were mixed with particles emitted from the generator operation at 25% load. Other metals were mixed with particles emitted at idle load.

NIOSH (1999)															
	TC (µg/filter)		M/C	EC/OC			Split Time			Char (Evolution)			Char (Transmission)		
Metal	w/cat	w/o cat	Ratio	w/cat	w/o cat	% diff	w/cat	w/o cat	Δ	w/cat	w/o cat	% diff	w/cat	w/o cat	%dif
$CaCl_2$	117.8	125.6	0.19	0.10*	0.14	-29	490*	506	-16	21	17	24	33	27	22
NaCl	122.9	125.6	0.22	0.09	0.14	-36	464	506	-42	20	17	18	37	27	37
$MnCl_2$	153.9	163.3	0.15	0.014	0.024	-42	543	532	11	23	15	53	53	47	13
CuCl	260.6	283.9	0.07	0.040	0.060	-33	473	520	-47	21	22	-5	57	55	4
$CuCl_2$	214.5	283.9	0.11	0.027	0.060	-55	513	520	-7	25	22	14	60	55	9
							Avg:	216							
							σ_d:	11							

Conny et al. (2003)															
	TC (µg/filter)		M/C	EC/OC			Split Time			Char (Evolution)			Char (Transmission)		
Metal	w/cat	w/o cat	Ratio	w/cat	w/o cat	% diff	w/cat	w/o cal	Δ	w/cat	w/o cat	% diff	w/cat	w/o cat	%dif
$CaCl_2$	128.7	146.7	0.19	0.12*	0.16*	-25	565*	587*	-22	24	21	14	33	27	22
NaCl	120.3	146.7	0.22	0.12	0.16*	-25	534	587*	-53	22	21	5	37	27	37
$MnCl_2$	158.3	166.0	0.15	0.016	0.035*	-54	595	599*	-4	28	24	17	53	47	13
CuCl	258.3	277.3	0.07	0.039	0.071*	-45	545	595*	-50	22	30	-27	57	55	4
$CuCl_2$	207.6	277.3	0.11	0.021*	0.071*	-70	595*	595*	0	30	30	0	60	55	9
							Avg:	593							
							σ_d:	5							

Table 3-7b: High OC diesel particles without sampling with a denuder. $CaCl_2$ and NaCl were mixed with particles emitted from the generator operation at 25% load. Other metals were mixed with particles emitted at idle load. Split times were manually adjusted to account for laser transmission.

A majority of the high OC diesel particles experiments were conducted at idle load with the use of a denuder upstream of the filter. Data for these experiments are shown in table 3-8a and 8b, with data with appropriate EC/OC split times in Table 3-9a and 9b. As opposed to previous experiments where there was a wide array of metals were tested, these experiments attempted to focus on how the M/C ratio deposited on the filter affected EGA measurements.

Figure 3-16 is a thermogram of the $CuCl_2$ and diesel particle sample (M/C ratio of 0.85) analyzed by the NIOSH (1999) protocol. There was very little difference in the carbon evolution during the inert phase, but during this period there was charring from both samples, with a much higher degree of charring from the $CuCl_2$ and diesel particle sample illustrated by the change in laser transmission. Once oxygen was introduced there was a drastic change in the carbon evolution. For the diesel particles mixed with $CuCl_2$, not only was there a higher carbon peak representative of removal of the charred carbon from the filter, but there was a shift in the second peak indicating removal of the native EC at lower temperatures. As the native EC was evolved off the filter, the laser transmission gradually increased indicating that the filter spot was getting lighter.

Catalyst	TC (µg/filter)		M/C	EC/OC			Split Time			Char (Evolution)			Char (Transmission)		
	w/cat	w/o cat	Ratio	w/cat	w/o cat	% diff	w/cat	w/o cat	Δ	w/cat	w/o cat	% diff	w/cat	w/o cat	%dif
$CuCl_2$	145.7	144.2	0.04	0.25	0.27	-8	361	496	-135	5	9	-80	25	18	39
	71.1	105.4	0.59	0.18	0.20	-11	451	492	-41	28	10	64	22	9	144
	58.7	50.5	0.92	0.10	0.19	-90	429	508	-79	13	17	-31	17	7	143
	171.3	176.5	0.49	0.18	0.27	-50	457	494	-37	29	15	48	54	18	200
	108.2	93.1	0.27	0.13	0.31	-150	451	494	-43	26	16	38	37	14	164
	72.3	65.8	0.59	0.13	0.30	-131	459	496	-37	33	12	64	43	11	291
	80.9	83.7	0.47	0.09	0.14	-55	471	514	-43	34	26	24	43	20	115
	78.2	80.9	0.85	0.12	0.28	-140	455	498	-43	30	15	50	37	12	208
$FeCl_3$	139.6	134.2	0.04	0.18	0.17	6	442	495	-53	9	9	0	34	22	55
NaCl	177.1	179.5	0.05	0.17	0.18	-6	456	503	-47	17	17	0	31	26	19
	45.7	36.7	0.13	0.15	0.19	-30	447	512	-65	15	20	-33	20	14	43
	80.5	68.6	0.10	0.19	0.18	5	443	512	-69	14	20	-43	20	15	33
	87.0	94.1	0.13	0.15	0.19	-26	457	510	-53	21	19	10	23	17	35
$MgSO_4$	106.1	108.8	0.04	0.17	0.22	-29	491	494	-3	12	12	0	19	16	19
KCl	113.4	107.3	0.05	0.22	0.20	9	443	500	-57	11	9	18	23	15	53
				Avg:	0.22			501							
				σ_d:	0.05			8							

Table 3-8a: Experiments conducted to determine the catalytic effect of metal salts and sulfates on the oxidation of high OC soot particles. Data shown is analysis by the NIOSH (1999) method.

Catalyst	TC (µg/filter)		M/C	EC/OC			Split Time			Char (Evolution)			Char (Transmission)		
	w/cat	w/o cat	Ratio	w/cat	w/o cat	% diff	w/cat	w/o cal	Δ	w/cat	w/o cat	% diff	w/cat	w/o cat	%dif
$CuCl_2$	143.9	147.6	0.04	0.33	0.24	27	339	586	-247	11	15	-36	36	17	112
	82.6	70.0	0.59	0.27	0.48	-78	511	581	-70	17	14	18	19	7	171
	71.5	51.4	0.92	0.12	0.33	-175	532	568	-36	21	10	52	19	6	217
	180.5	161.7	0.49	0.16	0.34	-113	537	572	-35	29	18	38	52	19	174
$FeCl_3$	140.7	138.8	0.04	0.19	0.17	11	509	583	-74	18	17	6	23	23	0
NaCl	191.9	138.8	0.04	0.24	0.23	4	526	576	-50	16	16	0	30	24	25
$MgSO_4$	102.3	100.7	0.04	0.26	0.24	8	558	574	-16	12	14	-17	18	14	29
KCl	110.9	106.9	0.06	0.20	0.19	5	536	587	-51	16	17	-6	24	18	33
				Avg:	0.28			578							
				σ_d:	0.10			7							

Table 3-8b: Experiments conducted to determine the catalytic effect of metal salts and sulfates on the oxidation of high OC soot particles. Data shown is analysis by the Conny et al. (2003) method.

Metal	TC (µg/filter)		M/C	EC/OC			Split Time			Char (Evolution)			Char (Transmission)		
	w/cat	w/o cat	Ratio	w/cat	w/o cat	% diff	w/cat	w/o cat	Δ	w/cat	w/o cat	% diff	w/cat	w/o cat	%dif
$CuCl_2$	145.7	144.2	0.04	0.29*	0.30*	-3	350*	487*	-137	3*	8*	-167	25	18	39
	71.1	105.4	0.59	0.18	0.23*	-28	451	473*	-22	28	8*	71	22	9	144
	58.7	50.5	0.92	0.17*	0.35*	-106	405*	472*	-67	8*	7*	13	17	7	143
	171.3	176.5	0.49	0.18	0.34*	-89	457	475*	-18	29	11*	62	54	18	200
	108.2	93.1	0.27	0.21*	0.40*	-48	425*	475*	-50	19*	11*	72	37	14	164
	72.3	65.8	0.59	0.13	0.39*	-67	459	475*	-16	33	7*	371	43	11	291
	80.9	83.7	0.47	0.15*	0.25*	-40	460*	497*	-37	30*	18*	67	43	20	115
	78.2	80.9	0.85	0.18*	0.41*	-56	447*	467*	-20	25*	8*	213	37	12	208
$FeCl_3$	139.6	134.2	0.04	0.14*	0.20*	-43	460*	485*	-25	12*	7*	42	34	22	55
NaCl	177.1	179.5	0.05	0.22*	0.22*	0	447*	495*	-48	14*	15*	-7	31	26	19
	45.7	36.7	0.13	0.22*	0.34*	-35	435*	490*	-55	10*	11*	-10	20	14	43
	80.5	68.6	0.10	0.15*	0.32*	-53	440*	490*	-50	10*	11*	-10	20	15	33
	87.0	94.1	0.13	0.32*	0.31*	3	435*	490*	-55	10*	11*	-10	23	17	35
$MgSO_4$	106.1	108.8	0.04	0.26*	0.27*	-4	468*	475*	-7	8*	9*	-13	19	16	19
KCl	113.4	107.3	0.05	0.25*	0.26*	-4	433*	478*	-45	8*	5*	38	23	15	53
				Avg:	0.31			482							
				σ_d:	0.06			9							

Table 3-9a: Resulting EC/OC measurements of diesel particles with and without the presence of metal catalysts. The cells noted with (*) indicate data which required manual adjustment of the EC/OC split point. Data shown is analysis by the NIOSH (1999) method.

Metal	TC (µg/filter) w/cat	w/o cat	M/C Ratio	EC/OC w/cat	w/o cat	% diff	Split Time w/cat	w/o cal	Δ	Char (Evolution) w/cat	w/o cat	% diff	Char (Transmission) w/cat	w/o cat	%dif
$CuCl_2$	143.9	147.6	0.04	0.33	0.29*	12	339	573*	-234	11	11*	0	36	17	112
	82.6	70.0	0.59	0.32*	0.72*	-125	475*	543*	-68	14*	11*	21	19	7	171
	71.5	51.4	0.92	0.18*	0.45*	-150	513*	520*	-7	16*	3*	81	19	6	217
	180.5	161.7	0.49	0.20*	0.40*	-100	530*	560*	-30	37*	15*	59	52	19	174
$FeCl_3$	140.7	138.8	0.04	0.20*	0.20*	0	495*	573*	-78	17*	15*	12	23	23	0
NaCl	191.9	138.8	0.04	0.27*	0.27*	0	493*	555*	-62	14*	14*	0	30	24	25
$MgSO_4$	102.3	100.7	0.04	0.32*	0.29*	9	535*	555*	-20	9*	11*	-22	18	14	29
KCl	110.9	106.9	0.06	0.27*	0.24*	11	486*	576*	-90	11*	14*	-27	24	18	33
				Avg:	0.36			557							
				σ_d:	0.17			19							

Table 3-9b: Resulting EC/OC measurements of diesel particles with and without the presence of metal catalysts. The cells noted with (*) indicate data which required manual adjustment of the EC/OC split point. Data shown is analysis by the Conny et al. (2003) method.

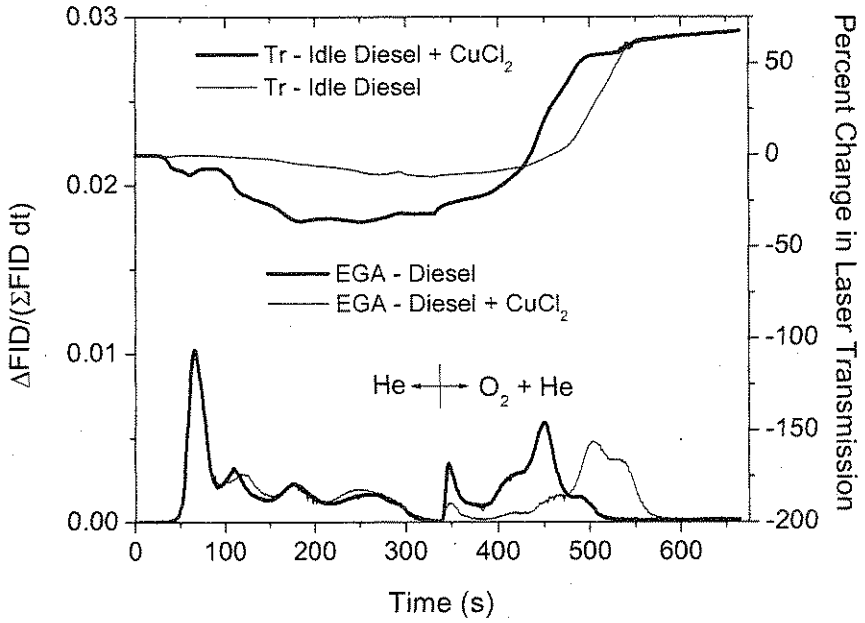

Figure 3-16: EGA thermogram of the $CuCl_2$ and idle diesel particles (M/C ratio of 0.85) analyzed by the NIOSH (1999) protocol.

Changes to the EC/OC ratio for diesel particles emitted during idle conditions seem to be sensitive to the M/C ratio, unlike particles emitted at maximum load. Figure 3-17 plots the two measures of char against the M/C ratio.

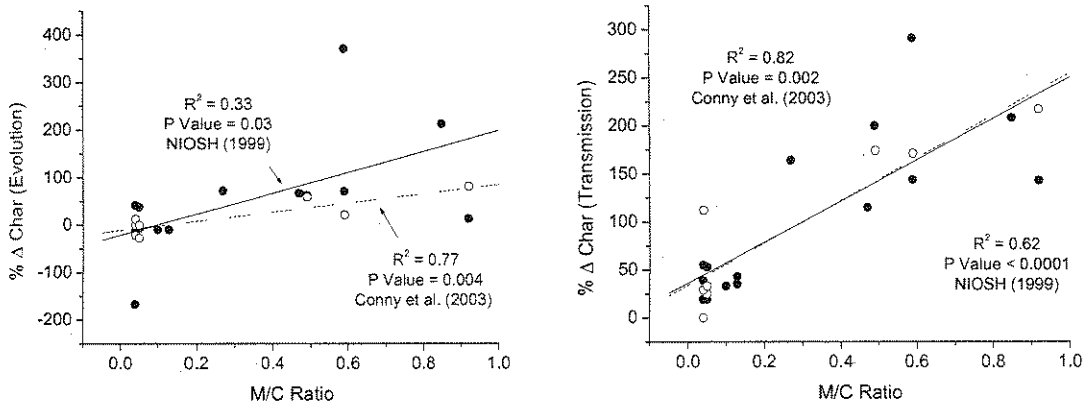

Figure 3-17: Correlations between the two measures of char to the M/C ratio deposited on the quartz filter

There was a relationship between the M/C ratio to the amount of laser reduction through the filter during EGA. As a higher proportion of metals were deposited on top of a layer of high OC diesel particles, the catalytic activity between the two aerosols during inert heating caused the filter spot to darken. The other measurement of char did not correlate well with the M/C ratio. This measurement of char may be negatively and/or positively biased due to the possibility that native EC which evolves earlier due to the catalytic activity of metals, may evolve during the period which was classified as char. Plotting the two measures of char against one another resulted in a slight correlation with low p-values (Figure 3-18).

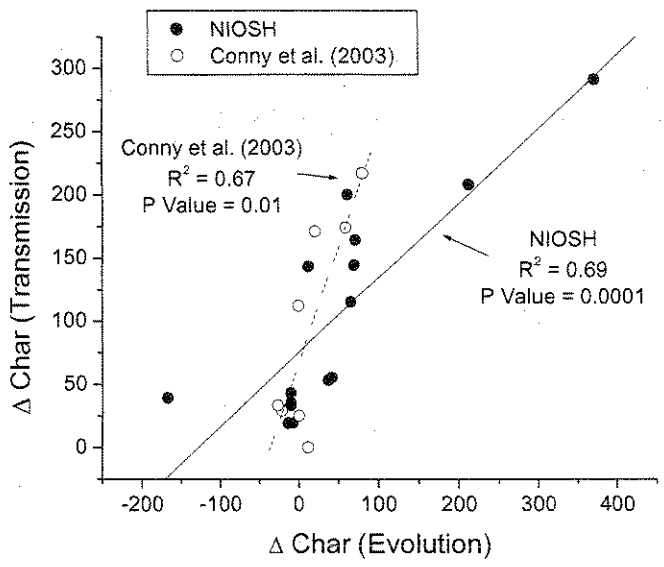

Figure 3-18: Correlation of the two measurements of char from EGA using the NIOSH (1999) and Conny et al. (2003) protocol for diesel particles emitted at idle load conditions sampled with a denuder.

For most of the data there were reductions in the EC/OC ratio, especially for the $CuCl_2$ catalyst. This catalyst over the range of M/C ratios tested showed large amounts of char for both methods of measurement. Unlike NaCl, which showed no conclusive relationship between EGA measurements and M/C ratio, $CuCl_2$ seemed to show a dependency between these two variables. Figure 3-19 plots the change in EC/OC ratio to the M/C ratio for data analyzed by the NIOSH (1999) protocol. Although there was significant spread in the limited data, the general trend was that the higher M/C ratios result in a larger decrease in the resulting EC/OC ratio.

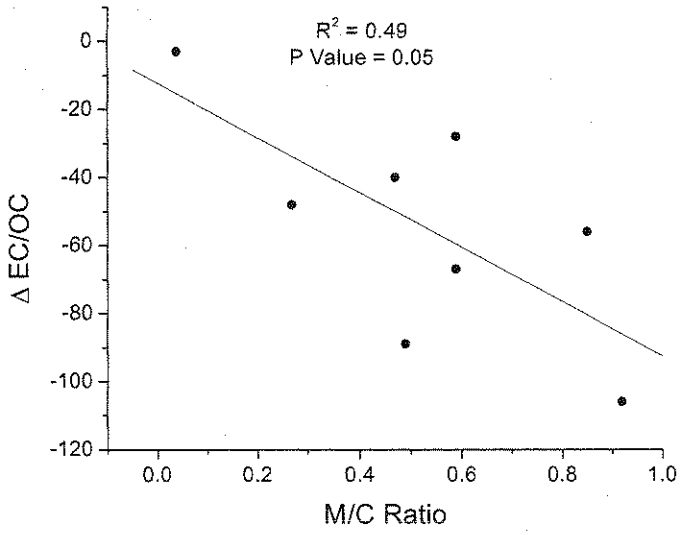

Figure 3-19: Correlation between the percentage of change in the EC/OC ratio and the M/C ratio of the sample. A relationship was observed only for $CuCl_2$.

3.4 Conclusions

Work by others and that presented here showed that components in the ambient aerosol affected the evolution of carbon in EGA. Lab generated metal salts deposited on top of a layer of high EC diesel particles resulted in lower oxidation temperatures of soot during EGA with $CuCl_2$ resulting in the largest reduction (143 to 170 °C). Only the magnesium compounds had no affect on the soot oxidation temperature. The degree of oxidation temperature reduction did not seem to depend on the amount of metal deposited on top of the diesel particles, confirming experiments using ambient aerosols as the catalyst. Examination of the control samples (i.e., diesel particles with no metal additives) showed a large spread in the measured EC/OC ratios reason being the location

of the EC/OC split. By manually adjusting the EC/OC split to the point where laser transmission equaled that initially, better repeatability of the control data resulted.

The effect of metals on EC/OC measurement for high EC diesel particles was highly variable resulting in reduction of 44% to increases of 89% when metals were mixed with diesel particles. The effect on measured EC/OC ratios was shown to possibly depend on the mobility diameter and melting point of the metal aerosol; however the correlations presented here were poor and are subject to additional experiments. The large variability in changes to the EC/OC ratio was attributed to the inconsistent thermal and optical characteristics of high EC diesel particles when mixed with metal aerosols during EGA. During analysis, the thermal evolution of a majority of the carbon for high EC diesel particles occurred during the region where the split point was typically assigned. This combined with the flat laser transmission profile during analysis made the resulting EC/OC ratio highly sensitive to the split location.

Similar to high EC diesel particles, measurements for high OC diesel particles required manual determination of the EC/OC split. The effect of metals on the thermal stability of high OC diesel particles was much more complex than that for high EC diesel particles. Not only do metals affect the oxidation temperature of the EC associated with these aerosols, they also affected the charring of the OC. Due to the increased amount of oxidized charred carbon combined with the earlier oxidation of EC with the addition of metals, most of the samples resulted in reductions of the EC/OC ratio. The amount of metals deposited on the high OC diesel particles was related to the amount of char

produced determined by the darkening of the filter spot. For the $CuCl_2$ additive, a larger affect on the EC/OC reduction was observed with high M/C ratios.

Further investigation into these findings is necessary to determine reasons as to why certain metals catalyze the evolution of carbon differently during EGA. Such steps such as the collection of more data or development of a new temperature program are necessary. Additional work is also necessary to evaluate the correct placement of the EC/OC split point. Regardless of these limitations, it is conclusive that metals do affect the measurement of diesel particles by EGA. Factors such as the reductions in oxidation temperature and increased production of char due to the presence of metals, in addition to knowing the emission source for the aerosol of interest are necessary to understand the uncertainties inherent in the EGA method.

References

Bell, T. L., et al. (2008). "Midweek increase in US summer rain and storm heights suggests air pollution invigorates rainstorms." Journal of Geophysical Research-Atmospheres **113**.

Bond, T. C. (2007). "Can warming particles enter global climate discussions?" Environmental Research Letters **2**(4).

Choularton, T. W., et al. (2008). "The influence of small aerosol particles on the properties of water and ice clouds." Faraday Discussions **137**: 205-222.

Chung, A., et al. (2001). "Comparison of real-time instruments used to monitor airborne particulate matter." Journal of the Air & Waste Management Association **51**(1): 109-120.

Chung, A., et al. (2008). "Particulate emissions by a small non-road diesel engine: Biodiesel and diesel characterization and mass measurements using the extended idealized aggregates theory." Atmospheric Environment **42**(9): 2129-2140.

Conny, J. M., et al. (2003). "Optimizing thermal-optical methods for measuring atmospheric elemental (black) carbon: A response surface study." Aerosol Science and Technology **37**(9): 703-723.

Edye, L. A., et al. (1993). "TRANSITION-METALS AS CATALYSTS FOR PYROLYSIS AND GASIFICATION OF BIOMASS." Acs Symposium Series **515**: 90-101.

Finlayson-Pitts, B. J. and J. N. Pitts (2000). Chemistry of the upper and lower atmosphere: theory, experiments, and applications. San Diego, Academic Press.

Fung, K., et al. (2002). "Evaluation of OC/EC speciation by thermal manganese dioxide oxidation and the IMPROVE method." Journal of the Air & Waste Management Association **52**(11): 1333-1341.

Grosjean, D., et al. (1994). "Evolved gas analysis of secondary organic aerosols." Aerosol Science and Technology **21**: 306-324.

Huebert, B. J. and R. J. Charlson (2000). "Uncertainties in data on organic aerosols." Tellus Series B-Chemical and Physical Meteorology **52**(5): 1249-1255.

Hughes, L. S., et al. (1998). "Physical and chemical characterization of atmospheric ultrafine particles in the Los Angeles area." Environmental Science & Technology **32**(9): 1153-1161.

Jacobson, M. Z. (2001). "Strong radiative heating due to the mixing state of black carbon in atmospheric aerosols." Nature **409**(6821): 695-697.

Kanakidou, M., et al. (2005). "Organic aerosol and global climate modelling: a review." Atmospheric Chemistry and Physics **5**: 1053-1123.

Keil, D. M. (2008). Climate Change and Sustainable Development - A Regulator's Perspective. IET Conference, London.

Kirchstetter, T. W., et al. (2001). "Laboratory and field investigation of the adsorption of gaseous organic compounds onto quartz filters." Atmospheric Environment **35**(9): 1663-1671.

Kirkevag, A., et al. (2008). "On the additivity of climate response to anthropogenic aerosols and CO2, and the enhancement of future global warming by carbonaceous aerosols." Tellus Series a-Dynamic Meteorology and Oceanography **60**(3): 513-527.

Koch, D., et al. (2007). "Linking future aerosol radiative forcing to shifts in source activities." Geophysical Research Letters **34**(5).

Levy, H., et al. (2008). "Strong sensitivity of late 21st century climate to projected changes in short-lived air pollutants." Journal of Geophysical Research-Atmospheres **113**(D6).

Lin, C. and S. K. Friedlander (1988). "SOOT OXIDATION IN FIBROUS FILTERS .2. EFFECTS OF TEMPERATURE, OXYGEN PARTIAL-PRESSURE, AND SODIUM ADDITIVES." Langmuir **4**(4): 898-903.

Mul, G., et al. (1998). "Catalytic oxidation of model soot by chlorine based catalysts." Catalysis and Automotive Pollution Control Iv **116**: 645-654.

Murphy, M. J., et al. (1981). "Assessment of diesel particulate control - direct and catayltyic oxidation." SAE Paper No. 810112.

Neeft, J. P. A., et al. (1996). "Catalysts for the oxidation of soot from diesel exhaust gases .1. An exploratory study." Applied Catalysis B-Environmental **8**(1): 57-78.

NIOSH (1999). Elemental Carbon (Diesel Particulate). NIOSH Manual of Analytical Methods (NMAM). NIOSH: Method 5040 Issue 3.

Novakov, T. and C. E. Corrigan (1995). "THERMAL CHARACTERIZATION OF BIOMASS SMOKE PARTICLES." Mikrochimica Acta **119**(1-2): 157-166.

Ramanathan, V. and G. Carmichael (2008). "Global and regional climate changes due to black carbon." Nature Geoscience **1**(4): 221-227.

Richards, G. N. and G. C. Zheng (1991). "INFLUENCE OF METAL-IONS AND OF SALTS ON PRODUCTS FROM PYROLYSIS OF WOOD - APPLICATIONS TO THERMOCHEMICAL PROCESSING OF NEWSPRINT AND BIOMASS." Journal of Analytical and Applied Pyrolysis **21**(1-2): 133-146.

Sardar, S. B., et al. (2005). "Seasonal and spatial variability of the size-resolved chemical composition of particulate matter (PM10) in the Los Angeles Basin." Journal of Geophysical Research-Atmospheres **110**(D7).

Senkan, D. S. Professor, Department of Chemical Engineering, UCLA.

Shah, S. D., et al. (2004). "Emission rates of particulate matter and elemental and organic carbon from in-use diesel engines." Environmental Science & Technology **38**(9): 2544-2550.

Shimada, N., et al. (2008). "Different action of alkali/alkaline earth metal chlorides on cellulose pyrolysis." Journal of Analytical and Applied Pyrolysis **81**: 80-87.

Silva, I. F., et al. (1997). "A kinetic and in situ XRD study of carbon reactions catalyzed by nickel, cobalt, molybdenum, and their mixtures." Journal of Catalysis **170**(1): 54-61.

Stanmore, B. R., et al. (2001). "The oxidation of soot: a review of experiments, mechanisms and models." Carbon **39**(15): 2247-2268.

Symonds, J. P. R., et al. (2007). "Diesel soot mass calculation in real-time with a differential mobility spectrometer." Journal of Aerosol Science **38**(1): 52-68.

Turner, J. R. and S. V. Hering (1994). "THE ADDITIVITY AND STABILITY OF CARBON SIGNATURES OBTAINED BY EVOLVED GAS-ANALYSIS." Aerosol Science and Technology **21**(4): 294-305.

Wang, S. H., et al. (2007). "Estimate of radiative forcing of Asian biomass-burning aerosols during the period of TRACE-P." Journal of Geophysical Research-Atmospheres **112**(D10).

Wang, Y. F., et al. (2003). "Emissions of fuel metals content from a diesel vehicle engine." Atmospheric Environment **37**(33): 4637-4643.

Wojas, B. and C. Almquist (2007). "Mass concentrations and metals speciation of PM2.5, PM10, and total suspended solids in Oxford, Ohio and comparison with those from

metropolitan sites in the Greater Cincinnati region." Atmospheric Environment **41**(39): 9064-9078.

Yin, J. X. and R. M. Harrison (2008). "Pragmatic mass closure study for PM1.0, PM2.5 and PM10 at roadside, urban background and rural sites." Atmospheric Environment **42**(5): 980-988.

Yu, J. L., et al. (2006). "Effect of iron on the gasification of Victorian brown coal with steam: enhancement of hydrogen production." Fuel **85**(2): 127-133.
sence of iron is discussed. (c) 2005 Elsevier Ltd. All rights reserved.

Yu, J. Z., et al. (2002). "Charring characteristics of atmospheric organic particulate matter in thermal analysis." Environmental Science & Technology **36**(4): 754-761.

Zhao, Y. L. and Y. Gao (2008). "Mass size distributions of water-soluble inorganic and organic ions in size-segregated aerosols over metropolitan Newark in the US east coast." Atmospheric Environment **42**(18): 4063-4078.

Chapter 4: The Catalytic Effects of Metal Salts and Sulfates on Secondary Organic Aerosols (SOA) and Biodiesel Aerosols

4.1 Introduction

Secondary organic aerosols (SOA) are formed in the atmosphere from the oxidation of volatile organic compounds (VOCs). It has been estimated that 10 to 40% of the global organic aerosol mass is attributed to SOA with about 90% of that being biogenic in nature (Volkamer et al. 2006); however, large variabilities remain in the estimate of the yearly SOA production (Bonn and Lawrence 2005). SOA can have significant impacts on visibility and climate however their impact relative to other aerosols is highly uncertain (Kanakidou et al. 2005). Model simulations have suggested that the global SOA burden will increase by 36% by 2100 with biogenic aerosols resulting in 26% of that increase (Heald et al. 2008). These estimates were achieved by updating the Community Atmosphere Model (CAM3) with recent laboratory results for SOA yield from various organic pre-cursors. Biogenic emissions were simulated using the Model of Emissions of Gases and Aerosols (MEGAN2) within the Community Land Model (CLM3).

Carbonaceous PM, both primary and secondary in nature, ranks as some of the most difficult aerosol to measure, such that basic atmospheric measurements of these materials carry uncertainties of at least 30-50% (Huebert and Charlson 2000). SOA comprises a large fraction of the particulate organic carbon (OC). OC combined with elemental carbon (EC) are often referred to as total carbon (TC). Categorically speaking,

some materials fall between OC and EC; for example, bound polyaromatic hydrocarbons (PAHs) on the surface of soot particles are not extractable by the same methods that other organics are, and have a higher C/H ratio than most organics, part way to soot.

The most common method of quantifying elemental and organic material in the atmosphere is the offline technique of using evolved gas analyzers (EGA), which provides EC and OC mass based on their respective thermal stabilities. The EGA works by evolving carbon off a quartz filter punch by heating, and oxidizing it downstream to CO_2 and then reducing it to methane and quantifying it with a flame ionization detector (FID). The step-wise heating process initially takes place in an inert (He) environment. During this phase, the evolved material is typically classified as OC. The oven then cools and then resumes the step-wise heating in an oxidizing (He/O_2) atmosphere. Ideally, the material evolved in the oxidizing phase is mainly classified as EC.

SOA concentrations from chamber studies and the ambient atmosphere are often measured by EGA (Edney et al. 2000; Saathoff et al. 2003; Salma et al. 2004; Plaza et al. 2006). One of the largest sources of uncertainties in using EGA is determining the exact location of the OC/EC split. During the inert phase, SOA will pyrolize and produce char, resulting in the darkening of the filter spot. Charred OC requires the addition of O_2 to remove it from the filter – similar to EC. The instrument accounts for charred OC that would otherwise be classified as EC by the laser transmittance or reflectance through the sample, otherwise known as thermo-optical transmittance (TOT) or thermo-optical reflectance (TOR). The EC/OC split is located at the point where the transmittance or reflectance level returns to its initial level after a reduction of laser response due to

charring. The National Institute of Occupational Safely and Health (NIOSH) specifies a standard temperature protocol for a TOT instrument (NIOSH 1999). In addition to the NIOSH (1999) method, (Conny et al. 2003) performed an extensive factorial study to optimize the temperature program of EGA-TOTs, to minimize the charring of OC and to eliminate the possibility of native EC evolving during the helium phase and being miscounted as OC.

Another complication in the analysis of OC and EC is the possibility that the non-carbonaceous components in aerosols may affect the thermal stability of carbon during EGA. Metals which are typically present in the atmosphere have been shown to affect the thermal stability of carbon during EGA (Grosjean et al. 1994; Turner and Hering 1994). Coarse (2.5 um < d_p < 10 um) and accumulation mode (0.1 um < d_p < 2.5 um) particles comprise the majority of the aerosol mass concentration (over 85%) in the Los Angeles area (Sardar et al. 2005). Coarse mode particles typically have high concentrations of metals (over 50% by mass) including aluminum, silicon, calcium, and iron and relatively low carbon mass concentrations. The accumulation mode frequently contains lower concentrations of metals and a higher fraction of carbon. For ultrafine particles, carbon often dominates the aerosol mass (Hughes et al. 1998; Sardar et al. 2005); however, (Chung et al. 2001) found that metals exceed 50% of the ultrafine particle mass for aerosols collected in Bakersfield, CA with calcium being the predominant metal. Few chamber studies have investigated mixtures of SOA and diesel particles (Saathoff et al. 2003; Lee et al. 2004); however they did not look into the affect of metals in the partitioning particulate carbon into EC and OC.

Biodiesel, an (at least partly) "carbon neutral" drop-in replacement for regular diesel fuel is currently gaining attention and market share as a source for alternative energy. Both the American Jobs Creation Act of 2004, which provided distributors of biodiesel fuel federal tax credits, and the Energy Policy Act of 2005, will significantly increase the demand for biodiesel fuel. The American Jobs Creation Act alone contributed to a 300% increase in the U.S. biodiesel production from just 2004 to 2005 (Swanson et al. 2007). LECG LLC, an international expert services company, has predicted that the demand for biodiesel fuel will increase from 75 million gallons in 2005 to over 600 million gallons by the year 2015 (Urbanchuk 2006). Due to its potential growth, the emissions of biodiesel combustion are important to quantify both from a chemical composition and climate standpoint.

Extensive literature is available examining innovative ways to produce biodiesel (Du et al. 2008; Jin et al. 2008; Ranganathan et al. 2008); however the research into biodiesel particulate emissions is limited. It has been determined that oxygenated fuels such as biodiesel have a higher soluble organic fraction (SOF) than non-oxygenated fuels such as petroleum diesel (Sidhu et al. 2001; Turrio-Baldassarri et al. 2004). The higher organic fraction in particles formed from biodiesel combustion may make it more susceptible to charring during the inert phase of EGA. (Jung et al. 2006) found that at 75% load, particles produced from a 100% soy methyl ester bidiesel fuel has reduced particle size, number, and mass in the accumulation mode where most of the mass is present. They attribute this decrease to the ease of biodiesel particles to be oxidized. Reaction rate constants showed about a 6 times higher oxidation rate compared to regular

diesel fuel in the range of 700 to 825° C. Similar trends in reduced particle size and mass was shown for particles produced from a biodiesel formulated from used cooking oil (Chung et al. 2008; Lapuerta et al. 2008).

Unlike diesel fuel which has its chemical composition regulated, biodiesel fuels can be made by a number of methods and sources. This inconsistency in biodiesel production introduces the possibility of data on biodiesel particulate matter being specific to the source fuel. The biodiesel fuel that is commercially available in Los Angeles is formulated from used vegetable oil (www.conservfuel.com) and will be a focus of this work. Particles emitted from biodiesel combustion have been shown to have metals similar in type and relative abundance to diesel particles (Dwivedi et al. 2006). Not only with the presence of metals in the atmosphere, but in the particles themselves, it is important to understand how metals affect the measurement of carbon from biodiesel particles in the EGA.

The extent of charring on lab generated α-pinene SOA in EGA with and without the addition of metal catalysts was investigated and any changes to the EC/OC ratio were analyzed. Mixtures of lab generated SOA and high EC diesel particles were analyzed for their sensitivity to catalytic metals during EGA. Finally, investigation into the veracity of EGA measurements of biodiesel EC and OC when metals are present was conducted. Results from the biodiesel experiments was compared to the data from diesel particles previously described in Chapter 3.

4.2 Experimental

Metal solutions were prepared by weighing out the appropriate mass of metal chloride/sulfate powder on a microbalance (± 0.001 g, Shimadzu) and were subsequently dissolved in purified de-ioninized water (18 M Ω). Solutions of metal chlorides and sulfates were nebulized into a small Teflon chamber for 2 min at a flow rate of 3.3 L min^{-1}. The chamber had a volume of approximately 0.13 m^3 in a pillow geometry and was constructed by sealing 2 mil FEP Teflon sheets with a impulse heat sealer (PI-G35, Packaging Aids). The seals were then reinforced with greenback tape (3M). The chamber air was less than 25% relative humidity, so the aerosol leaving the nebulizer was directly injected into the chamber without the use of a drier. Chamber air was supplied by an oil-free air compressor and was purified prior to filling the chamber by a series of packed bed scrubbers filled with Purafil Triple Blend (Purafil Inc.), activated charcoal, and a HEPA capsule filter (Gelman). The background particle concentration in a clean filled chamber was < 20 particles cm^{-1}. Conductive rubber tubing was used to sample from the chamber through Teflon sampling ports. 47 mm filter holders equipped with a Teflon and quartz filter sampled the nebulized aerosols from the chamber simultaneously at a flow rate of 20 L min^{-1} for 30 seconds. The scanning mobility particle sizer (SMPS) was also used to characterize the aerosol size distribution. Teflon filters were pre-weighed in a temperature and humidity controlled room using a microbalance (± 1 μg, Sartorius) after removing charges from the filters by passing them over a polonium strip. Prior to weighing, the filters were allowed to re-equilibrate for 24 hrs in the weighing room. After gravimetric analysis, the Teflon filters were placed in sterile polycarbonate

petri dishes and material was extracted with 10 mL of 5% HNO_3 solution for 48 hours. The extract was analyzed for metals by inductively coupled plasma atomic emission spectroscopy (ICP-AES). Calibration solutions were provided by Dr Amir Liba (Director, UCLA Molecular and Instrumentation Center) and calibration curves were performed at concentrations of 0, 50, 100, 400, 700, and 1000 ppm for the desired metals with correlation coefficients for these calibrations being above 0.999.

SOA was formed by photo-oxidizing α-pinene in an outdoor Teflon chamber (as described in Chapter 2). Liquid α-pinene was volatilized in a glass bulb and then injected into the chamber using purified compressor air. A cylinder of nitric oxide (NO) supplied the desired concentration of NO to provide a VOC/NO_x ratio of about 10. During injection of α-pinene and NO, the chamber was covered with tarps to allow mixing of the gas phase species before interaction with the incoming solar radiation. Adequate mixing of the α-pinene and NO was allowed before removing the cover. SOA formed after about an hour of exposure to sunlight. From SMPS measurements, SOA was first observed at around 60 nm and then rapidly grew to 300 nm.

SOA was sampled from the chamber using a parallel plate diffusion denuder filled with activated carbon strips (Sunset Labs). The denuder removed gas phase organics which may lead to an overestimation of particle phase OC. A ¼" copper tube connected to the denuder was inserted about 1 to 2' into the chamber. Both a clean quartz filter (control) and a metal doped quartz filter sampled downstream of the denuder. The metals investigated were NaCl, KCl, $MgSO_4$, $CuCl_2$, and $FeCl_3$. Sampling occurred at 20 L/min for 10, 15, or 20 minutes depending on the estimated mass concentration of carbon

particulate matter (PM) inside the chamber. Sampling began once a significant peak indicating the formation of SOA measured by the SMPS. After collecting SOA on the quartz filters, diesel particles were injected into the chamber using a small portable diesel generator using diesel fuel operating at 100% load. This resulted in an external mixture of a highly organic (SOA) and elemental (diesel particles) carbon aerosol (Figure 4-1). Before use, the diesel generator was warmed up for 5 minutes at idle and then another 5 minutes at the load investigated. Also in figure 4-1 is a SMPS mass distribution showing the bi-modal distribution representative of the diesel particle and SOA mixture.

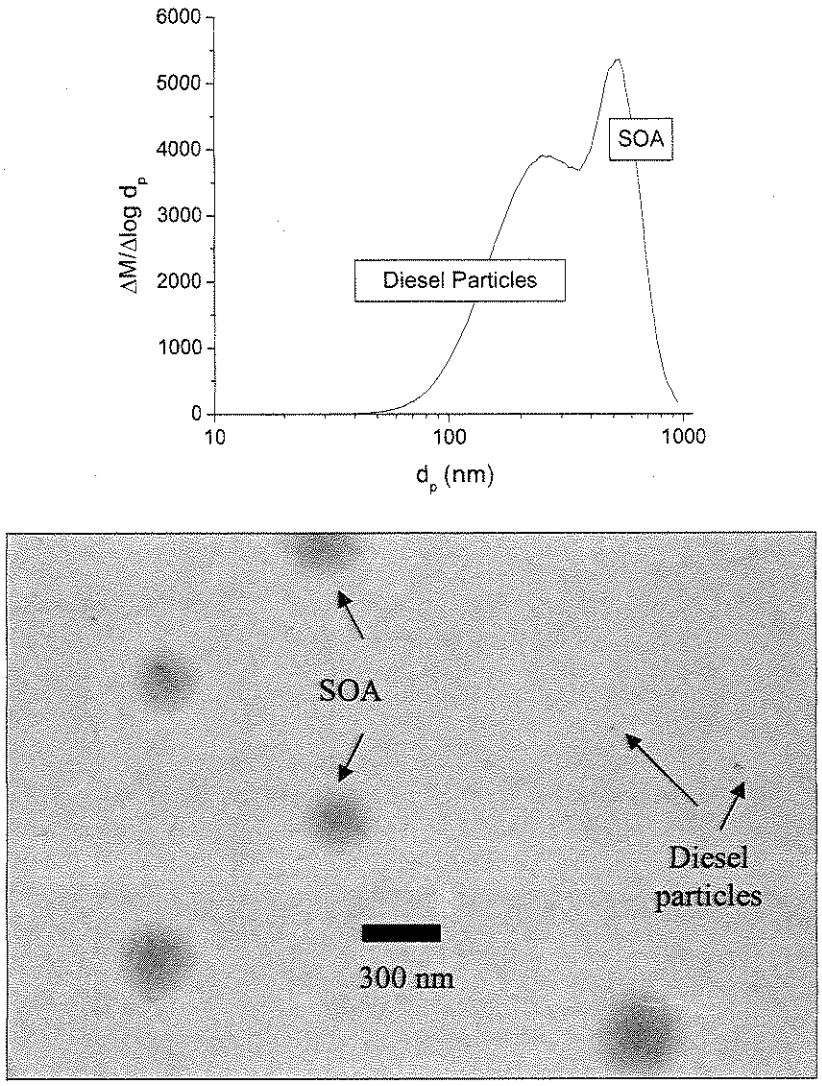

Figure 4-1: SMPS distribution showing a bi-modal distribution for the mixture of diesel particles and SOA (top). TEM image of SOA and diesel particles (bottom).

Once SMPS size distribution measurements stabilized, sampling resumed from the chamber using the denuder upstream of a clean and metal doped quartz filter. Filters were stored in Petri dishes sealed with Teflon tape in a freezer. Analysis of the carbon content was conducted using TOT-EGA using both the NIOSH (1999) and Conny et al.

(2003) temperature protocol (Table 4-1). Two separate SOA/diesel experiments were conducted with the hopes of varying the amount of metal to carbon PM deposited on the sample.

		NIOSH (1999)		Conny et al. (2003)	
	Step	Temp (°C)	Time (s)	Temp (°C)	Time (s)
He Phase	1	250	90	190	90
	2	500	60	365	60
	3	650	60	610	60
	4	850	90	835	72
O_2-He Phase	1	650	30	550	180
	2	750	30	700	60
	3	850	60	850	60
	4	940	120	900	90-120

Table 4-1: Temperatures and durations of each step for the NIOSH (1999) and Conny et al. (2003) method used for TOT-EGA. After step 4 there is a about a 50 second period of cooling before the O_2-He phase begins.

The primary carbon emissions from a generator running on biodiesel fuel were tested producing particles higher in OC than diesel particles. The denuder was placed 0.5 m from the engine and sampled directly from the exhaust. Both a control and a metal laden quartz filter were used downstream of the denuder. The same metals selected for the SOA/diesel experiments were also chosen for analysis for the biodiesel experiments. Sampling was conducted at 20 L/min for 10 min when operating the generator at maximum load, and for 60 min when at idle load.

4.3 Results

SOA

Measurements for the two SOA experiments are shown in Table 4-2. The SOA experiments collected samples with a range of metal to carbon mass ratios (M/C ratio) from 0.06 to 0.45 deposited on the quartz filters.

NIOSH (1999) Protocol										
					Char (Evolution)			Char (Transmission)		
	Metal	TC (μg/filter) w/cat	TC (μg/filter) w/o cat	M/C Ratio	w/cat	w/o cat	% Δ	w/cat	w/o cat	% Δ
Exp 1	NaCl	18.1	17.5	0.45	9	6	50	18	12	50
	KCl	22.0	21.3	0.26	11	9	22	17	10	70
	$MgSO_4$	25.6	30.5	0.14	11	8	38	14	11	27
	$CuCl_2$	35.5	36.8	0.13	15	7	114	45	14	221
	$FeCl_3$	43.5	43.3	0.11	16	10	60	40	16	150
Exp 2	NaCl	39.7	40.3	0.19	10	7	43	30	15	100
	KCl	47.2	53.9	0.1	12	11	9	35	24	46
	$MgSO_4$	45.2	46.7	0.09	7	6	17	25	18	39
	$CuCl_2$	76.5	101.4	0.06	12	10	20	50	35	43
	$FeCl_3$	71.2	83.9	0.06	13	9	44	48	31	55
Conny et al. (2003) Protocol										
	Metal	TC (μg/filter) w/cat	TC (μg/filter) w/o cat	M/C Ratio	w/cat	w/o cat	% Δ	w/cat	w/o cat	% Δ
Exp 1	NaCl	19.2	18.7	0.44	14	12	17	19	9	111
	KCl	23.1	21.8	0.27	13	10	30	21	10	110
	$MgSO_4$	27.7	34.8	0.13	21	20	5	11	10	10
	$CuCl_2$	40.0	37.3	0.12	22	14	57	43	14	207
	$FeCl_3$	45.3	43.9	0.11	19	14	36	43	17	153
Exp 2	NaCl	38.5	40.2	0.19	17	13	31	29	18	61
	KCl	47.1	55.7	0.1	17	17	0	33	21	57
	$MgSO_4$	43.5	43.3	0.09	16	14	14	22	19	16
	$CuCl_2$	78.9	82.0	0.06	16	12	33	60	29	107
	$FeCl_3$	69.6	83.8	0.06	15	14	7	52	31	68

Table 4-2: EC/OC ratios and measures of char for SOA. Data using the NIOSH (1999) and Conny et al. (2003) temperature protocols are shown.

Much like the other samples discussed in Chapter 3 and in this work, it was determined from the EGA data that adjustment of the EC/OC split time was necessary. Adjustment of the split point resulted in no effect on the EC/OC ratio in that all carbon

was still classified as OC. This was in sharp contrast to the high OC diesel samples which showed a large an affect on the measured EC/OC ratio when manually setting an EC/OC split time.

Char was quantified by two methods. The first was the amount of carbon removed from the filter between the introduction of oxygen into the carrier gas to the point where laser transmission increases to its initial value. The amount of carbon evolved during this period was expressed as a percentage of the total carbon evolved during the entire analysis, and is called char by evolution. The second measure of char was the percent reduction of laser transmission through the filter during the inert heating phase of EGA and is called char by transmission.

Although not affecting the EC/OC ratio, the metal catalysts did result in increased charring. Among the metals tested, the transition metal chlorides were the most effective in catalyzing the reaction of SOA to charred carbon. Figure 4-2 illustrates an EGA thermogram of SOA and a mixture of $CuCl_2$. The FID response was normalized to the total FID response so that the area under the curve was proportional to the total carbon evolved. The bold lines for the carbon evolution and laser transmission represented the measurement of SOA with the $CuCl_2$ catalyst. The carbon evolved during the inert phase was decreased when the aerosols are mixed with $CuCl_2$. This decrease in carbon evolution was compensated by the increase in carbon evolution beyond the introduction of oxygen caused by the catalyst, especially immediately after the addition of oxygen. The enhancement of charring was also evident in the laser transmission profiles. The laser transmission profile (darker line) for SOA and $CuCl_2$ not only decreased to a greater

degree but also at a faster rate than the transmission signal without the $CuCl_2$ catalyst. When attempting to compare the amount of char produced for the two samples with different mass to carbon mass ratio on the filter, results were not consistent. For the NIOSH (1999) method it seemed that more char was produced for the higher metal to carbon ratios when $CuCl_2$ was used; however for the Conny et al. (2003) method, this trend was reversed. $FeCl_3$ was the other transition metal chloride that had a large effect on the amount of char produced. Conversely to $CuCl_2$, it seemed that the increased amount of char produced with the presence of $FeCl_3$ was dependent on the M/C ratio on the sample in that the more Fe (III) fraction on the sample, the more char was produced.

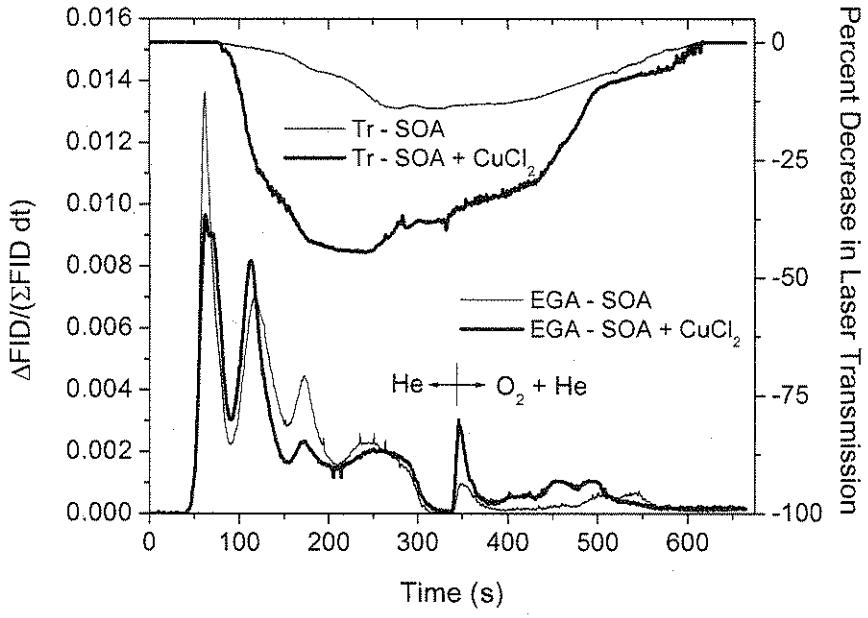

Figure 4-2: EGA thermogram of SOA and a mixture of SOA and $CuCl_2$. Carbon evolution (left y-axis) and laser transmission through the filter (right y-axis) are shown. This is analyzed using the NIOSH (1999) method.

Although it was shown in Chapter 3 that $MgSO_4$ did not catalyze the early oxidation of carbon, it did catalyze the reaction of OC to char for both temperature programs evident by the increased charring in the presence of this metal chloride. Both sodium and potassium chloride catalyzed the OC to char reaction to a greater extent than $MgSO_4$; however, not to the degree of the transition metal chlorides.

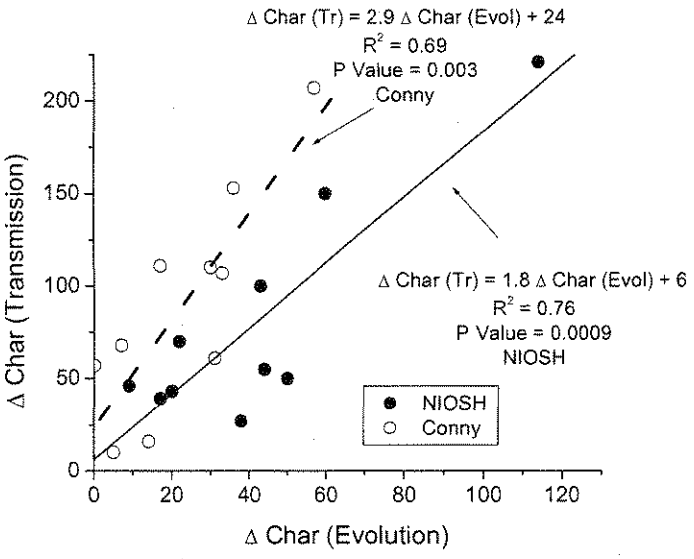

Figure 4-3: Correlation between the two measures of char for SOA.

There was a correlation between the two measures of char for SOA (Figure 4-3), and the R^2 and P-values were much more favorable compared to high OC diesel particles (Chapter 3). A possible explanation for the better correlation for SOA was the uniformity in its chemical composition. Diesel particles are a mixture of EC and OC, metals (Wang et al., 2003; Dwivedi et al. 2006), and sulfur, whereas the lab generated SOA is a by-product of the photo-oxidation of α-pinene. A particle consisting of a mixture of various

types of carbonaceous and non-carbonaceous species may introduce more uncertainty in the measurement of carbon.

Due to the lack of data, it was difficult to determine what factors influence the enhancement of char in the presence of metals. Although being unable to determine this, it was found that metals will enhance the production of char during the inert phase of the EGA for lab generated SOA. Although not affecting the measured EC/OC ratios, the enhancement of char production by these metals became a factor when mixing different aerosols of different carbon composition (i.e., SOA and diesel particles)

SOA and Diesel Particles

Figure 4-4 shows an EGA thermogram measuring a mixture of SOA with high EC diesel particles using the NIOSH (1999) method in the presence of $CuCl_2$ (metal to carbon mass ratio of 0.09)

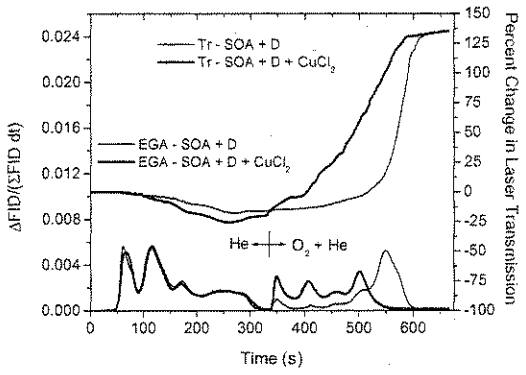

Figure 4-4: EGA thermogram of SOA and diesel particles (D) formed at maximum load with and without $CuCl_2$ analyzed by the NIOSH (1999) method. The bold lines for carbon evolution and laser transmission are representative of measurements for the SOA/D mixed with a metal catalyst.

The complications involved with metals affecting the thermal stability of carbon during EGA were once again clearly seen. First there was an increased amount of char produced by the catalytic activity of $CuCl_2$ by way of laser reduction through the filter sample. There was a 25% reduction in laser transmission through the filter when $CuCl_2$ was added to the aerosol as opposed to 17% when it was only SOA and diesel particles. Not only was there increased amount of darkening on the filter spot but the laser transmission decreased more rapidly when the reaction was catalyzed by $CuCl_2$. Second there were different carbon evolution profiles once oxygen was introduced to the carrier gas. When there was no metal catalyst, the carbon evolution was similar to that of high EC diesel particles, with the addition of a small initial peak representative of char. It was reasonable to assume that a bulk of the native EC was in the second larger peak. When examining the carbon evolution profile due to the addition of $CuCl_2$, a more complex carbon evolution profile was observed. The peak that was associated with native EC not only oxidized at lower temperatures due to the catalyst, but it was also the same magnitude as the other peaks in the oxidative phase. This lack of discontinuity between charred OC and the peak that was predominantly native EC may introduce problems in the determination of the EC/OC split.

The results for the EC/OC ratio, split time, and measures of char are shown in Table 4-3a and 3b with data representative of corrected split times shown in Table 4-4a and 4b. Both tables showed that there was little change in EC/OC ratio due to the catalytic metal compounds regardless of the M/C mass ratio deposited on the filter. Both

methods were very capable of measuring the EC/OC ratios for this aerosol, which was in sharp contrast to diesel paricles.

A possible hypothesis for this difference was that the charring effect of SOA eliminated the complication observed for high EC diesel particles which exhibited very little change in the laser transmission profile during EGA. By having the transmission change only a few percent during inert heating of pure high EC particles, the location of the EC/OC split becomes arbitrary. Since there was extensive charring of SOA, with or without the presence of metals, this noticeable drop in laser transmission through the filter allowed a more obvious determination of the EC/OC split location once transmission levels reached its initial level. By having the laser transmission through the filter decrease significantly below the initial level, this eliminated the possibility of extremely early split times which were encountered for samples containing high EC diesel particles and metals.

NIOSH (1999) Protocol														
		TC (μg/filter)			EC/OC		Split Time		Char (Evolution)			Char (Transmission)		
	Metal	w/cat	w/cat	M/C Ratio	w/cat	w/o cat	w/cat	w/o cat	w/cat	w/o cat	%Δ	w/cat	w/o cat	%Δ
Exp 1	NaCl	58.7	55.4	0.15	0.19	0.19	467	535	15	12	25	21	19	11
	KCl	46.9	47.6	0.13	0.16	0.13	464	548	15	13	15	23	19	21
	$MgSO_4$	60.6	57.5	0.07	0.28	0.29	534	521	11	10	10	13	13	0
	$CuCl_2$	41.4	44.6	0.10	0.16	0.17	433	546	13	13	0	29	12	142
	$FeCl_3$	53.1	54.5	0.09	0.26	0.27	456	524	10	7	43	26	13	100
Exp 2	NaCl	57.5	63.3	0.12	0.37	0.39	462	529	11	11	0	20	13	54
	KCl	60.5	57.8	0.08	0.29	0.39	479	512	9	7	29	21	14	50
	$MgSO_4$	56.6	52.6	0.07	0.33	0.36	507	518	8	8	0	15	14	7
	$CuCl_2$	56.2	57.8	0.09	0.32	0.33	405	518	11	10	10	26	18	44
	$FeCl_3$	57.6	63.5	0.07	0.35	0.34	406	507	12	11	9	26	17	53
					Avg.	0.29		526						
					σ_d:	0.09		14						

Table 4-3a: EC/OC ratios and measures of char for mixtures of SOA and high EC diesel particles with and without the presence of metals. Data show is analysis by the NIOSH (1999) method.

Conny et al. (2003) Protocol															
					EC/OC		Split Time		Char (Evolution)			Char (Transmission)			
	Metal	TC (μg/filter) w/cat	w/cat	M/C Ratio	w/cat	w/o cat	w/cat	w/o cat	w/cat	w/o cat	%Δ	w/cat	w/o cat	%Δ	
Exp 1	NaCl	56.5	55.6	0.15	0.23	0.22	542	599	15	13	15	18	15	20	
	KCl	46.3	48.2	0.13	0.21	0.21	600	540	14	12	17	23	16	44	
	$MgSO_4$	61.1	58.7	0.07	0.34	0.33	598	595	12	11	9	14	11	27	
	$CuCl_2$	41.6	42.1	0.11	0.21	0.23	387	600	16	12	33	32	12	167	
	$FeCl_3$	51.1	50.3	0.10	0.29	0.33	598	496	13	12	8	29	12	142	
Exp 2	NaCl	63.2	62.9	0.13	0.44	0.46	522	592	13	12	8	24	15	60	
	KCl	60.2	56.8	0.09	0.39	0.43	541	590	14	13	8	24	14	71	
	$MgSO_4$	54.3	51.8	0.08	0.38	0.39	583	590	13	13	0	16	14	14	
	$CuCl_2$	54.6	53.6	0.09	0.39	0.39	356	591	13	13	0	24	14	71	
	$FeCl_3$	54.4	58.5	0.08	0.38	0.38	480	590	15	13	15	29	16	81	
					Avg.	0.34		578							
					σ_d:	0.09		34							

Table 4-3b: EC/OC ratios and measures of char for mixtures of SOA and high EC diesel particles with and without the presence of metals. Data show is analysis by the Conny et al. (2003) protocol.

NIOSH (1999) Protocol														
		TC (μg/filter)		M/C	EC/OC		Split Time		Char (Evolution)			Char (Transmission)		
	Metal	w/cat	w/o cat	Ratio	w/cat	w/o cat	w/cat	w/o cat	w/cat	w/o cat	%Δ	w/cat	w/o cat	%Δ
Exp 1	NaCl	58.7	55.4	0.15	0.21*	0.21*	460*	528*	14	11	27	21	19	11
	KCl	46.9	47.6	0.13	0.18*	0.19*	459*	530*	12	11	9	23	19	21
	$MgSO_4$	60.6	57.5	0.07	0.34*	0.35*	512*	498*	7	8	-13	13	13	0
	$CuCl_2$	41.4	44.6	0.18	0.18*	0.20*	421*	537*	12	12	0	29	12	142
	$FeCl_3$	53.1	54.5	0.09	0.26	0.29*	456	510*	10	7	43	26	13	100
Exp 2	NaCl	57.5	63.3	0.12	0.45*	0.48*	448*	500*	7	7	0	20	13	54
	KCl	60.5	57.8	0.08	0.35*	0.46*	459*	490*	6	4	50	21	14	50
	$MgSO_4$	56.6	52.6	0.07	0.40*	0.43*	487*	496*	5	5	0	15	14	7
	$CuCl_2$	56.2	57.8	0.09	0.35*	0.38*	398*	502*	10	8	25	26	18	44
	$FeCl_3$	57.6	63.5	0.07	0.32*	0.37*	420*	497*	9	9	0	26	17	53
					Avg.	0.37		509						
					σ_d:	0.11		17						

Table 4-4a: EC/OC ratios and measures of char for mixtures of SOA and high EC diesel particles with and without the presence of metals. Data indicated by a (*) are those which required adjustment of the EC/OC split time. Analysis of samples conducted using the NIOSH (1999) method.

Conny et al. (2003) Protocol															
					EC/OC		Split Time		Char (Evolution)			Char (Transmission)			
	Metal	TC (µg/filter) w/cat	w/o cat	M/C Ratio	w/cat	w/o cat	w/cat	w/o cat	w/cat	w/o cat	%Δ	w/cat	w/o cat	%Δ	
Exp 1	NaCl	56.5	55.6	0.15	0.26*	0.22	531*	599	13	13	0	18	15	20	
	KCl	46.3	48.2	0.13	0.24*	0.23*	593*	533*	13	11	18	23	16	44	
	$MgSO_4$	61.1	58.7	0.07	0.39*	0.36*	580*	588*	8	11	-27	14	11	27	
	$CuCl_2$	41.6	42.1	0.11	0.25*	0.26*	360*	594*	13	12	8	32	12	167	
	$FeCl_3$	51.1	50.3	0.1	0.26*	0.32*	539*	590*	17	11	55	29	12	142	
Exp 2	NaCl	63.2	62.9	0.13	0.45*	0.56*	513*	550*	13	8	63	24	15	60	
	KCl	60.2	56.8	0.09	0.44*	0.52*	530*	553*	14	9	56	24	14	71	
	$MgSO_4$	54.3	51.8	0.08	0.44*	0.45*	565*	575*	11	10	10	16	14	14	
	$CuCl_2$	54.6	53.6	0.09	0.43*	0.49*	349*	550*	11	9	22	24	14	71	
	$FeCl_3$	54.4	58.5	0.08	0.40*	0.45*	450*	566*	14	10	40	29	16	81	
					Avg.	0.39		570							
					σ_d:	0.12		23							

Table 4-4b: EC/OC ratios and measures of char for mixtures of SOA and high EC diesel particles with and without the presence of metals. Data indicated by a (*) are those which required adjustment of the EC/OC split time. Analysis of samples conducted using the Conny et al. (2003) method.

Biodiesel Particles – Maximum Load

Table 4-5 and 4-6 shows the EGA results from mixing metal compounds with biodiesel particles emitted from a generator operating at maximum load with and without adjusting for an appropriate EC/OC split point. The change in oxidation temperature (ΔT_{ox}) was defined as the difference in temperatures at which the peak of the carbon oxidation occurs. As stated in Chapter 3, going forward with the analysis, focus will be given attention to the data with adjusted EC/OC split times.

Significant changes, mainly reductions, in the EC/OC ratio were observed when mixing biodiesel particles with a metal compound. For the NIOSH (1999) and Conny et al. (2003) method, reductions up to 24 and 31% respectively, were observed for the data in Table 4-5. Comparing the oxidation temperature of the EC for the control case (i.e., no metals added) there was a very narrow range for the biodiesel particles with standard deviations of 5 and 0.5 for the NIOSH (1999) and Conny et al. (2003) method. This was much narrower than that observed for diesel particles which showed standard deviations of 20 to 28, depending on the temperature program used. Comparing the change in oxidation temperature caused by a specific metal between biodiesel and diesel particles, a very good correlation was observed (Figure 4-5). Although the oxidation temperature of the diesel particles for the control showed more spread, the resulting effect of metals on the reduction in the oxidation temperature between diesel and biodiesel particles was very similar.

NIOSH (1999) Protocol												
	TC (µg/filter)		M/C	EC/OC			Split Time			ΔTox		
Metal	w/cat	w/o cat	Ratio	w/cat	w/o cat	% diff	w/cat	w/o cat	Δ	w/cat	w/o cat	Δ
KCl	30.2	32.2	0.16	1.11	1.26	-12	463	490	-27	793	863	70
NaCl	31.9	29.4	0.25	1.30	1.54	-16	448	319	129	794	864	70
$MgSO_4$	30.9	31.8	0.11	1.19	1.36	-13	473	475	-2	862	862	0
$CuCl_2$	39.0	38.4	0.10	1.34	1.67	-20	355	478	-123	654	860	196
$FeCl_3$	30.6	33.7	0.14	1.62	1.30	25	300	474	-174	765	852	87
				Avg.	1.4			447			860	
				σ_d:	0.2			72			5	
Conny et al. (2003) Protocol												
	TC (µg/filter)		M/C	EC/OC			Split Time			ΔTox		
Metal	w/cat	w/o cat	Ratio	w/cat	w/o cat	% diff	w/cat	w/o cal	Δ	w/cat	w/o cat	Δ
KCl	30.4	31.3	0.16	1.69	1.98	-15	439	465	-26	861	865	4
NaCl	30.9	30.5	0.24	1.37	1.33	3	528	573	-45	851	865	14
$MgSO_4$	29.3	31.1	0.11	1.66	1.07	55	526	577	-51	864	864	0
$CuCl_2$	37.9	38.0	0.10	1.76	2.04	-14	334	539	-205	725	864	139
$FeCl_3$	31.9	30.3	0.14	2.31	2.08	11	264	557	-293	785	865	80
				Avg.	1.7			542			864	
				σ_d:	0.5			46			0.5	

Table 4-5: Effect of metal compounds on the EC/OC measurement of biodiesel particles emitted by a diesel generator operating at maximum load.

NIOSH (1999) Protocol													
	TC (µg/filter)		M/C	EC/OC			Split Time			ΔTox		
Metal	w/cat	w/o cat	Ratio	w/cat	w/o cat	% diff	w/cat	w/o cat	Δ	w/cat	w/o cat	Δ
KCl	30.2	32.2	0.16	1.75	1.73	1	463	490	-27	793	863	70
NaCl	31.9	29.4	0.25	1.45	1.54 *	-6	448	319	129	794	864	70
$MgSO_4$	30.9	31.8	0.11	1.53 **	1.71 **	-11	335 **	335 **	0	862	862	0
$CuCl_2$	39.0	38.4	0.10	1.83	2.41	-24	355	478	-123	654	860	196
$FeCl_3$	30.6	33.7	0.14	1.51 **	1.91	-21	335 **	474	-139	765	852	87
				Avg.	1.86			419				
				σ_d:	0.33			85				
Conny et al. (2003) Protocol												
	TC (µg/filter)		M/C	EC/OC			Split Time			ΔTox		
Metal	w/cat	w/o cat	Ratio	w/cat	w/o cat	% diff	w/cat	w/o cal	Δ	w/cat	w/o cat	Δ
KCl	30.4	31.3	0.16	1.77	1.98 *	-11	400	390	10	861	865	4
NaCl	30.9	30.5	0.24	1.72	1.91	-10	400	453	-53	851	865	14
$MgSO_4$	29.3	31.1	0.11	1.68	1.69	-1	330	440	-110	864	864	0
$CuCl_2$	37.9	38.0	0.10	1.96	2.25	-13	330	400	-70	725	864	139
$FeCl_3$	31.9	30.3	0.14	1.91 **	2.78	-31	318 **	410	-92	785	865	80
				Avg.	2.12			419				
				σ_d:	0.42			27				

*Adjusting EC/OC split time had no effect on EC/OC ratio

** Transmission reaches initial level before introduction of oxygen so set split time at the point where oxygen is first introduced in EGA

Table 4-6: Effect of metal compounds on the EC/OC measurement of biodiesel particles emitted by a diesel generator operating at maximum load. All data required manual setting of the EC/OC split time.

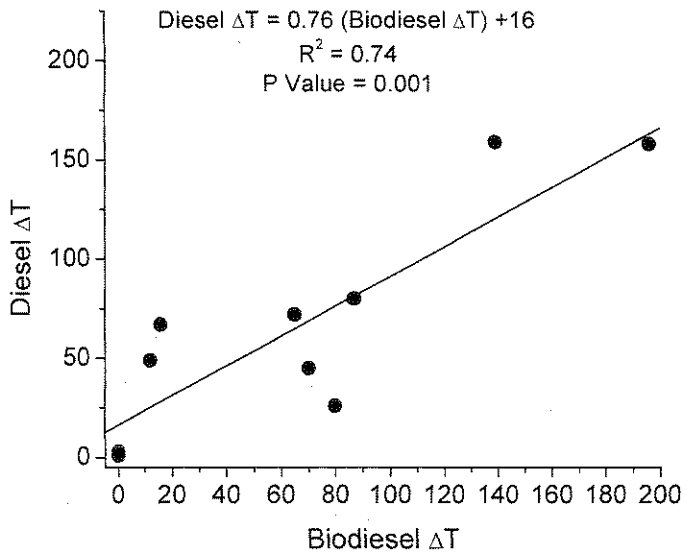

Figure 4-5: Correlation between the change in oxidation temperature of biodiesel and diesel particles in the presence of catalytic metals.

The complications with measurements of high EC diesel particles, regardless of the source of fuel, were illustrated in the EGA thermograms. Figure 4-6 is a thermogram of biodiesel particles in the presence of NaCl. The carbon evolution of biodiesel was very similar to that of diesel particles. For the inert phase there was no noticeable difference in carbon evolution. Once oxygen was introduced, the carbon began to oxidize earlier and was completely removed from the filter at lower temperatures when in the presence of NaCl. A characteristic shared between diesel and biodiesel particles in the EGA thermograms which led possibly to complications in the EC/OC measurement was the relatively flat transmission profiles. During the inert heating and for most of the oxidative heating, there was a very small decrease in transmission indicative of little

charring. The significant change in laser transmission began when the predominately EC carbon begins to oxidize from the filter. Beyond the analysis time of 400 seconds, changes of the split time by a few seconds had a huge affect on both biodiesel and diesel particles; however, considering that biodiesel particles contained more OC than diesel particles, the EC/OC ratio was less sensitive to any changes in the split time as compared to diesel particles.

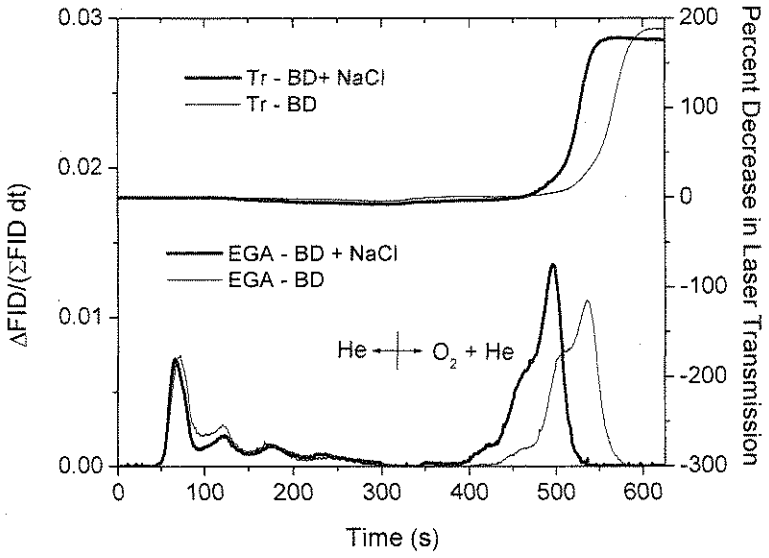

Figure 4-6: EGA thermogram of biodiesel particles with and without NaCl. Transmission profiles are also shown. The analysis is conducted using the NIOSH (1999) protocol. The bold profiles for carbon evolution and laser transmission is representative of the biodiesel/NaCl aerosol.

Biodiesel Particles – Idle Load

Table 4-7 and 4-8 presents the EC/OC ratios and measures of char for biodiesel particles produced at idle load for non-adjusted and adjusted EC/OC ratios.

NIOSH (1999) Protocol													
	TC (μg/filter)		M/C	EC/OC			Split Time		Char (Evolution)		Char (Transmission)		
Metal	w/cat	w/o cat	Ratio	w/cat	w/o cat	% diff	w/cat	w/o cat	w/cat	w/o cat	w/cat	w/o cat	% Δ
NaCl	205.7	204.5	0.03	0.066	0.073	-10	454	494	9	8	40	30	33
KCl	214.4	221.1	0.02	0.037	0.035	6	458	501	12	8	55	40	38
$MgSO_4$	468.5	474.6	0.02	0.024	0.026	-8	503	497	7	5	50	36	39
$CuCl_2$	657.6	659.5	0.01	0.026	0.026	0	428	497	4	4	83	45	84
$FeCl_3$	634.1	608.8	0.01	0.029	0.029	0	433	496	4	4	69	41	68
				Avg:	0.038			497					
				St. Dev:	0.02			3					

Conny et al. (2003) Protocol													
	TC (μg/filter)		M/C	EC/OC			Split Time		Char (Evolvolution)		Char (Transmission)		
Metal	w/cat	w/o cat	Ratio	w/cat	w/o cat	% diff	w/cat	w/o cat	w/cat	w/o cat	w/cat	w/o cat	% Δ
NaCl	209.7	202.8	0.03	0.073	0.083	-12	535	571	9	8	40	29	38
KCl	214.1	216.8	0.02	0.040	0.048	-17	537	568	8	7	56	34	65
$MgSO_4$	433.7	429.3	0.02	0.031	0.036	-14	560	578	5	4	44	35	26
$CuCl_2$	671.9	647.7	0.01	0.041	0.032	28	356	560	4	3	74	40	85
$FeCl_3$	587.7	573.8	0.01	0.041	0.036	14	419	564	4	4	63	38	66
				Avg:	0.047			568					
				St. Dev:	0.021			7					

Table 4-7: Effect of metal compounds on the EC/OC measurement of biodiesel particles emitted by a diesel generator operating at idle load.

NIOSH (1999) Protocol														
	TC (μg/filter)		M/C	EC/OC			Split Time		Char (Evolution)		Char (Transmission)		
Metal	w/cat	w/o cat	Ratio	w/cat	w/o cat	% diff	w/cat	w/o cat	w/cat	w/o cat	w/cat	w/o cat	% Δ
NaCl	205.7	204.5	0.03	0.075 *	0.073	3	449 *	494	8	8	40	30	33
KCl	214.4	221.1	0.02	0.046 *	0.043 *	7	451 *	493 *	7	7	55	40	38
$MgSO_4$	468.5	474.6	0.02	0.030 *	0.029 *	3	488 *	495 *	5	6	50	36	39
$CuCl_2$	657.6	659.5	0.01	0.028 *	0.028 *	0	417 *	491 *	4	4	83	45	84
$FeCl_3$	634.1	608.8	0.01	0.031 *	0.032 *	-3	427 *	490 *	4	4	69	41	68
				Avg:	0.041			493					
				St. Dev:	0.02			2					

Conny et al. (2003) Protocol													
	TC (μg/filter)		M/C	EC/OC			Split Time		Char (Evolvolution)		Char (Transmission)		
Metal	w/cat	w/o cat	Ratio	w/cat	w/o cat	% diff	w/cat	w/o cat	w/cat	w/o cat	w/cat	w/o cat	% Δ
NaCl	209.7	202.8	0.03	0.085 *	0.099 *	-14	523 *	545 *	8	7	40	29	38
KCl	214.1	216.8	0.02	0.046 *	0.048	-4	526 *	568	7	7	56	34	65
$MgSO_4$	433.7	429.3	0.02	0.031	0.036	-14	560	578	5	4	44	35	26
$CuCl_2$	671.9	647.7	0.01	0.035 *	0.032	9	371 *	560	4	3	74	40	85
$FeCl_3$	587.7	573.8	0.01	0.036 *	0.036	0	450 *	564	4	4	63	38	66
				Avg:	0.050			563					
				St. Dev:	0.028			12					

*Data which required adjustment of the EC/OC split time

Table 4-8: Effect of metal compounds on the EC/OC measurement of biodiesel particles emitted by a diesel generator operating at idle load with adjusted split times.

Adjustment of the EC/OC split time for these particles had very little affect on the resulting measurements in part due to the little amount of carbon evolved during the period where the split point was normally set and the large change in transmission which allows the software to set the split time with more accuracy. This was evident in the thermograms in figure 4-7 of biodiesel particles in the presence of $CuCl_2$. A lognormal axis was used for the carbon response to encompass the entire range of carbon measured, since for these samples there was an overwhelmingly large amount of OC compared to EC. The dark line is the carbon evolution of idle biodiesel particles in the presence of $CuCl_2$. Both the NIOSH (1999) and Conny et al. (2003) showed a higher initial peak once oxygen was introduced in the carrier gas indicative of charred OC being removed from the filter. In addition to a higher initial peak, the second peak, which was composed of both char and native EC was oxidized at lower temperatures due to the catalytic ability of the metal to oxidize carbon at lower temperatures. Consistent with both methods, the sample composed of biodiesel and $CuCl_2$ aerosols becomes darker at a faster rate than the sample of biodiesel particles, indicating a higher degree of char. Coinciding with the earlier oxidation of carbon, the laser transmission was observed to increase rapidly.

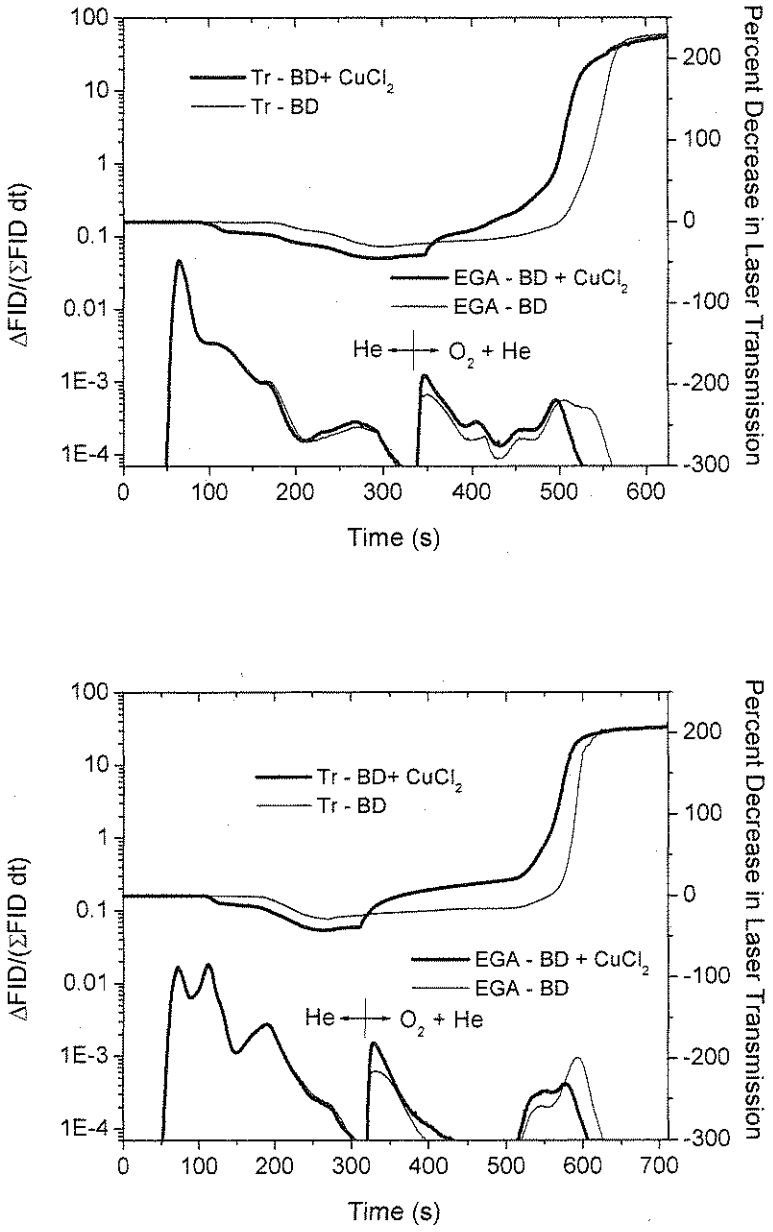

Figure 4-7: EGA thermograms of idle biodiesel particles (BD) alone and in the presence of $CuCl_2$. Top panel and bottom panels are analyses conducted using the NIOSH (1999) and Conny et al. (2003) protocol. Bold lines represent the BD mixed with the metal catalyst.

Correlations between the two measures of char were not good for the two temperature protocols. From the limited data in table 4-7, biodiesel particles during EGA undergo significant charring indicated by the reduction in laser transmission through the filter, but this darkening was not accompanied by an increase in the amount of carbon evolved that was defined as char. Better, but still poor correlation was observed for high OC diesel particles in chapter 3. A possible explanation for the lack of correlation was the nature of carbon for combustion produced particles and lab generated SOA. The chemical composition of the lab generated SOA was largely OC as opposed to the OC associated with combustion particles which can be mixed with a variety of non-carbonaceous species. As has been shown, metal aerosols externally mixed with combustion particles affected charring, and it is possible that the non-carbonaceous species such as native metals, sulfur, and oxygenated compounds (mainly for biodiesel particles) can lead to increased complexity in analyzing the thermal stability of combustion particles.

4.4 Conclusions

The catalytic effects of metals on carbonaceous aerosols during EGA varied according to the type of aerosol measured. The EC/OC ratio of lab generated SOA produced from the photo-oxidation of liquid α-pinene was unaffected when mixed with metal aerosols. Although having no affect on this measurement, the metals did catalyze the formation of char during heating of the samples. The two measures of char for SOA correlated well with one another and was attributed to the relatively simple chemical

composition of the lab generated SOA. In addition to SOA, metals had very negligible effect on the EC/OC measurements of an external mixture of SOA with high EC diesel particles, even though the metals still catalyzed the oxidiation of high EC soot at lower temperatures.

Metal catalyst particles had a similar effect on biodiesel particles as for diesel particles (discussed in Chapter 3). Metal catalysts resulted in large changes to the EC/OC ratio. Also, depending on the metal tested, similar affects on reductions of the oxidation temperature of carbon were observed between biodiesel and diesel particles. In contrast to high EC biodiesel particles, biodiesel particles emitted at idle load conditions were not significantly affected by the presence of metals in the sample. This was attributed to the large amounts of OC in the control aerosol. By having very little carbon in the region where the EC/OC split time was typically set, the resulting EC/OC ratio was largely unaffected by the catalytic of metals during the oxidative phase of analysis.

Measurements of SOA illustrated that charring may be beneficial in the selection of an appropriate EC/OC split time thus facilitating accurate measurements of the EC/OC ratio. High EC diesel and biodiesel particles emitted at high loads were very problematic for EGA for the following reasons – one, there was very minimal charring during EGA and two, a bulk of the carbon evolved from the filter during the time period where the split time was normally set. By having the laser transmission stay near constant during analysis, the split time location became difficult to discern. Especially during the region where most of the carbon was oxidized, slight changes in the split time resulted in large changes to the EC/OC ratio. By having an aerosol char during analysis, the change in

laser transmission was more noticeable and a better selection of the EC/OC split time occurred. This point was exemplified from the experiments involving the addition of a high charring aerosol such as SOA to a low charring one being high EC diesel particles. This external mixture of high OC and EC particles, was largely unaffected by the catalytic characteristics of metal additives. By understanding the type of aerosol, whether it was from an urban or rural setting or from emissions testing directly from an engine, the measurements and shortcomings of EGA can be better understood.

References

Bonn, B. and M. G. Lawrence (2005). "Influence of biogenic secondary organic aerosol formation approaches on atmospheric chemistry." Journal of Atmospheric Chemistry **51**(3): 235-270.

Chung, A., et al. (2001). "Comparison of real-time instruments used to monitor airborne particulate matter." Journal of the Air & Waste Management Association **51**(1): 109-120.

Chung, A., et al. (2008). "Particulate emissions by a small non-road diesel engine: Biodiesel and diesel characterization and mass measurements using the extended idealized aggregates theory." Atmospheric Environment **42**(9): 2129-2140.

Conny, J. M., et al. (2003). "Optimizing thermal-optical methods for measuring atmospheric elemental (black) carbon: A response surface study." Aerosol Science and Technology **37**(9): 703-723.

Du, W., et al. (2008). "Perspectives for biotechnological production of biodiesel and impacts." Applied Microbiology and Biotechnology **79**(3): 331-337.

Dwivedi, D., et al. (2006). "Particulate emission characterization of a biodiesel vs diesel-fuelled compression ignition transport engine: A comparative study." Atmospheric Environment **40**(29): 5586-5595.

Edney, E. O., et al. (2000). "Impact of aerosol liquid water on secondary organic aerosol yields of irradiated toluene/propylene/NOx/(NH4)(2) SO4/air mixtures." Atmospheric Environment **34**(23): 3907-3919.

Grosjean, D., et al. (1994). "EVOLVED GAS-ANALYSIS OF SECONDARY ORGANIC AEROSOLS." Aerosol Science and Technology **21**(4): 306-324.

Heald, C. L., et al. (2008). "Predicted change in global secondary organic aerosol concentrations in response to future climate, emissions, and land use change." Journal of Geophysical Research-Atmospheres **113**(D5).

Huebert, B. J. and R. J. Charlson (2000). "Uncertainties in data on organic aerosols." Tellus Series B-Chemical and Physical Meteorology **52**(5): 1249-1255.

Hughes, L. S., et al. (1998). "Physical and chemical characterization of atmospheric ultrafine particles in the Los Angeles area." Environmental Science & Technology **32**(9): 1153-1161.

Jin, G., et al. (2008). "Producing biodiesel using whole-cell biocatalysts in separate hydrolysis and methanolysis reactions." Journal of Environmental Science and Health Part a-Toxic/Hazardous Substances & Environmental Engineering **43**(6): 589-595.

Jung, H. J., et al. (2006). "Characteristics of SME biodiesel-fueled diesel particle emissions and the kinetics of oxidation." Environmental Science & Technology **40**(16): 4949-4955.

Kanakidou, M., et al. (2005). "Organic aerosol and global climate modelling: a review." Atmospheric Chemistry and Physics **5**: 1053-1123.

Lapuerta, M., et al. (2008). "Diesel particulate emissions from used cooking oil biodiesel." Bioresource Technology **99**: 731-740.

Lee, S. D., et al. (2004). "SOA formation from the photooxidation of alpha-pinene in the presence of freshly emitted diesel soot exhaust." Atmospheric Environment **38**(16): 2597-2605.

NIOSH (1999). Elemental Carbon (Diesel Particulate). NIOSH Manual of Analytical Methods (NMAM). NIOSH: Method 5040 Issue 3.

Plaza, J., et al. (2006). "Estimation of secondary organic aerosol formation from semicontinuous OC-EC measurements in a Madrid suburban area." Atmospheric Environment **40**(6): 1134-1147.

Ranganathan, S. V., et al. (2008). "An overview of enzymatic production of biodiesel." Bioresource Technology **99**(10): 3975-3981.

Saathoff, H., et al. (2003). "Coating of soot and (NH4)(2)SO4 particles by ozonolysis products of alpha-pinene." Journal of Aerosol Science **34**(10): 1297-1321.

Salma, I., et al. (2004). "Elemental and organic carbon in urban canyon and background environments in Budapest, Hungary." Atmospheric Environment **38**(1): 27-36.

Sardar, S. B., et al. (2005). "Seasonal and spatial variability of the size-resolved chemical composition of particulate matter (PM10) in the Los Angeles Basin." Journal of Geophysical Research-Atmospheres **110**(D7).

Senkan, D. S. Professor, Department of Chemical Engineering, UCLA.

Sidhu, S., et al. (2001). "Semi-volatile and particulate emissions from the combustion of alternative diesel fuels." Chemosphere **42**(5-7): 681-690.

Swanson, K. J., et al. (2007). "Biodiesel exhaust: The need for health effects research." Environmental Health Perspectives **115**(4): 496-499.

Turner, J. R. and S. V. Hering (1994). "THE ADDITIVITY AND STABILITY OF CARBON SIGNATURES OBTAINED BY EVOLVED GAS-ANALYSIS." Aerosol Science and Technology **21**(4): 294-305.

Turrio-Baldassarri, L., et al. (2004). "Emission comparison of urban bus engine fueled with diesel oil and 'biodiesel' blend." Science of the Total Environment **327**(1-3): 147-162.

Urbanchuk, J. M. (2006). "Contribution of the Biodiesel Industry to the Economy of the United States." Prepared for the National Biodiesel Board.

Volkamer, R., et al. (2006). "Secondary organic aerosol formation from anthropogenic air pollution: Rapid and higher than expected." Geophysical Research Letters **33**(17).

Chapter 5: Conclusions

The objectives outlined in Chapter 1 were addressed and the conclusions are presented as follows,

1. Characterize the emissions of a small non-road diesel generator operating on diesel fuel and compare to published data for larger on-road diesel engines.

   Number distributions measured by the SMPS showed that particle mobility diameters rose with increasing engine loads similar to that of larger on-road diesel engines. The EC/OC ratio, measured by thermo-optical transmission EGA, with careful attention to the potential for an OC artifact, increased from about 0.5 at idle load to 3.8 at 100% load when using diesel fuel. TEM images of the particles showed that at idle, the majority of the particles were liquid droplets the small remaining fraction were aggregates. When a load was applied, the droplets were replaced by chain aggregates, which had a mean primary particle size of 29 ± 9 nm at 100% load. Fractal dimensions averaged 1.63 ± 0.13, consistent with much larger diesel engines emissions reported in the literature. By showing that the emissions produced from a small non-road diesel generator are similar to that of larger on-road diesel generators, these smaller and more economical engines can be used as surrogates for emission and health studies involving diesel particles. Also, physical and chemical data of diesel particles alone is insufficient in distinguishing emissions between a on-road and non-road diesel engine.

2. Add to the limited amount of data regarding the particle characteristics resulting from the combustion of biodiesel fuel.

The use of biofuel (B100) results in emissions of particles that have smaller mobility diameters than particles emitted from diesel fuel combustion. TEM images verified this by showing that these particles were more compact and more tightly bound, and lacked the clearly defined primary particles of diesel aggregates. Due to the defined nature of primary particles being a prerequisite for the analysis of aggregates for morphology for our method, D_f and N_p were not determined. This type of characterization of biodiesel particles is unique in that it served as one of the first studies to analyze the physical and chemical composition of particles emitted by a non-road diesel generator operating on biodiesel fuel.

3. Extend the idealized aggregate (IA) theory developed by Lall and Friedlander (2006) to determine the mass concentrations of diesel particles from real-time measurements, possibly presenting an advantage over gravimetric measurement methods which offer poor time resolution.

Correlations between the SMPS measurements, corrected with the extended IA theory, and the filter-based measurements, were excellent in both cases ($R^2 = 0.99$) with slopes close to unity - 1.04 for the gravimetric-corrected SMPS comparison and 0.89 for the TC-corrected SMPS comparison. The ability of the extended IA theory to use real-time number distributions to calculate mass concentrations is a powerful

tool which can possibly be used in lieu of the limited, labor intensive method of gravimetric analysis.

4. Study the effect of metals, which are typically in the ambient atmosphere, on the thermal stability of carbonaceous particles during their measurement for carbon content and to correlate the effects to any resulting biases to the measured EC/OC ratio.

It was shown that metals in the presence of carbonaceous aerosols impacted its thermal stability during EGA and affected the resulting measurement of EC/OC ratios. Understanding the shortcomings of this popular method to analyze carbon is necessary in providing accurate data for climate change calculations involving carbonaceous aerosols. This is one of the first studies to present a systematic method in quantifying the impact of metals on carbon analysis; however, more work is still needed.

Lab generated metal salts mixed with high EC diesel particles resulted in lower oxidation temperatures, with the exception of the magnesium species. The effect of metals on EC/OC measurement for high EC diesel particles was highly variable resulting in reduction of 44% to increases of 89% when metals are mixed with diesel particles. Correlations presented attempted to relate observations on the thermal stability of carbon resulting from being mixed with metals to the resulting change in the EC/OC ratio; however more work is needed to verify these correlations.

The effect of metals on the thermal stability of high OC diesel particles was much more complex than that for high EC diesel particles. Not only did metals affect the oxidation temperature of the EC associated with these aerosols, they also affected the charring of OC. Due to the increased amount of oxidized charred carbon combined with the earlier oxidation of EC with the addition of metals, most of the samples resulted in reductions of the EC/OC ratio.

The presence of metals with high EC biodiesel particles caused a reduction in the EC/OC ratio. The resulting change in oxidation temperature was very similar to that of diesel particles resulting in the conclusion that the thermal stability of high EC diesel and biodiesel particles was very similar.

5. Determine if the type of carbon within a particle plays an important role in its interactions with metals during EGA.

Understanding the type of carbon measured by the EGA is important in realizing potential shortcomings associated with the analysis of carbon. For example, there are different concerns when source testing from a diesel engine or SOA collection from a rural environment for carbon content by EGA. Diesel and biodiesel particles emitted at high loads were very problematic for EGA for the following reasons – one, there was very minimal charring during EGA and two, a bulk of the carbon evolved from the filter during the time period where the split time is normally set. By having the laser transmission stay near constant during analysis, the split time location became

uncertain. Especially during the region where most of the carbon was oxidized, slight changes in the split time potentially resulted in large changes to the EC/OC ratio.

Metals had little effect on the EC/OC ratio for SOA or mixtures of SOA and high EC diesel particles using EGA. A possible explanation for the consistent EC/OC ratios was the charring effect of SOA. Since there was extensive charring of SOA, with or without the presence of metals, this noticeable drop in laser transmission through the filter allowed the EGA software to set a more obvious EC/OC split location once transmission levels reaches its initial level. By having the laser transmission through the filter decrease significantly below the initial level, this eliminated the possibility of extremely early split times which were encountered for samples containing high EC diesel particles and metals. By having an aerosol char during analysis, the change in laser transmission was more noticeable and a better selection of the EC/OC split time occurred.

Recommendations

A key objective that was not addressed was relating the effects of metals on the thermal stability of carbon during EGA to any changes to the EC/OC ratio. Correlations were presented throughout Chapter 3 and 4; however, further work is necessary to determine the validity of the proposed correlations. Such steps such as the collection of more data or development of a new temperature program may be necessary. An aspect that was not addressed, but yet possibly important to pursue, is the possible bias caused by laser transmission though a blank quartz filter during EGA. The laser transmission

through the filter is the key component in determining the location of the EC/OC split and if the filter itself presents any alteration of the laser transmission during heating then this needs to be addressed. Priority in future research should be given towards understanding the uncertainty in the software designated EC/OC split point and analysis of the transmission of laser light through a blank quartz filter during heating. By correcting the data to account for the laser transmission through a blank quartz filter, it is possible that the correlations presented in Chapter 3 and 4 will have improved R^2 and P-values.